ARTIFICIAL TACTILE SENSATION BY MICROSTIMULATION OF THE HINDPAW REPRESENTATION IN THE PRIMARY SOMATOSENSORY CORTEX OF BEHAVING RATS

by

İsmail Devecioğlu

B.S., Electronics and Communication Teaching, Marmara University, 2009

M.S., Biomedical Engineering, Boğaziçi University, 2011

Submitted to the Institute of Biomedical Engineering

in partial fulfillment of the requirements

for the degree of

Doctor

of

Philosophy

Boğaziçi University

2016

To my wife

and son...

ACKNOWLEDGMENTS

I am grateful to my advisor, Assoc. Prof. Dr. Burak Güçlü, for his great mentoring and support during my PhD work.

I specially thank to my wife for her patience and encouragement when I really needed. I also thank to my parents for their support during my graduate study.

I thank to Prof. Dr. Can Yücesoy, Assoc. Prof. Dr. Rifat Koray Çiftçi, Assist. Prof. Dr. Özgür Kocatürk and Assist. Prof. Dr. Hale Pınar Zengingönül for their precious comments.

I also thank to Sevgi Öztürk for revising my MATLAB scripts and for her help during training animals; Bige Vardar and Samet Kocatürk for their help in training animals; Deniz Kılınç and Sedef Yusufoğlu for their support; Bora Büyüksaraç, Erhan Uyanık and Ahmet Turan Talaş for their help in manufacture of the multi-probe tip adaptor.

This PhD work was supported by TÜBİTAK grant no: 113S901 and Boğaziçi University BAP no: 15XD2 to Assoc. Prof. Dr. Burak Güçlü.

ACADEMIC ETHICS AND INTEGRITY STATEMENT

I, İsmail Devecioğlu, hereby certify that I am aware of the Academic Ethics and Integrity Policy issued by the Council of Higher Education (YÖK) and I fully acknowledge all the consequences due to its violation by plagiarism or any other way.

Name :

Signature:

Date:

ABSTRACT

ARTIFICIAL TACTILE SENSATION BY MICROSTIMULATION OF THE HINDPAW REPRESENTATION IN THE PRIMARY SOMATOSENSORY CORTEX OF BEHAVING RATS

In this thesis, rats were trained to detect the presence or absence of bursts of mechanical sinusoidal vibrations (duration: 0.5 s, zero-to-peak amplitude: 200 μm, frequency: 40 Hz) delivered to the volar surface of their hindpaws in a novel vibrotactile operant chamber. In psychophysical experiments, psychometric curves were obtained for three frequencies (40 Hz, 60 Hz and 80 Hz). Then, the rats were implanted with microelectrodes in the hindpaw representation of the primary somatosensory cortex and trained to detect trains of biphasic charge-balanced current pulses (pulse width: 600 μs, current intensity: 20-200 μA)(ICMS). They further tested in psychophysical experiments and psychometric curves were obtained for ICMS detection as in vibrotactile experiments. The psychometric data collected from vibrotactile and ICMS experiments were fitted with surface functions using the stimulus intensity and frequency. Psychometric correspondence functions (PCFs) were constructed based on the psychometric functions of five rats. The PCFs were used to estimate current intensities for a given tactile stimulus intensity and frequency. The PCFs were validated in an additional experiment at five frequencies (40 Hz, 50 Hz, 60 Hz, 70 Hz and 80 Hz). In this experiment, the rats performing vibrotactile detection task were presented with unrewarded trials containing either a vibrotactile or an ICMS stimulus. The vibrotactile and ICMS intensities were matched based on PCFs. Kolmogorov-Smirnov statistic showed that the vibrotactile and ICMS stimuli produced similar psychometric curves in validation experiments (all p values >0.05 for 5 frequencies and 5 rats). Therefore, the PCF based method seems to be feasible for modulating the current intensities and frequency of ICMS in a somatosensory neuroprosthetic application.

Keywords: Vibrotactile stimulation, intracortical microstimulation, somatosensory neuroprosthesis, rat.

ÖZET

DAVRANIŞ HALİNDEKİ SIÇANLARDA BİRİNCİL BEDEN DUYUSU KORTEKSİNİN MİKRO-UYARIMI İLE YAPAY DOKUNMA HİSSİNİN OLUŞTURULMASI

Bu tez çalışmasında, sıçanlar mekanik sinuzoidal titreşimlerin (uyarı süresi: 0.5 s, tepe genliği: 200 μm, frekans: 40 Hz) varlığını ya da yokluğunu algılamaya şartlandırılmıştır. Şartlandırma için yeni bir mekanik uyarım sistemi ile donatılmış işlemsel şartlandırma kabini tasarlanmıştır. Psikofiziksel deneylerde, sıçanlara ait psikometrik eğriler üç frekansta (40 Hz, 60 Hz ve 80 Hz) elde edilmiştir. Daha sonra, sıçanların birincil beden duyusu korteksinin arka ayak bölgesine mikro-elektrotlar yerleştirilmiş ve sıçanlar iki-fazlı yük-dengeli akım darbelerini (ICMS) (darbe genişliği: 600 μs, akım seviyesi: 20-200 μA) algılamaya şartlandırılmıştır. Psikofiziksel deneylerle mekanik deneylerde olduğu gibi psikometrik eğriler elde edilmiştir. Mekanik ve ICMS deneylerinden toplanan psikometrik verilere uyaran genlik ve frekansına göre yüzey eğrileri uydurulmuştur. Elde edilen psikometrik fonksiyonlar ile beş sıçan için psikometrik denklik fonksiyonları (PCF) üretilmiştir. PCF'ler belirlenen bir frekansta verilen mekanik titreşim genliğine psikometrik olarak denk gelen akım genliğini hesaplamakta kullanılmıştır. PCF'ler ile oluşturulan modelin doğruluğu ayrı bir davranışsal deneyde beş frekansta (40 Hz, 50 Hz, 60 Hz, 70 Hz ve 80 Hz) test edilmiştir. Bu deneylerde, yüksek genlikte bir mekanik uyaran ile algılama görevi yapan sıçanlara içerisinde mekanik ya da ICMS uyaranlardan birinin bulunduğu ödül verilmeyen denemeler sunulmuştur. Bu denemelerde kullanılan mekanik ve ICMS uyaranların genlikleri PCF ile birbirlerine eşleştirilmiştir. Kolmogorov-Smirnov testinin sonucuna göre, mekanik ve ICMS uyaranlar benzer psikometrik eğriler üretmiştir (beş frekans ve beş sıçan için tüm p değerleri >0.05). Böylelikle, psikometrik denkliklere dayalı bu metot beden duyusu protezlerinde kullanılan ICMS uyaranına ait genlik ve frekansın modüle edilmesi için uygun görünmektedir.

Anahtar Sözcükler: Mekanik titreşimsel uyarım, korteks içi elektriksel uyarım, beden duyusu nöro-protezi, sıçan.

TABLE OF CONTENTS

LIST OF FIGURES

LIST OF TABLES

LIST OF SYMBOLS

p	Probability
$p(h)$	Hit rate
$p(f)$	False alarm rate
$p^*(h)$	Corrected hit rate
e	Euler's number
α,a	Midpoint of the sigmoid (the mean of the normal distribution)
β,b	The parameter related to the slope of the sigmoid at the midpoint
Ω	Ohm, unit of electrical resistance
A	Amplitude
R^2	Goodness of fit
Na^+	Sodium ion
K^+	Potassium ion
Cl^-	Chloride ion
A^-	Organic anions
$\delta\phi$	Resting membrane potential
R_s	Electrical impedance of electrolyte
C_{dl}	Capacitance of electrical double layer
$Z_{Faradaic}$	Faradaic impedance
V_e	Extracellular potential
I, i	Current
r	Radius, distance
σ	Conductivity of extracellular fluid
τ	Duration
a, b, c, d	Coefficients of psychometric surface function
f	Frequency
$z(.)$	z-score
$d^{'}$	Sensitivity index

LIST OF ABBREVIATIONS

ICMS	Intracortical microstimulation
PCF	Psychometric correspondence function
RA	Rapidly adapting. RA type I afferents (for human; FAI)
SA	Slowly adapting
PC	Pacinian afferent (for human; FAII)
SAI	Slowly adapting type I afferent
SAII	Slowly adapting type II afferent
RF	Receptive field
MCN	Merkel cell-neurite complex
CNS	Central nervous system
TN	Trigeminal nucleus of brainstem
VPN	Ventral posterior nucleus of thalamus
VPM	Ventral posterior medial nucleus of thalamus
SI	Primary somatosensory cortex
SII	Secondary somatosensory cortex
P	Pacinian channel
NPI-III	Non-Pacinian channels I-III
LED	Light emitting diode
dB SPL	Decibel of sound pressure level
dB ref 1μm	Decibel referenced to 1μm
dB ref 1μA	Decibel referenced to 1μA
VDC	DC voltage
DAQ	Data acquisition
GUI	Graphical user interface
ROC	Receiver operant characteristic
N/A	Not available
DBS	Deep brain stimulation
BMI	Brain machine interface

EPSP,IPSP	Excitatory/inhibitory postsynaptic potential
AP	Action potential
FBR	Foreign body response
CSC	Charge storage capacity
IPI	Inter-pulse interval
PW	Pulse width
IP	Intraperitoneal
SQ	Subcutaneous
PI	Post-implantation
EEG	Electroencephalography
ECoG	Electrocorticography
TES/TMS	Transcranial electrical/magnetic stimulation
EMG	Electromyography
ENG	Electroneurography
PEF	Psychometric equivalence function

1. INTRODUCTION

1.1 Motivation

In 1992, the prevalence of traumatic spinal cord injury was 12.7 per million in Turkey [1]. To my knowledge, there is not any study reporting the current prevalence of any kind of paralysis and the total incidences in Turkey. In the United States of America (USA), 5.6 million people (1.9 % of US population) were living with motor disabilities in 2008 [2]. In France, annual incidence of traumatic spinal cord injury was 19.4 per million in 2000, whereas it was 23.5 per million in Spain between the years of 2000-2009 [3]. Between the years of 1995 and 2005, 218 upper limb amputations were recorded only in the city of Van, Turkey [4]. In 1995, there were 1.4 million amputees in USA [5]. The latest survey performed in USA revealed that; 185,000 people were amputated in 1996 [6]. Ziegler-Graham et al. estimated this number to reach 2.21 million in 2020 [7].

Amputation and palsy as a result of either a chronic disease or trauma seriously affects subject's daily living quality in both physical and psychological aspects [8]. Amputees and paralytic patients have to deal with lack of independency in their daily living activities as well as other social problems and psychopathological conditions [9]-[14]. Altered body appearance, independency and social acceptance anxiety are the primary driving forces beneath these conditions [13, 14]. Furthermore, while some patients are not able to return to work as a result of physical disabilities after amputation, the others may have to find new jobs that require less work but higher educational profiles [15]. On the other hand, paralytics who is bound to bed do not have a chance to be occupied for a job. Furthermore, considering the annual amputation rates [4, 7] and prevalence of palsy [1]-[3], costs for the society and the economy are considerably high [2]. According to the report of Christopher & Dana Reeve Foundation, caregiver services cost $306 billion annually in USA [2]. Education and getting a quality profession are other issues to be dealt.

In order to improve physical and psychological conditions of these subjects and

to regain them to society, there is a great effort to develop functional prostheses that can help them to move and even feel. The most common prostheses are the passive ones and used only for aesthetic improvements which would diminish the body image anxiety [11]. However, subjective well-being does not depend only on the appearance but also on the independency and the future aims after the trauma [11, 14]. Functional prostheses have been proposed to improve daily-living quality of amputees and paralytics. Nevertheless, expectations from functional prostheses vary depending on the level of amputation (e.g., upper limb or wrist) or paralysis (e.g., cervical or thoracic) and occupation (e.g. profession or daily living activities) [16]-[18].

Different motorized prostheses have been proposed in the literature [19]-[22]. Otto Bock HealthCare GmbH (Germany) commercialized a robotic hand controlled by myoelectric signals recorded from muscles in residual limb [23]. In addition, The BrainGate Co. (USA) have been testing a robotic arm controlled by the activity of cortical neurons recorded via electrode arrays implanted on human subjects [24]. The motorized prosthesis users mostly rely on their vision in order to control their prostheses [16]. However, in a survey performed by Lewis et al. (2012), amputees reported that they would prefer a sensory feedback as vibration, electrical stimulation, pressure or temperature instead of watching or listening to their prosthesis [16].

Keeping the needs of prothesis users in mind, it is also important to understand the role of sensory feedback from our limbs. Movement planning and precise control of the limbs mostly depends on integration of multisensory cues (i.e., vision, proprioception and touch) [25]. Cutaneous afferents from our skin signal the information about contact with an object, its shape and its movement with respect to the skin [26, 27]. Proprioceptive afferents innervating the muscles signal the posture of the limbs and their position in space with respect to the body [26]. These two senses together with vision and sound are used to coordinate the movement with high precision (e.g. grasping an object with adequate force to prevent slipping). Without the cutaneous and/or proprioceptive feedback, limb coordination would be disrupted and movements would be clumsy [27]. This is the case for motorized prostheses; actions take longer and are less accurate compared to natural movements. Implementing the sensory feedback on neural prostheses would improve the quality of the movement. Gaunt et al. (2013) studied the effects of proprioceptive feedback in control of a robotic arm on a tetraplegic

patient [28]. The patient had complete paralysis but had intact sensation of touch and proprioception. She was implanted with microelectrode arrays in motor cortex and trained to control the robotic arm through a brain-computer interface. During the control experiments, she had no feedback except her vision and was successfully controlling the robotic arm (i.e., moving the arm across two points in horizontal plane). When she was blindfolded, she failed to control the robotic arm. However, she regained the control when one moved her arm in synchrony with the robotic arm (providing proprioceptive feedback) while she was still blindfolded.

In addition to the movement planning, multisensory feedback constitutes the basics of body embodiment (the feeling of own body/limb) [29]-[32]. De Vignemont proposed that if the spatial, sensorimotor and affective properties of a limb or an object are processed in the same manner as the properties of one's own body, then it is embodied [32]. If neural prostheses are expected to be more than a tool [33], it is important to implement naturalistic sensory feedback in these devices.

Improvements in neural interfaces encourage the sensory prostheses applications [34]. Neural interfaces can be used not only for recording but also for electrical stimulation of peripheral and/or central nervous systems [35]-[37]. Electrical stimulation of sensory afferents or cortical neurons in sensory cortices through these interfaces elicits artificial sensations [36]-[38]. However, in order to induce a naturalistic sensation, it is important to develop feasible and versatile methods for translating natural stimuli (e.g., pressure on a robotic finger) into electrical stimulation patterns.

Therefore, in this thesis, I focused on how to convert vibrotactile stimuli, for example, applied on a sensorized robotic finger into intracortical microstimulation patterns in order to elicit similar sensations as in the case of natural stimulation.

1.2 Objectives

The aim of this PhD work was to model the psychophysical correspondence between the vibrotactile stimuli applied on the volar surface of rat's hindpaws and intracortical microstimulation (ICMS) in the hindpaw representation of the primary somatosensory cortex of the rats. The model -psychometric correspondence function

(PCF)- was used to convert vibrotactile stimuli into ICMS trains. I hypothesized that PCFs can be used to modulate ICMS trains in order to generate neural activity, therefore, an artificial sensation, which results in similar psychophysical performances as in the tactile experiments.

As the secondary objective of the thesis, a vibrotactile operant conditioning chamber for freely behaving rats is proposed. Also, a training schedule is presented for training unrestrained rats to detect vibrotactile cues delivered to the volar surface of their hindpaws. Furthermore, sensitivity of rats to vibrotactile and ICMS stimuli was studied.

1.3 Outline

In the first section here, I presented the motivation and objectives of the study. In Chapter II, design of vibrotactile operant conditioning chamber and vibrotactile sensitivity of freely behaving rats are presented. Operant conditioning of the rats by ICMS and their sensitivity to ICMS is presented in Chapter III. Chapter IV presents the construction and validation of PCFs. A general conclusion for the thesis is given in Chapter V. In the final chapter of the thesis, future research directions are discussed.

2. VIBROTACTILE OPERANT CONDITIONING OF FREELY BEHAVING RATS AND THEIR SENSITIVITY TO VIBROTACTILE STIMULI

2.1 Introduction

Rodents have been good models for studying nervous system during behavior. Various behavioral tasks have been used to train this model animal based on sensory inputs from different modalities, such as hearing [39], olfaction [40], vision [41] and touch [42]-[46]. Furthermore, they can be conditioned to perform various tasks for drug self-administration [47] or electrical microstimulation in the cortex [48]. In this study, I focused on conditioning rats based on vibrotactile stimulation of their hind-paw glabrous skin. Therefore, an extensive review of tactile sensation is presented in following sections.

2.1.1 The Sense of Touch

The sense of touch is mediated by mechanoreceptive afferents innervating the skin. Glabrous (hairless) and hairy skins are innervated by different types of mechanorecetive afferents. In addition to glabrous and hairy skins, rodents have a distinct tactile sensory organ used in active exploration; whiskers.

- **Mechanoreceptors of The Hairy Skin**

The hairy skin is innervated by afferents associated with hair follicles or cutaneous mechanoreceptors (e.g., Merkel cells, Pacinian corpuscles and Ruffini endings) (Figure 2.1) [49]-[53]. Touch domes are the elevated skin regions where 5-10 Merkel cells are grouped together [49, 51]. Each of these Merkel cells might be innervated by two or more large myelinated fibers. Each fiber may innervate several Merkel cells located in different touch domes. Touch domes have small receptive fields (RF) (e.g.,

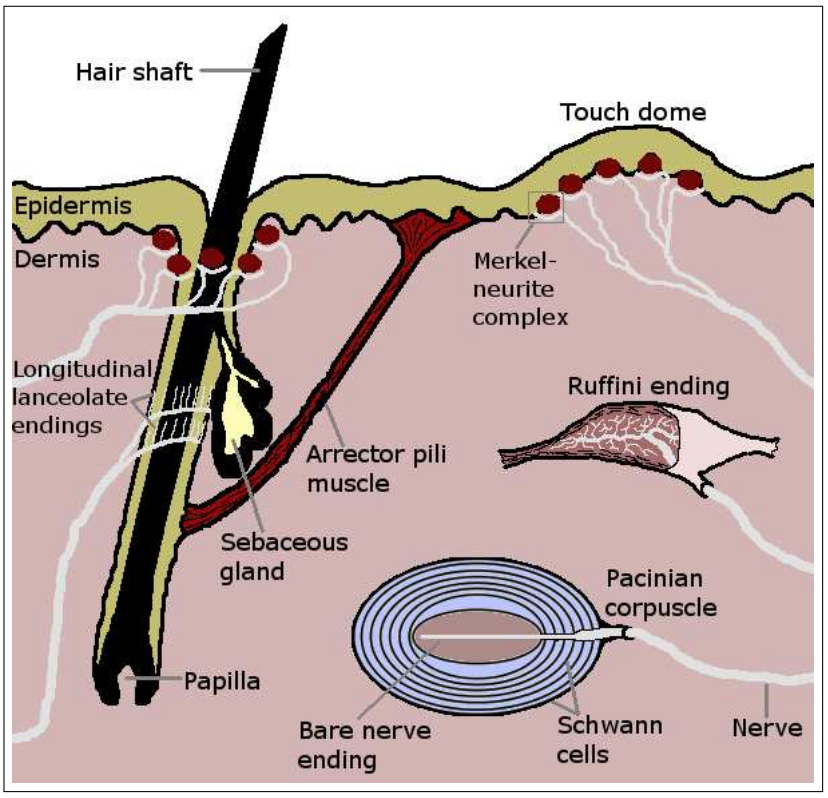

Figure 2.1 An illustration of mechanoreceptors in mammalian hairy skin. (Hair follicle drawing is reproduced from Figure 2.12 of Willis and Coggeshall, 2004 [49]. Drawing of Ruffini ending is reproduced from Figure 5 of Andres and von Düring, 1973 [50])

skin area sensitive to indentation) and they are responsive to light skin indentations [49]. Under static indentation, they show a sustained response. In addition to the touch domes, Merkel cells can be found in hair follicles too. Three types of hair follicles are defined in mammalian skin; down hairs (D-hairs or zigzag hairs; the shortest and the most abundant hair type), guard hairs (the longest and thickest hairs on the skin) and auchene/awl hairs [52]. Follicles of these hairs are innervated by different sets of low-threshold mechanoreceptive afferents. For example, follicles of guard hairs are surrounded by Merkel cells and thickly myelinated nerve endings called *longitudinal lanceolate endings*, whereas D-hair and auchene/awl hair follicles are innervated by both myelinated and unmyelinated nerve fibers [54]. A single fiber may innervate more than one hair follicle [55]. Hair follicles are sensitive to hair movement but do not respond to static stimuli [49, 52]. In addition to those hairs on their fur, rodents are equipped with specialized sinus hairs on their snout called *mystacial vibrissae* or *whiskers* (Figure 2.2). In rats, whiskers are arranged in 5 rows (rows A-E) and each

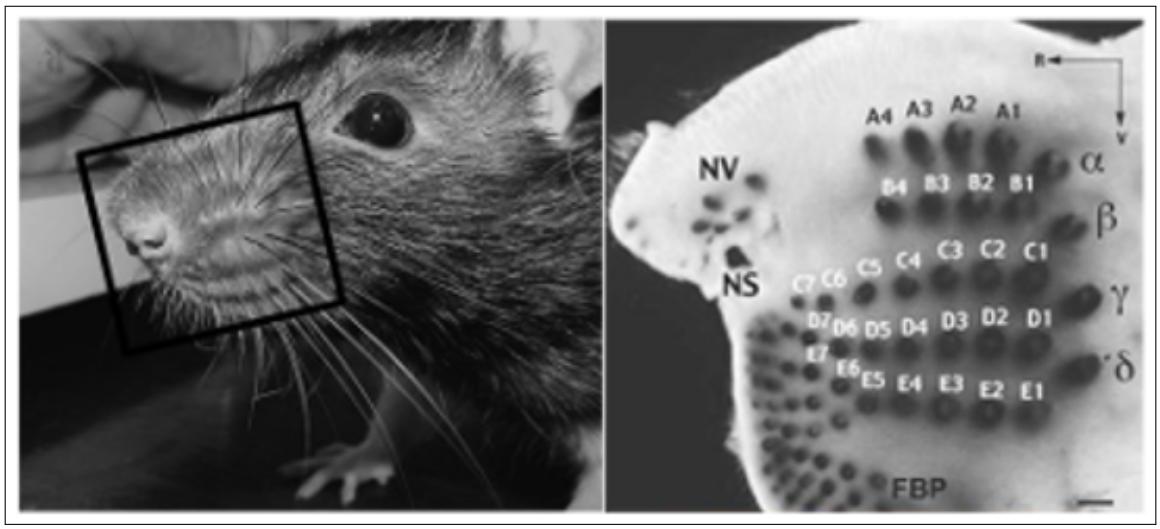

Figure 2.2 Photograph showing the rat whiskers (on the left) and micrograph showing arrangement of vibrissal follicles in the skin (on the right). Follicles were visualized by threating blood sinuses surrounding whisker roots with xylene. A-E: vibrissal rows, α-δ: caudal-most vibrissa follicles, NV: nasal vibrissae, NS: nostril, R: rostral, V: ventral, FBP: furry buccal pad. Scale bar = 1 mm. [57, 58]

row has 5-9 whiskers [56]-[58]. Their length vary between 1.5 to 5 cm [56]. Rodents use their whiskers for tactile exploration of their environment. These sinus hairs are innervated by slowly and rapidly adapting mechanoreceptive afferents, such as Merkel's cells, longitudinal and branched lanceolate nerve endings, lamellated corpuscles and free nerve endings [49, 51]. Furthermore, striated muscle fibers attached to the hair follicle enables the voluntary movement of the vibrissae. Motor and sensory innervation of vibrissae forms a sensorimotor loop which enables encoding of complex tactile features (e.g. curvature, texture, size, etc.) of the objects [56, 59, 60].

In addition to hair units, field units are sensitive to rapid movements of the skin and hairs [61]. However, there is not much detailed information about their end organs. They differ from hair units with their receptive field structure; while hair units have discrete and small low-threshold spots, field units have larger low-threshold spots which are connected to each other [55]. Other than field units, tactile C afferents (or C mechanoreceptors) innervate the hairy skin. They are sensitive to stimuli slowly moving on the skin [49, 62]. These unmyelinated, low-threshold mechanoreceptors are thought to be mediate pleasant (affective) touch in social interactions [62]. Pacinian corpuscles and Ruffini endings are also found in hairy skin. Structures and response properties of these mechanoreceptors are presented in the following section.

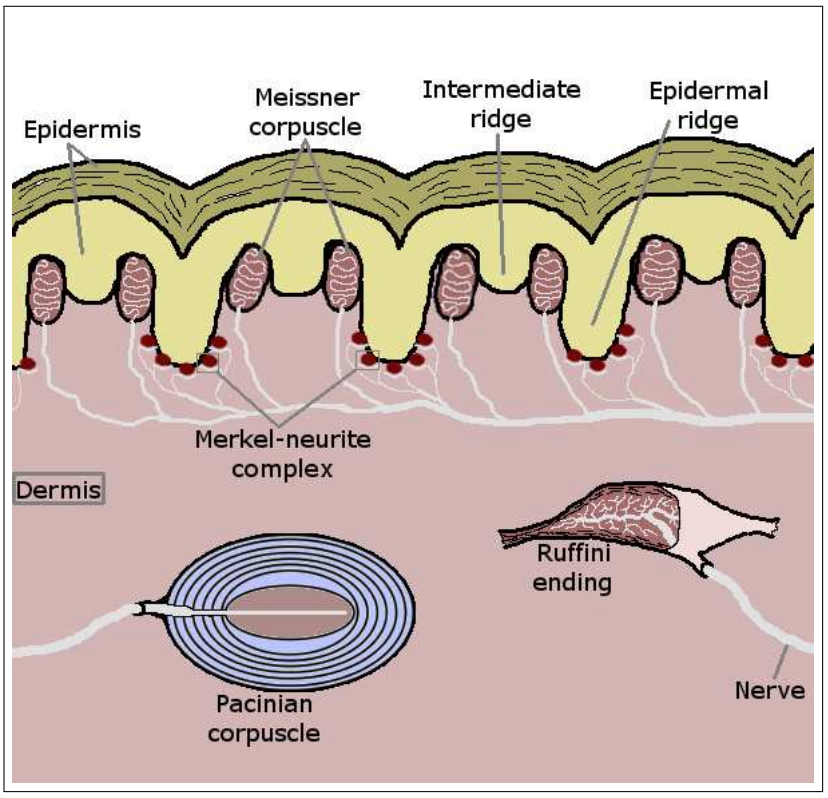

Figure 2.3 An illustration of mechanoreceptors in mammalian glabrous skin. (Drawing of Ruffini ending is reproduced from Figure 5 of Andres and von Düring, 1973 [50])

- **Mechanoreceptors of The Glabrous Skin**

Mammalian glabrous skin is innervated by four types of mechanoreceptors: Pacinian corpuscles, Meissner corpuscles, Merkel's discs and Ruffini endings (Figure 2.3) [27, 49, 51, 63, 64]. Meissner corpuscles and Merkel's discs are superficial mechanoreceptors [65, 66]. On the other hand, Pacinian corpuscles and Ruffini endings are located in deeper dermis and subcutaneous tissue [65]. These mechanoreceptors can be classified according to their receptive field sizes, innervation densities and response properties such as adaptation and tuning frequency [55, 67]-[75]. Meissner corpuscles and Merkel's disks have small RFs whereas Pacinian corpuscles and Ruffini endings have larger receptive fields [65]. Furthermore, innervation densities of Meissner corpuscles and Merkel's disks are higher than those of Pacinian corpuscles and Ruffini endings (Figure 2.4). Based on their response to a ramp-and-hold stimulus, these mechanoreceptors can be classified as rapidly adapting (RA) or slowly adapting (SA) (Figure 2.4) [65, 66, 76]. Afferent associated with Pacinian Corpuscles (denoted as *FAII -fast adapting II-* in human and *PC* in other mammals) and Meissner corpuscles (denoted

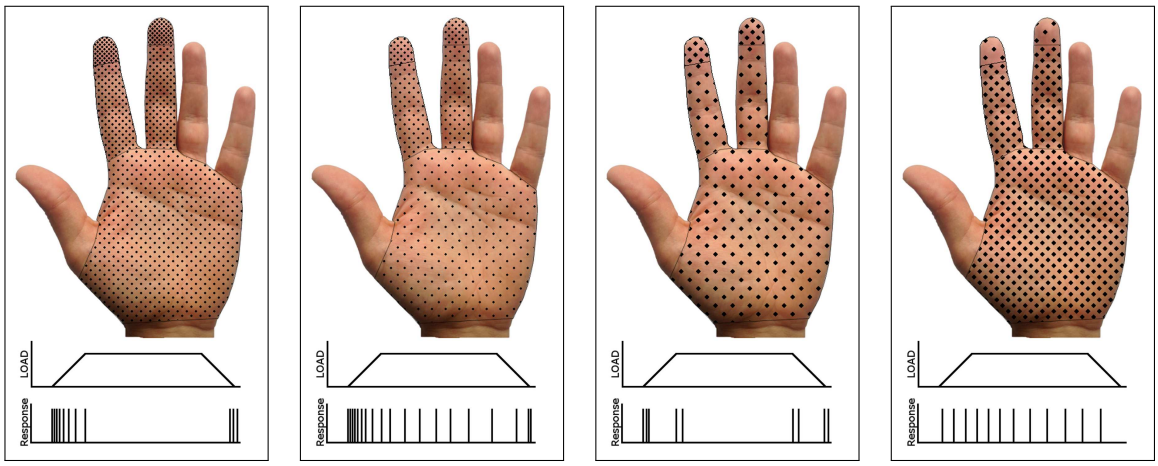

(a) RA (FAI) (b) SAI (c) PC (FAII) (d) SAII

Figure 2.4 Innervation density and response properties of cutaneous mechanoreceptive afferents. (a) RA fibers innervating Meissner corpuscles have higher innervation density in fingertips. They respond during the rise and fall of a ramp and hold stimulus. (b) SAI fiber innervating Merkel's disk have a innervation pattern similar to RA fibers. However, their innervation density is lower. They display a high onset respond and fire irregularly during the persistent indentation. (c) Innervation density of PC afferents is lower compared to type I afferents and their distribution is relatively homogeneous on the glabrous skin of the hand. They respond to transient events such as static-to-ramp or ramp-to-static transition. (d) SAII afferents innervating Ruffini endings have relatively higher innervation density than PCs. They respond regularly during the ramp and hold stimulus. (Drawings are reproduced from Bolanowski, 2002 [65])

as *FAI* in human and *RA* in other mammals) respond at the onset and offset of a ramp-and-hold stimulus, and hence, they are called rapidly adapting mechanoreceptors [27, 65]. On the other hand, afferents associated with Merkel's disks (*SAI*) and Ruffini endings (*SAII*) fire during a sustained stimulus. Since their firing rates decrease at a constant rate as the constant indentation persists, they are called slowly adapting mechanoreceptors.

Meissner corpuscles are built of flattened supportive cells surrounded by a connective tissue. Meissner corpuscles are located in the finger-like projections of the dermis into the epidermis called *dermal papillae* [77, 78]. Both myelinated and unmyelinated afferents innervate these corpuscles like a coil [79]. However, the role of unmyelinated afferents innervating Meissner corpuscles is not clear. Myelinated afferents ends with an unmyelinated section of axon in the corpuscle [51]. When the corpuscles are deformed by a mechanical stimulus, the nerve endings are excited. A single RA afferent innervates up to 20 Meissner corpuscle while a Meissner corpuscle might be innervated by 5 RA afferents [27]. Their innervation density is higher in

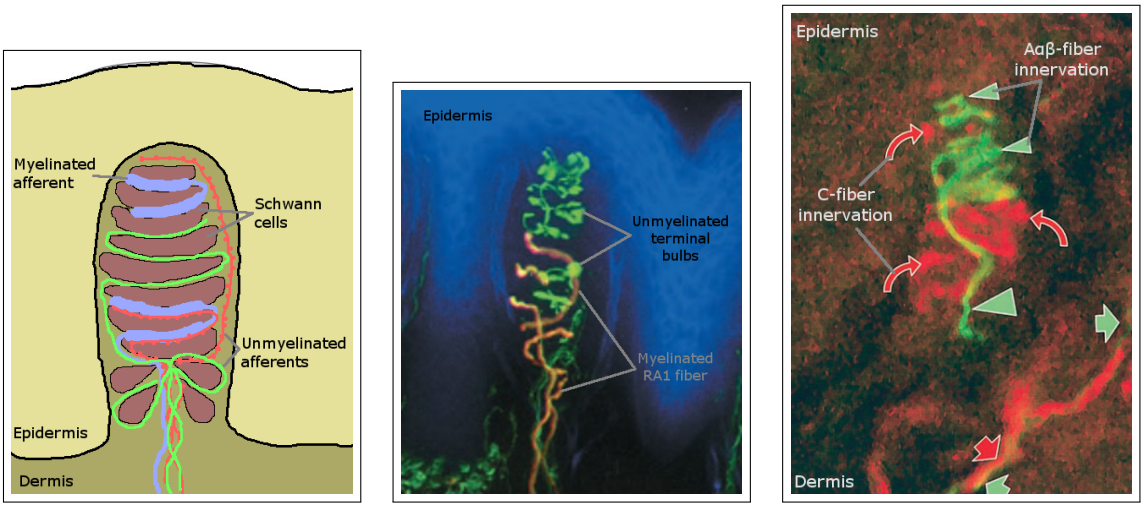

(a) (b) (c)

Figure 2.5 Structure of Meissner Corpuscle. (a) Arrangement of Schwann cells and innervation of C- (green and red) and A$\alpha\beta$-fibers (purple) (reproduced from Figure 1 of Paré et al., 2001 [79]). (b) A confocal image of Meissner corpuscle located in dermal papilla. Myelinated fibers are shown in yellow and unmyelinated fibers and/or fiber terminals are show in green. (Modified from Figure 23-3 of Gardner and Johnson, 2012 [27].) (c) Confocal image showing C- and A$\alpha\beta$-fibers innervating a Meissner corpuscle. C-fibers are shown in red (curved arrows) and A$\alpha\beta$-fibers are shown in green (arrow heads). (Modified from Figure 4 of Paré et al., 2001 [79].)

distal regions (e.g. finger tips). In the literature, innervation density was reported as 141 afferents/cm^2 in the fingertips and 25 afferents/cm^2 in the palm of human [80]. In monkeys, innervation density varies between 40 to 178 afferents/cm^2 in the fingertip depending on the species [78, 81]. RAs' close proximity to the skin surface makes them very sensitive to skin displacement. They are highly sensitive to dynamic stimuli such as flutter. Their sensitivity is high at frequencies near 40 Hz [65, 71]. The Meissner corpuscle surrounding the nerve endings acts as a mechanical filter and eliminates the static portions of the stimuli. RAs can entrain with a vibratory stimuli by firing one or two spikes per cycle [75, 82]. Their high innervation density (especially in fingers) and high sensitivity to dynamic events on the skin makes them appropriate for slip detection on the skin. Therefore, they may have a role in grip force adjustment and detection of surface features [27, 74].

Pacinian corpuscles are located in the deep dermis or subcutaneous tissue [27, 49, 51]. They are formed by laminated structure of Schwann cells [83, 84]. Unmyelinated endings of PC afferents rest in the fluid-filled inner core of the corpuscle which has a denser arrangement of Schwann cells. The corpuscle surrounding the nerve

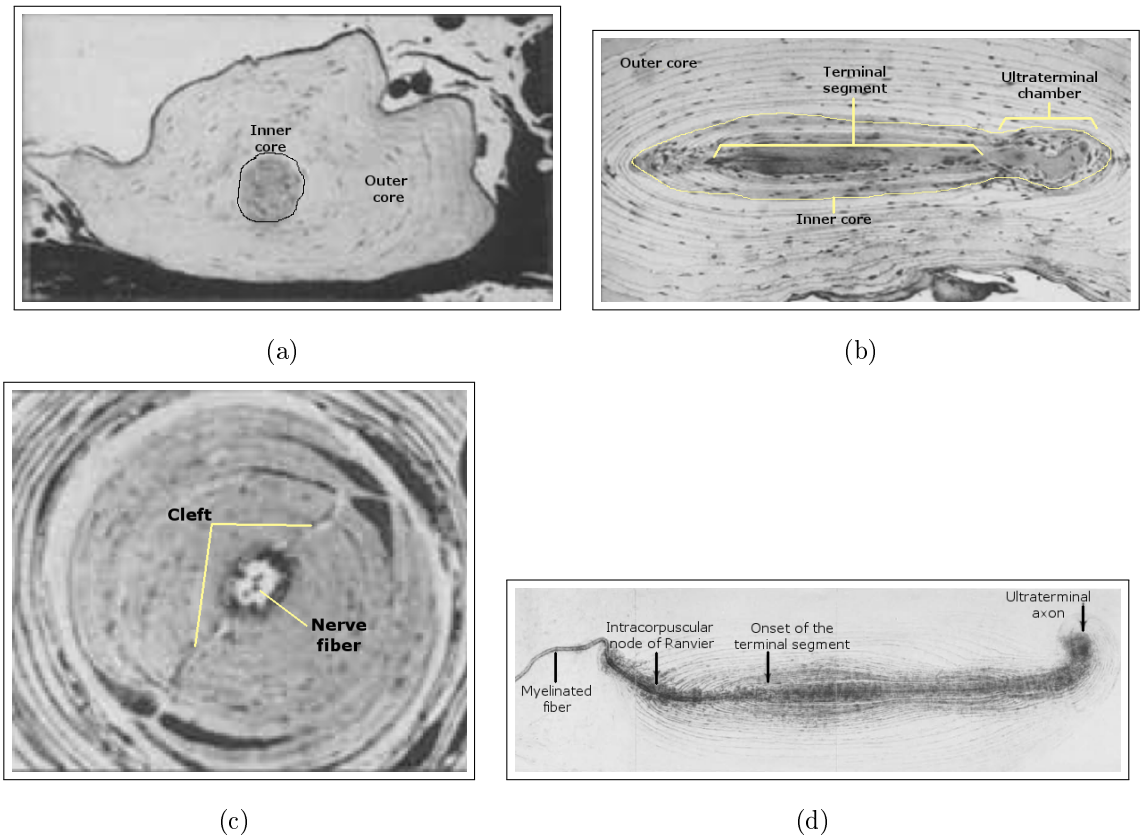

Figure 2.6 Structure of the Pacinian Corpuscle. (a) Cross-section of a PC. PCs are formed of laminated Schwann cells. The space between laminae is filled with fluid. Denser arrangement of Schwann cells in the center form the inner core of PC. (b) Longitudinal section showing the center of PC. At the center of inner core, unmyelinated axon terminal rests. (c) Magnified image of inner core. At the center, nerve fiber rests. Inner core is divided into two halves by a cleft. (d) The myelinated PC afferent enters the PC and loses its myelination after an intracorpuscular node of Ranvier. The fiber terminates in ultraterminal chamber surrounded by outer core cells. (Modified from Figures 2, 3 and 8 of Spencer and Schaumburg, 1973 [83].)

ending filters the maintained pressure and low-frequency stimuli [49]. Therefore, PCs are highly sensitive to transient or high frequency events [66, 71, 74]. PCs' sensitivity is higher between 180-415 Hz for the criterion of one spike per stimulus cycle [70]. Like RA fibers, PCs can entrain with vibrotactile stimuli [70, 71, 74]. Although they are located in deep structures, they can sense a 10-nm vibration on the skin [74]. The laminated structure is thought to amplify transient events on the skin surface [27]. Therefore, they can sense the distant events such as vibration at the tip of a hand-held tool [27, 74, 85]. In addition to mechanical roles of the corpuscle, Pawson et al. proposed that there might be a mechanochemical interaction between the nerve and the surrounding glial tissue [86]. In contrast to their high mechanical sensitivity, PCs

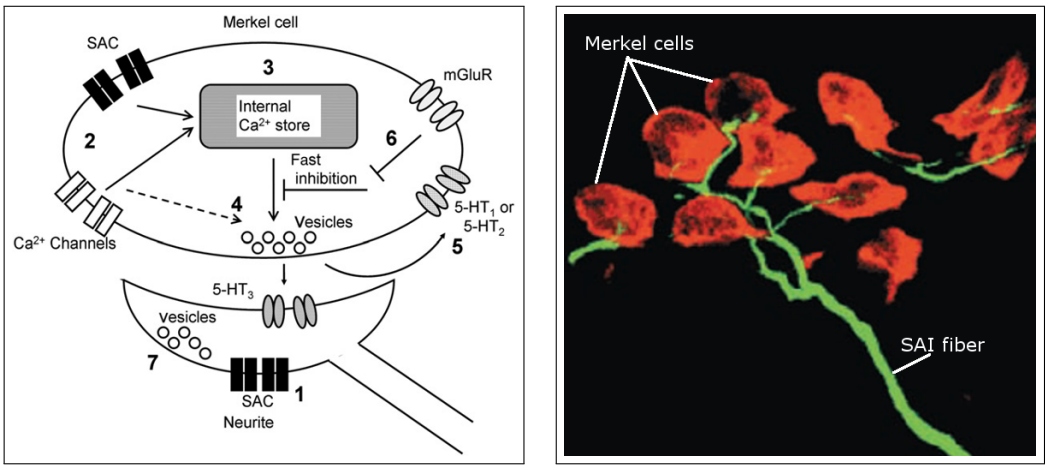

(a) (b)

Figure 2.7 Structure of a Merkel's disk-neurite complex. (a) A model showing the mechanochemical interaction between a Merkel's disk and an SAI axon terminal. Mechanical stimulation excites both Merkel's disk and the neurite by activating stretch activated ion channels (SAC) (steps 1 and 2). Accumulation of high amount of Ca^{2+} in the Merkel's disk (step 3) causes neurotransmitter (serotonin and glutamate) release into synaptic cleft (step 4). Neurotransmitters not only excite serotonin activated channels on the neurite but also affects serotonin and glutamate activated channels on the Merkel's disk (step 5). This elongates the neurotransmitter release by the Merkel's disk (step 6). In the meantime, some neurotrasmitter might be released by the neurite (step 7). [87] (b) Image showing the innervation of SAI afferent on Merkel's disks. (Modified from Figure 23-3 of Gardner and Johnson, 2012 [27].)

are very sparsely distributed in the skin and have a low spatial resolution [27, 74]. Their innervation density is 10 afferents/cm^2 in the palm and 20 afferents/cm^2 in the fingertip [80]. Their RFs may span a finger or the entire hand [27, 71].

Merkel's disks (also called Merkel cell) are located at the tip of epidermal ridges (indentation of epidermis into the dermis) and they are the end organs of SAI afferents [27]. Merkel's disk and the end terminal of the innervating axon form the *Merkel cell-neurite complex* (MNC). Merkel's disks not only mechanically filter the stimuli but also mechanochemically interact with the axon terminal determining the response properties of the afferent [87]. Serotonin and glutamate are released from Merkel's disk when a mechanical stimulus is applied. SAI's innervation density varies between 70-134 afferents/cm^2 at the finger tip depending on species [74, 80, 81]. They have small RFs and show a long-lasting irregular discharge under a constant pressure [67, 71, 72, 88]. SAIs display a two-phased response when a ramp-and-hold stimulus is applied; their firing rate is higher at the onset of the stimulus and show a rapid adaptation decreasing the firing rate which than display an adaptation at lower rates.

The latter adaptation phase may continue for >30 min [67]. Stimulation of tissue surrounding RF center (the most sensitive point) together with RF center suppress the response of SAI [89]. This is called *surround suppression*. SAIs are sensitive to frequencies below 8 Hz and static indentations of the skin [71]. Furthermore, their sensitivity below 4 Hz is better than RAIs [90]. Strong coupling between the Merkel's disk and the epidermal tissue improves its sensitivity to corners, edges and curvature of the objects [27, 74, 89]. Therefore, SAI may contribute to the shape and texture perception.

Ruffini endings are located in the dermis and innervated by SAII afferents. They resemble a spindle and consist of collagen and Schwann cells [49]. SAII fibers are sensitive to skin stretch rather than skin indentation [71, 74]. They are concentrated at skin parts around joints and skin folds [27]. Therefore, they contribute to the perception of hand posture together with proprioceptive afferents. Furthermore, they convey the information about the direction of movement on the skin. Although they are found

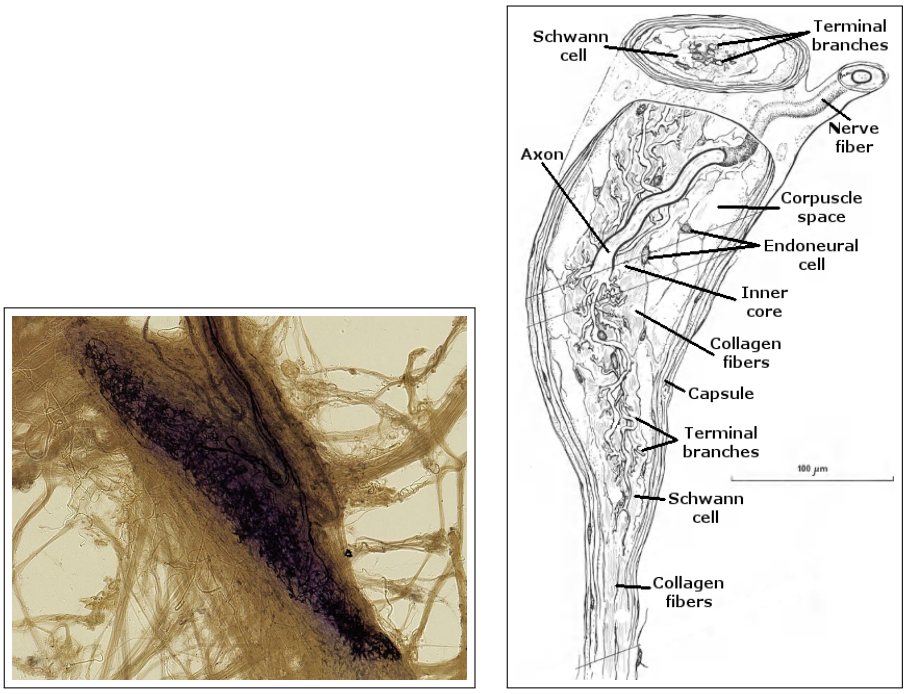

(a) (b)

Figure 2.8 Structure of the Ruffini ending. (a) Image of original slide showing Ruffini ending sent by Angelo Ruffini to Charles Sherrington in 1898 [91, 92]. The specimen is collected from a human and stained with gold chloride. (b) Drawing of a Ruffini ending showing the internal structures and innervation of SAII afferent. (Adapted from Figure 5 of Andres and von Düring, 1973 [50])

in humans and rats, monkeys and mice do not have SAII afferents [27, 71, 74, 75]. Their innervation density is 50 afferents/cm^2 [80]. SAIIs have greater RFs and regular firing pattern under constant indentation compared to SAIs [27, 71].

2.1.2 Central Processing of Tactile Stimuli

Tactile information from cutaneous mechanoreceptors are conveyed by pseudo-unipolar nerve cells into the central nervous system (CNS) (Figure 2.9). These nerve cells consist of a single axon projecting from cutaneous mechanoreceptors to the brain stem and a soma resting at dorsal root ganglion -a cluster of nerve cell somas located outside the vertebra. Primary mechanoreceptive afferents enter CNS from dorsal root of the spinal nerve and ascend from ipsilateral dorsal column to cuneate nucleus of medulla oblongata [26]. Here, they make synapses to the second-order nerve fibers which cross the midline and ascend contralaterally towards the thalamus. The second-order fibers terminate in the ventral posterior nuclei (VPN) of the thalamus. From there, tactile information is conveyed to primary somatosensory cortex (SI). This pathway is called *dorsal column medial lemniscal system* [26].

Each neuron in SI receives inputs from many mechanoreceptors via thalamus. Therefore, their response properties and RF structures depend on the properties of inputs and how they are organized (i.e., excitatory or inhibitory). For example, while Type-I afferents innervating the glabrous skin of the hand have small RFs, a cortical neuron's RF may span two or more fingers. Furthermore, RF sizes becomes even larger and may form functional structures (e.g., fingers of both hands) in higher cortical areas (Figure 2.10(b)). In addition, cortical neurons do not receive only excitatory inputs; their RFs may consist of excitatory and inhibitory regions [27]. Stimulation of inhibitory skin regions together with excitatory field would decrease the firing rate of the neuron. Lateral inhibition enhance the tactile contrast for a more detailed perception (e.g. texture). Despite all, neither the response properties nor RF structures of cortical neurons are persistent, instead, they reshape with experience or other external factors such as (limb or cortical) injuries [27].

Furthermore, SI is segregated into different cytoarchitectural regions special-

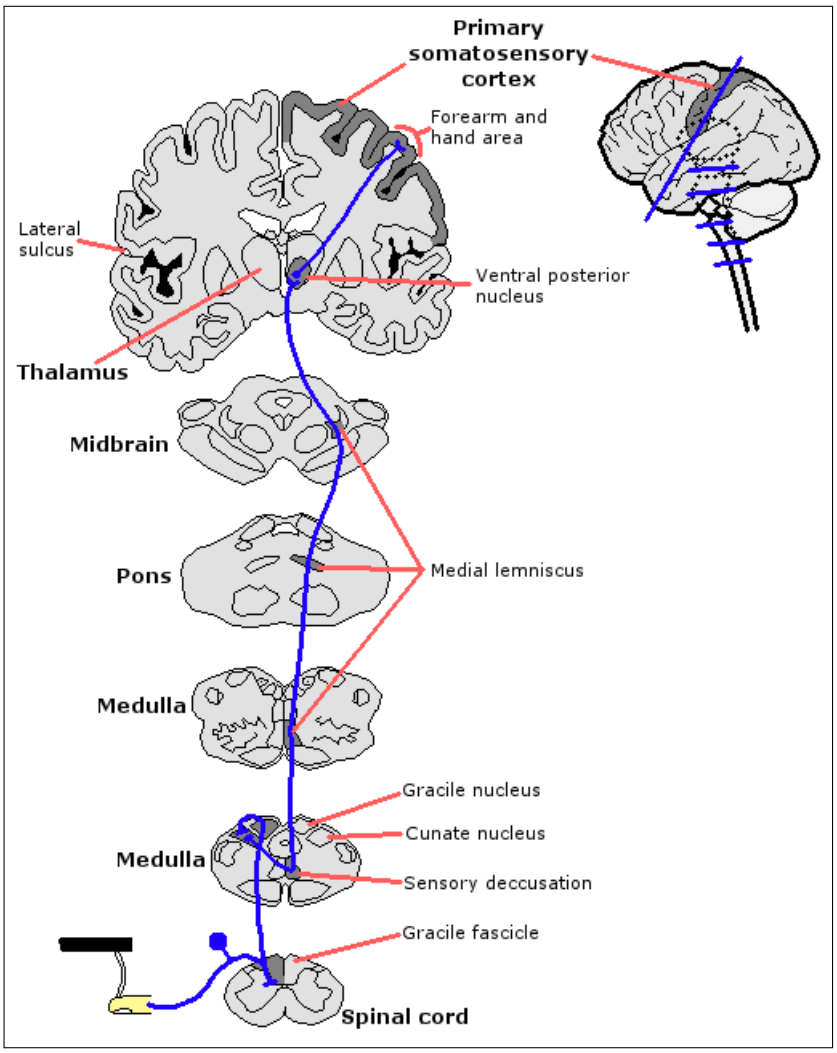

Figure 2.9 Somatosensory pathway. The sense of touch is conveyed by pseudo-unipolar nerve cells up to medula oblongata where information is passed on second-order neuron. While primary afferent ascend ipsilaterally, second-order neuron crosses the midline in medula and ascend contralaterally. Information is processed by one more synapse in ventral posterior nuclei of the thalamus before reaching the cortex. (Reproduced from Figure 22-11 of Gardner and Johnson, 2012a [26])

ized in processing different (aspects of) sensory information: Brodmann's areas 3a, 3b, 1 and 2 [27]. These regions are highly interconnected to each other and responsible for parallel and serial processing of sensory information. For example, areas 3a and 3b receive a massive input from VPN and they project their outputs to areas 1 and 2 (Figure 2.10(a)). On the other hand, tactile information is processed in areas 3b and 1, whereas areas 3a and 2 process proprioceptive information. These areas convey information to higher cortical areas in parietal cortex, such as secondary somatosensory cortex (SII) and Brodmann's area 5. As the information passes on higher cortical regions, it becomes more abstract. For example, while neurons in SI may respond to

one physical aspect of a tactile stimulus (e.g. indentation rate), neurons of SII respond to complex features such as roughness, grooves, shape, etc. Information processed in these higher cortical areas is transmitted to temporal and motor areas to support other perceptual and executional processes.

Each area of SI has a somatotopic arrangement, so that different skin regions are

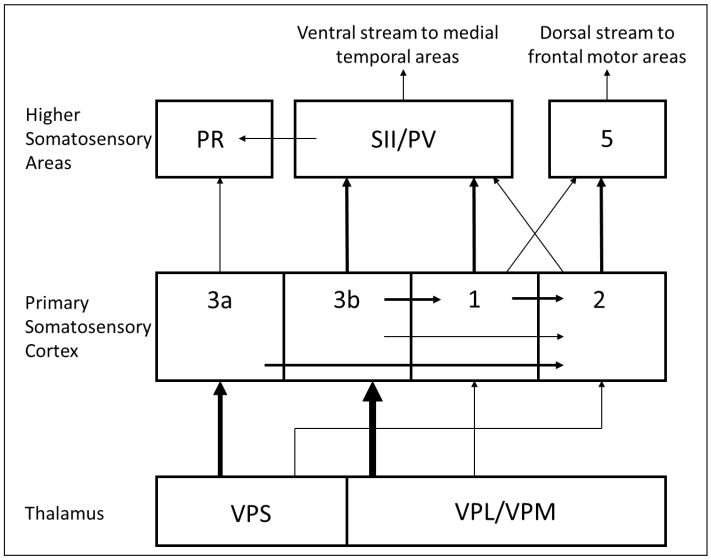

(a)

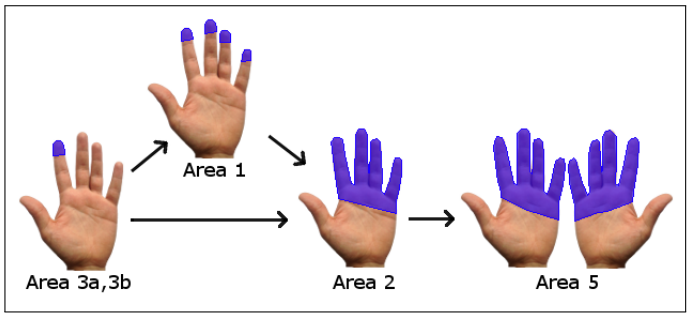

(b)

Figure 2.10 (a) Connections between somatosensory areas. Tactile information from mechanoreceptive afferents are conveyed to the primary somatosensory cortex by ventral posterior nuclei of thalamus (VPS: ventral posterior superior nucleus, VPL: ventral posterior lateral nucleus, VPM: ventral posterior medial nucleus). While Bordmann's areas 3b and 1 receives cutaneous mechanoreceptive inputs, 3a and 2 receives proprioceptive inputs. These areas process information in serial and parallel manner. Output neurons of SI project into higher cortical areas such as secondary somatosensory cortex (SII) and other parietal cortices (i.e., PR: parietal rostroventral cortex, PV: parietal ventral cortex and Brodmann's area 5). As the information passes on higher cortical regions, it becomes more abstract. Finally, information is conveyed to temporal and motor areas to support emotional and executional processes. (Reproduced from Figure 23-10 of Gardner and Johnson, 2012a [26]) (b)Receptive field sizes of cortical neurons. Neurons of higher cortical regions process inputs from a wider and functionally organized area. (Reproduced from Figure 23-11 of Gardner and Johnson, 2012a [26])

represented by a different set of cortical neurons (Figure 2.11) [27]. The somatotopic organization is not uniform; the organs (e.g. hands) that we use extensively have a bigger representation than others in the SI. Other cortical regions (e.g.,VPN and SII) processing somatosensory information also have such somatotopic arrangement [27]. Gardner and Johnson, 2012b, proposed that SII has four and posterior parietal cortex has at least two somatotopic maps. These maps are obtained by electrophysiologic recording and electrical stimulation experiments [93]. It should be noted that Figure 2.11 shows a generic somatotopic map. Somatotopic maps differ subject to subject but share a similar outline. In addition, these maps are subject to change by experiences because of the dynamic nature of the cortex. For example, a piano player's finger representations would be much more wider and discrete than those of a laborer.

Rodent vibrissal sensory inputs follow a similar pathway as other cutaneous inputs but synapse locations are different. Trigeminal ganglion nerve fibers innervate the follicles of vibrissae at one end and they terminate in trigeminal nuclei (TN) of the brainstem on the other end [56, 60]. Trigeminal ganglion is located just outside

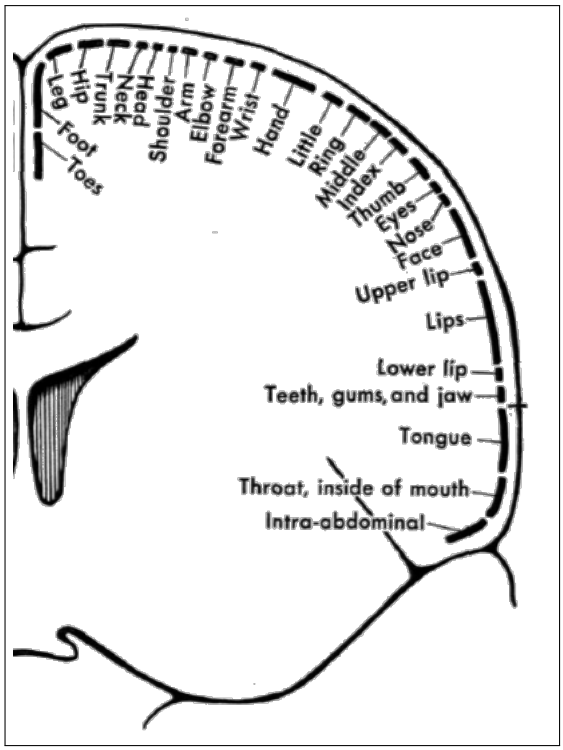

Figure 2.11 Sensory somatotopic map of human. Different skin regions are represented by a different set of neuron in the SI. Lengths of the lines show the relative cortical representation of the particular skin region. (Drawing by Penfield and Rasmussen, 1950 [93])

the brainstem. Second-order neurons convey information from brainstem to ventral posterior medial nuclei (VPM) of the thalamus. Finally, the thalamus relays information to SI. Similar to the primates, rodents also have a sensory somatotopic map in their cortex (Figure 2.12). However, this map is not well segregated; motor and sensory regions may overlap [94]-[96]. Furthermore, submodalities of somatic sensation are also overlapping [95]. Since most of the rodents use their whiskers extensively, their vibrissae have a more elaborate topographic representation comprising approximately 1/4 of the cortical surface [95]. Each vibrissa is represented by a different cortical column which is called a *barrel*. The region comprises these barrels is called *barrel cortex*. The barrel structures can be seen easily by simple staining techniques (Figure 2.12). The vibrissal system is also supplied with descending pathways which enables the movement of individual whiskers forming a complex network of sensorimotor loop [56, 59, 60]. This network enables rodents to extract detailed tactile information from their environment by means of active tactile exploration. The animals can voluntarily move their whiskers and palpate objects. Although each barrel mainly process information from their principle whisker, interactions between neighboring barrels still exist [59].

2.1.3 The Psychophysics of Touch

The nervous system encodes specific features of the external stimuli as a population. When this population code reaches to the cortex, we perceive the stimuli. We recognize objects and distinguish them from each other with the differences in perceptions that they elicit. Also, we depend on our perceptions in our daily living activities. Therefore, it is important to understand how quantitative aspects of a physical stimulus relate to the perception that it elicited. Psychophysics inspects the psychological processes elicited by a physical stimulus by systematically changing one or two dimensions of the stimulus [97]. Psychophysical experiments are designed to determine the limits of perception. Experiments mostly focus on three parameters; (1) absolute detection threshold [98, 99], (2) discrimination threshold [100]-[102], and (3) scaling [103, 104]. Absolute detection threshold can be defined as the lowest amplitude level of

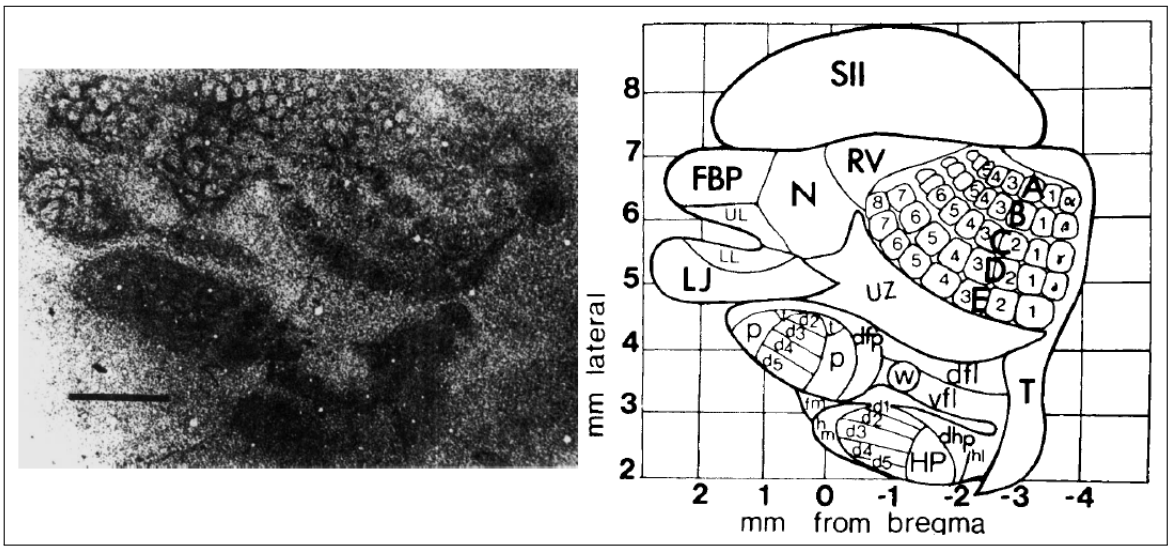

Figure 2.12 Sensory somatotopic map of rat. (Left) A section stained with thionin showing the cytoarchitectonic topography of rat SI. (Right) Somatotopic representation of body in S1. SII: secondary somatosensory cortex, FBP: furry buccal pad, N: nose, RV: rostral small vibrissae, A-E: rows of barrels (barrel cortex), UL: upper lip, LL: lower lip, LJ: lower jaw, UZ: zone unresponsive in anesthetized recordings, p: palm, t: thumb, d2-5: digits of forepaw, dfp: dorsal forelimb, w: whiskers on wrist, dfl: dorsal forelimb, vfl: ventral forelimb, T: trunk, fm: forelimb muscle, hm: hindlimb muscle, d1-d5: digits of hindpaw, HP: hindpaw, dhp: dorsal hindpaw, hl: hindlimb [95].

a stimulus that elicits a sensation. Discrimination threshold is the minimum difference between one dimension (e.g. amplitude, frequency, duration, etc.) of two stimuli that can be discriminated. In scaling experiments, subjects are asked to scale one or more dimensions of a stimulus with or without a reference.

Tactile psychophysical experiments have been performed to reveal how tactile information is processed by central nervous system and how we perceive and utilize this information. Although different tactile stimuli (e.g. ramp-and-hold stimuli with single cylindrical probes or gratings scanned across the skin surface) have been used, using vibratory stimuli has been a general habit because of frequency specificity of peripheral mechanoreceptive afferents (e.g. PCs are more sensitive to high frequencies whereas RAs are sensitive to flutter stimuli) and easy control of amplitude and frequency of sinusoidal vibrations. Based on this physiological basis, tactile psychophysical channels have defined for glabrous touch in order to extract more details about how information conveyed by different mechanoreceptive afferents are perceived [63].

• **The Psychophysical Channels of Touch**

In humans and primates, the relationship between the absolute detection threshold and the frequency of stimulus consist of a frequency independent region between 20-40 Hz and a frequency dependent region between 40-700 Hz (black data points in Figure 2.13(a)) [63]. Trend of psychophysical detection thresholds at high frequencies resembles the change of absolute spike thresholds of PC afferents in the same range of frequency. On the other hand, low frequency profile is in parallel with threshold levels of RA fibers. After extensive studies on response properties of mechanoreceptive afferents and psychophysical experiments in the literature, Bolanowski et al., 1988, proposed four psychophysical channels contributing to the sense of touch; Non-Pacinian I (NPI) channel is mediated by RA (FAI) fibers innervating Meissner corpuscles, NPII channel is mediated by SAII fibers innervating Ruffini endings, NPIII channels is mediated by SAI fibers innervating Merkel's disks, and Pacinian (P) channel mediated by PC (FAII) afferents (Figure 2.13) [105]. When threshold-frequency characteristics of psychophysical channels and mechanoreceptive afferents are compared (Figure 2.13), each channel resembles the characteristic of corresponding afferent population. However, while comparing Figure 2.13(a) and 2.13(b), it should be noted that threshold criteria for each afferent is different. Furthermore, tactile psychophysical channels, therefore, the tactile sensation, depends on the population response of mechanoreceptive afferents. Then, absolute psychophysical detection thresholds are much more lower than thresholds of mechanoreceptive afferents.

Each tactile psychophysical channel is proposed to convey information in specific frequency ranges [63]. For example, NPI channel conveys flutter sensation in the range of 2-40 Hz, whereas P channel conveys the sense of vibration between 40-500 Hz. On the other hand, NPII channel conveys a "buzz-like sensation" in the range of 100-500 Hz, and NPIII channel produces pressure sensation between 0.4-2 Hz. Although sensations around threshold levels might be conveyed by the most sensitive channel at that frequency, higher amplitude levels may evoke sensations with contribution of other activated channels. Each sensory channel differs from each other not only with their frequency range and the sensation that they produce but also with their response properties under different stimulation conditions [63]. For example, the best frequencies -the frequency with minimum threshold level- of P and NPII channels varies with

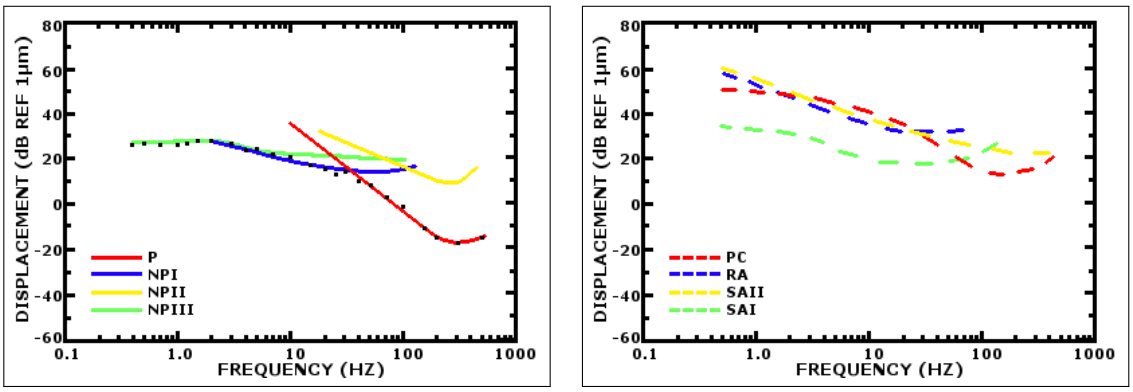

(a) (b)

Figure 2.13 Tactile psychophysical channels. (a) The four-channel model proposed by Bolanowski et al, 1988. Each channel is shown in different colors. Black data points show the absolute detection thresholds for the thenar eminence stimulated with a 2.9-cm^2 probe. NPI-III: Non-Pacinian channels mediated by RA, SAII ans SAI fibers, respectively. P: Pacinian channel mediated by PC afferents. (Reproduced from Figure 8 of Bolanowski et al., 1988 [105]) (b) Threshold-frequency characteristics of mechanoreceptive afferents with following threshold criteria; 4 spikes/stimulus for PC, 1 spike/stimulus for RA, 5 spikes/second for SAII, and 0.8 spikes/second for SAI. (Reproduced from Figure 7 of Bolanowski et al., 1988 [105])

temperature. Among four tactile channels, only P channel has the properties of temporal and spatial summation. Temporal summation is the improvement in detection threshold as the stimulus duration is elongated. Spatial summation is the improvement in detection threshold as the stimulation area is increased.

2.1.4 The Classical Psychophysical Methods

There are three techniques used in classical psychophysical experiments: Methods of constant stimuli, limits and adjustment [106].

In the method of constant stimuli, the subject is presented with a predetermined set of stimuli (e.g., 5-9 amplitude levels for detection task). Each stimulus is presented randomly and repeated many times to obtain a statistical measure (e.g., detection probability). The experiment can be designed for measuring the detection or discrimination threshold of the subjects. If the task is to determine detection threshold, 5-9 amplitude levels are used [106]. Experimenter has to make sure that the biggest amplitude level could be detected in most of the trials whereas the minimum amplitude level should be almost undetectable. If it is a discrimination experiment, there

would be a standard stimulus and 5-9 comparison stimuli at different magnitudes (e.g., frequency, amplitude, duration, etc.). As in detection task, the maximum difference should be easily detectable. The subject is asked to report whether s/he perceived the stimulus or whether the comparison stimulus is bigger than the standard one in each trial. At the end of the experiment, the rate of reporting "yes, I felt the stimulus" or "comparison is bigger" is recorded for each constant stimulus. Finally, the data points are plotted and fitted with a sigmoid curve (Figure 2.14, Equation 2.1).

$$p = \frac{1}{1 + e^{(\alpha - x)/\beta}} \tag{2.1}$$

where p is the probability of detecting a stimulus with an amplitude of x, α is the midpoint of the sigmoid curve (the mean of normal distribution), β is related to the slope of the sigmoid at α. The reason for the sigmoid fit is the variable nature of the sensory system. Variation of the sensory inputs and processes is normally distributed [106]. The sigmoid curve is the cumulative version of this distribution (Figure 2.14). For example, the upper panel of Figure 2.14 shows the distribution of momentary thresholds (i.e., the instant threshold at a given trial). A stimulus would be perceived if it is equal to or greater than the momentary threshold. Therefore, the area under the normal distribution that is below the applied intensity would give the detection rate. In this example, when a stimulus intensity of 24 units is applied, it would exceed the momentary threshold in 20% of the time. If the stimulus intensity is 31 units, it would be detected 80% of the time. In the method of constant stimuli, it is possible to determine the threshold level defined as a statistical value (e.g. %50 detection threshold) in addition to the detection/discrimination probabilities at different magnitude levels.

In the methods of limits and adjustment, the amplitude level or the difference between standard and comparison stimuli is adjusted depending on the subjects performance. In a detection task, for example, the experiment starts with a too high amplitude level which is certainly detectable, and the amplitude level is decreased as the subject reports the detection until it is not detected. The amplitude level where the detection to no-detection transition occurred is recorded. Then, the stimulus is started from a low amplitude level and increased until the subject reports a detection. After repeating increasing and decreasing cycles many times, the mean of amplitude

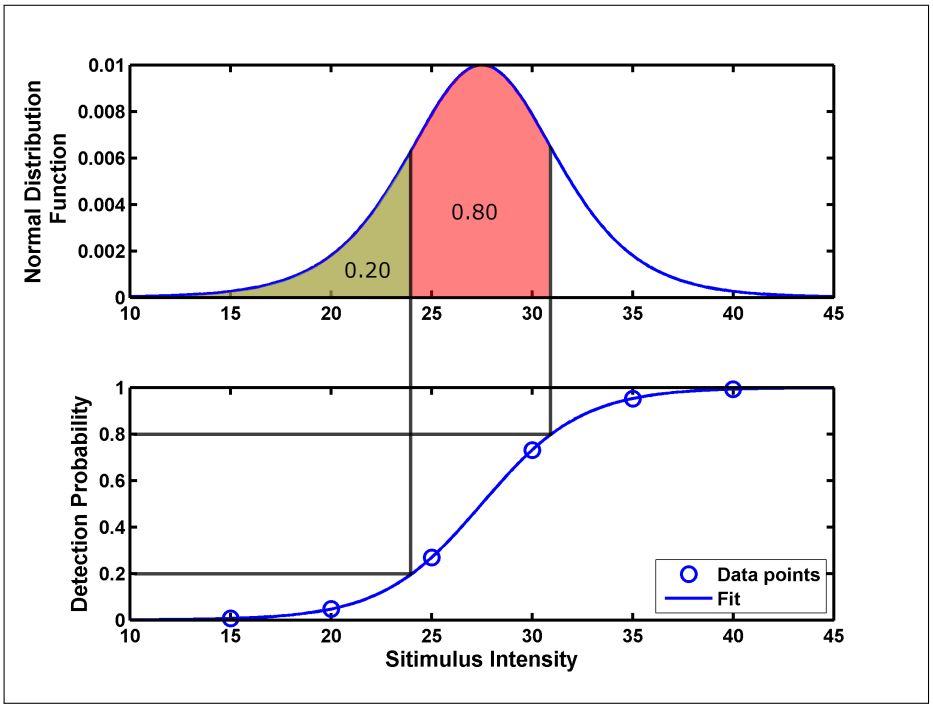

Figure 2.14 Derivation of psychometric curves from a normal distribution. Psychometric curves are the cumulative version of the normal distribution of biological and psychological events. (Adapted from Figure 3.2 of Gescheider, 1997 [106].)

levels where transitions occurred is accepted as the absolute detection threshold. The difference between the methods of limits and adjustment is the participation of the subject in method of adjustment [106]. In this method, the subject controls the variation of the stimulus intensity. The staircase method is a variation of the method of limits [106]. The staircase method is mostly combined with two-interval forced-choice. In this method, stimulus is presented in one of two intervals and the subject is asked to report in which interval s/he perceived the stimulus. The intensity of the stimulus is started at a suprathreshold level. It is decreased in succession of a few (e.g., three) correct responses and increased after each false response. The experiment is terminated when the variation of stimulus intensity is ± 1 step for last few trials. The mean of these trials would give the detection threshold. In the case of 3 correct responses and 1 false response criteria, 75% threshold level would be measured (3 correct responses in 4 responses). This method is a fast approach for determining the the detection threshold at any statistical criterion. However, a few sessions has to be performed with different statistical criteria if a psychometric curve is desired.

2.1.5 Animal Psychophysics

Rodents and monkeys have been valuable models for behavioral experiments on sensory perception. They can be trained for different behavioral task in operant chambers. Operant chambers can vary in design and equipment depending on the aim of the training and modality of the stimuli. Head- or body-restrainment, for example, has been used to deliver a controlled stimulus in awake animals by preventing them to move. In these kind of systems, animals' movements are restrained by either a harness [107] or restrainment bars implanted on the skull [108]. On the other hand, if freely behaving animals would be accompanied in experiments, nose poking holes equipped with infrared beam detectors [39, 46], licking spouts [40, 42], touch screens [41] or levers [44] can be used for recording the behavioral responses. After a desired behavioral response, the rodents are presented with a reward. Liquid rewards generally given by solenoid valves [39, 40, 42, 44]-[46] whereas pellet foods are supplied through magazines [41].

In order to motivate behavior in rodents, either water or food deprivation can be used. If a water/food-deprived rodent is presented with water/food after each time it performs a desired behavior (i.e., pressing a lever), an association would form between this behavior and the reward which is water/food [109]. This type of rewarding strategy is called positive reinforcement. On the other hand, aversive stimuli can be used to drive behavior in rodents. In this case, a stimuli that is aversive for the rodent (i.e., electric shock) can be delivered until a behavioral response, such as pressing a lever, occurs [110]. By time, the rodent would associate that pressing the lever would cease the unpleasant stimulus. This strategy is called negative reinforcement (reinforcement by removing an unpleasant stimulus). Furthermore, a sensory cue, such as an auditory signal, preceding the aversive stimulus might be elicit the same behavioral response, since the sensory cue would be associated with the aversive stimuli by time. This is called conditioned avoidance. Although conditioned avoidance could be used for studying sensory systems in rats [111], researchers mostly prefer positive reinforcement since it is more appropriate for different behavioral tasks such as forced choice detection or discrimination tasks [39]-[46].

In a very simple way, animals can be trained in a Go/No-Go paradigm where

animals are rewarded for their respond (e.g., pressing/releasing a lever) within a limited time window after the presence of a sensory cue [44, 108, 112]-[115]. Those responses performed after the response-interval or without the presence of the stimulus are not rewarded. On the other hand, the animals can be trained to respond on one of two or more options (e.g., one of two levers or licking spouts). This approach has been widely used for testing animals ability to detect [42, 116, 117], discriminate [46, 107, 118] or localize [119] sensory cues. In most cases, the animal itself starts a trial by pressing a lever or putting their nose into the nose-poking hole. This action is followed by a stimulus-observation interval. At the end of this interval, the animal is expected to make a respond based on their observation. Finally, they are rewarded if their respond is correct (e.g., a correct detection or rejection) or they are not rewarded and a punishment may follow the response [109]. In a detection task, a stimulus is either presented or not in the observation interval. The animals are trained to report stimulus and no-stimulus conditions by, for example, pressing different levers. During training, a supra-threshold stimulus is used to assure it is detected by the animal all the time. After the animal experts on the task, they are also presented with lower intensity levels to further test their sensitivity. Depending on the animals momentary threshold and the perceived intensity level (see Section 2.1.4), animal would report either a stimulus or no-stimulus. When the responses are plotted against intensity levels, psychometric curves would be obtained revealing the sensitivity of the animals for different intensity levels. On the other hand, in a discrimination tasks, a stimulus is presented in each trial but it varies in its one dimension (e.g., frequency or amplitude). The rats are trained to respond, for example, on different levers for two extreme stimuli (e.g., high vs low frequency). Then, they are presented with other intermediate stimuli and forced to classify these intermediate values as either high or low in frequency/amplitude. A further improvement in forced-choice task is done by presenting two stimuli together and training animals to respond based on the difference between these stimuli [42, 115]. This method is called two-alternative forced-choice task and mostly used to test laterality in a sensory organs such as vibrissae and olfaction. It is also possible to train animals in a two-interval forced-choice paradigm [120]. However, this method has been mostly used for primates, whereas there is no literature on rodents to my knowledge. The task is identical to those used in humans (see Section 2.1.4), except that animals

are restrained in a chair during the experiments.

Rats have been widely studied for their vibrissal system because of highly magnified representation of each vibrissa in SI [42]-[46, 56, 107]. Furthermore, vibrissal system is a good model for studying active touch because the sensory and motor innervation form a closed-loop sensorimotor network [59, 60]. However, in order to deliver a controlled stimulus on the whiskers, it might be necessary to restrain head movements or to wait for a stationary head position in behaving animals. Furthermore, humans mostly use their glabrous skin equipped with mechanoreceptors for tactile exploration. In literature, it was shown that rat glabrous skin contains all the mechanoreceptive afferents that human does [71, 72, 75, 121]. However, according to my knowledge, all operant chambers designs reported in the somatosensory literature were for tactile stimulation of the whiskers. For example, operant chamber proposed by Tahon et al. (2011) had a drum in vertical axis to stimulate whiskers only on one side of the nose [44]. The drum was positioned just outside an opening near the lever which is used to start a trial and measure reaction time. A motor was used to control the drum rotation and an adhesive tape was placed on a particular surface of the drum. Rats were trained to initiate the drum rotation by pressing the lever and to release the lever when they sense the adhesive tape. While pressing the lever, rats learned to position their nose close to the drum surface. However, this design would not be suitable for designing tasks with more complex stimuli (e.g., stimulation of individual whiskers). Wiest et al. (2010) built an operant chamber with different compartments for stimulus and respond/reward [46]. Compartments were separated from each other by a sliding door. A nose-poke hole was placed on the stimulus compartment. The stimulus was presented through sliding bars placed on each side of the nose-poking hole. These bars were controlled by step motors allowing to adjust the aperture width. Aperture size was adjusted just before each trial and a trial was started when the sliding door was open. The rats were trained to enter stimulus compartment, poke their nose in the hole and observe the width of the aperture with their whiskers. Then, they got back to the reward compartment equipped with two licking spouts and responded on a spout. Each spout was associated with either the wide or the narrow aperture. However, it was not possible to apply dynamically changing stimuli since aperture widths were predefined. Adibi and Arabzadeh (2011) used an operant chamber similar to the one

used by Wiest et al., except that they used vibrating plates to stimulate whiskers of behaving rats. Piezoelectric actuators were used to vibrate plates placed at both side close to the nose-poking hole. In order to verify contact between the whiskers and the stimulator, video recordings were controlled after each session. The contact between a stimulator and the stimulated surface is important because the behavioral responses depend on the stimulus when it is presented. On the other side, head-restrainment was used in many other studies in order to stimulate whiskers accurately [122]-[124]. For example, Gerdjikov et al. (2010) used a glass capillary to stimulate a single whisker [122]. They fixed the whisker in the glass capillary and moved sinusoidally by a piezoelectric bender. Sachdev et al. (2000) applied air puffs similarly in a head-restrained rat. However, cautious observation of the whiskers by a dissection microscope was necessary to verify the deflection of a single whisker.

2.2 The Aim

In this chapter, I presented a novel computer-controlled operant chamber for various behavioral tasks in which vibrotactile stimuli was applied to the glabrous skin of freely behaving rats. Mechanoreceptors in the volar surface of the hindpaw were specifically stimulated. The novel multi-probe tip adaptor mounted on the mechanical shaker provided accurate stimulation of the skin regardless of the rat's position in the chamber. A detailed training schedule is also provided for this design. Furthermore, I studied the sensitivity of freely behaving rats to vibrotactile stimuli at different frequencies. Psychometric curves obtained in psychophysical experiments were also used in Chapter 4 where I proposed a model for translation of vibrotactile stimuli into ICMS trains.

The vibrotactile operant chamber and training schedule presented in this chapter were published in;

Devecioğlu İ. and Güçlü B., A novel vibrotactile system for stimulating the glabrous skin of awake freely behaving rats during operant conditioning. *J Neuroscience Methods* 242: 41-51, 2015. [125]

2.3 Materials and Methods

2.3.1 Animals

59 Wistar albino rats (44 males and 15 females, ages between 3-7 months) were used in this study. The rats were acquired from Vivarium of Center for Life Sciences and Technologies, Boğaziçi University. All experiments were approved by the Boğaziçi University Institutional Ethics Committee for the Local Use of Animals in Experiments.

The animals used in next chapters of the thesis were selected from these 59 rats as they failed at different stages of the training schedule. The rats which failed to perform behavioral tasks were used in other electrophysiological experiments in Tactile Research Laboratory, Boğaziçi University or sent back to the vivarium.

Rats were housed in standard cages under reversed 12:12-h day-night cycle. In order to motivate rats for behavioral experiments, they were water-deprived 24 h before experiments. Water was only available in the operant chamber while rats were performing a task. Rats were kept at >80% of their normal weights. Additional water was provided if their weight decreased more than 20%. Food was ad libitum in both home cages and the operant chamber.

2.3.2 Operant chamber and vibrotactile stimulator

Figure 2.15 shows the custom-built operant chamber used in this study. Letter labels (a-v) were used to indicate each component on the chamber. The chamber walls (e) are made of Plexiglas (length: 25 cm, width: 25 cm, height: 30 cm) and the ground plate (r) is made of aluminum. An aluminum frame (o) was constructed to elevate the chamber 24.5 cm from the table top, so that the vibrotactile stimulating system (j-n) could be placed beneath it. The aluminum ground plate has 230 holes (diameter: 4 mm, center-to-center distance: 6 mm) precisely spaced in a hexagonal pattern (q). The perforation covers an area with a diameter of ∼10 cm. The probes (s) of the multi-probe tip adaptor (j) moved through these holes during mechanical stimulation. The location and the size of perforation assures that several probes simultaneously

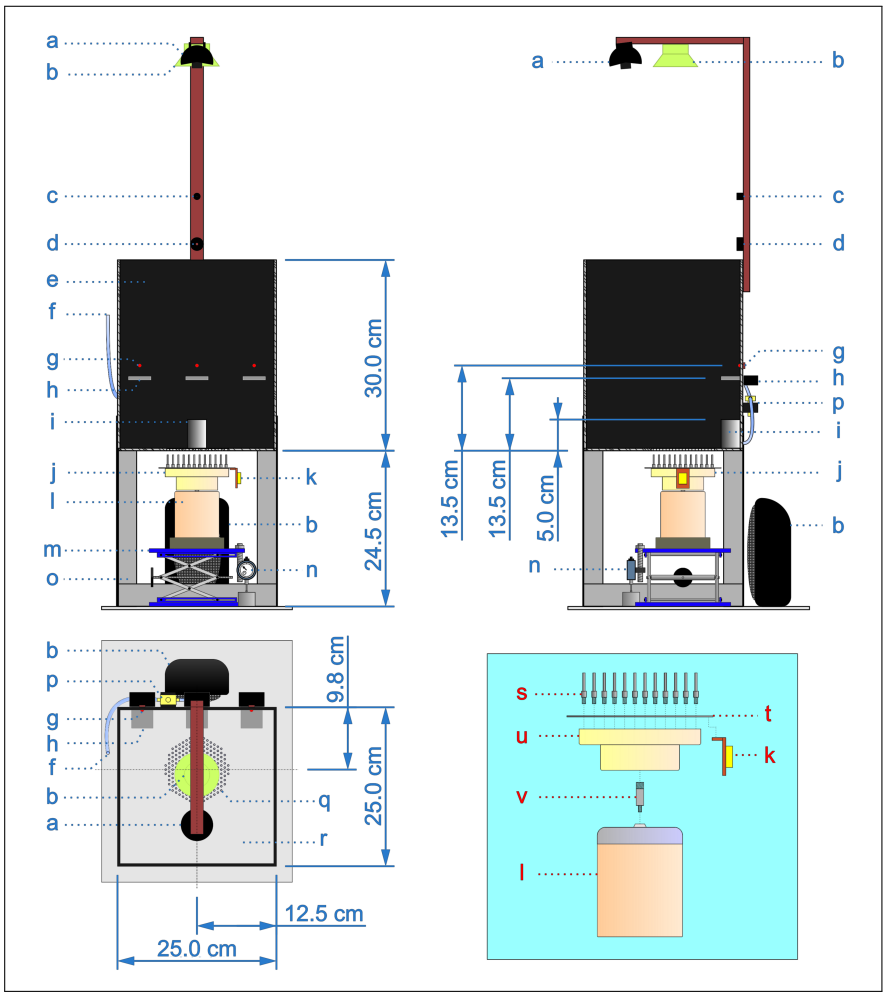

Figure 2.15 The custom-made operant chamber and the assembly of the tactile stimulator. (a) Infrared camera, (b) white-noise speakers, (c) reward buzzer, (d) error buzzer, (e) Plexiglas walls, (f) hose from the water reservoir, (g) LEDs, (h) levers, (i) water receptacle, (j) multi-probe tip adaptor, (k) accelerometer and resistance measurement circuit, (l) mechanical shaker, (m) laboratory jack, (n) dial indicator, (o) aluminum frame, (p) solenoid valve, (q) hexagonal hole pattern, (r) aluminum ground plate, (s) stainless steel probes, (t) aluminum conductor, (u) plastic adaptor, (v) armature connection screw. (The figure was published in Devecioğlu and Güçlü, 2015 [125])

contact to the rat skin in each trial. A battery driven electrical circuit (k) was built to monitor the probe-skin contact. This circuit simply consists of a 9-V battery and a 1-kΩ resistor connected in series with the probes touching the skin surface. When the rat step on the stimulating area, it closes the circuit by touching the ground plate and contactor probe(s). The voltage across the resistor changes depending on the number of probes in contact with the skin. The circuit also has a single chip accelerometer (ADXL05, Analog Devices, USA). Accelerometer used to monitor the movement of the multi-probe tip adaptor in vertical axis. A holder was used for the reward buzzer (Digi-Key part #: 102-1124-ND, operated at 5 VDC, frequency: 2.3 kHz, intensity: 90

dB SPL) (c) and error buzzer (Digi-Key part #: 458-1351-ND, operated at 24 VDC, frequency: 3.5 dB, intensity: 105 dB SPL) (d), white-noise speaker (generic speakers) (b) and the camera (a generic webcam) (a).

The front wall of the chamber was equipped with three non-retractable levers (h), three blue light emitting diodes (LEDs) aligned with each lever (g) and a water receptacle (i). Levers are 4 cm in width and protrude 2.5 cm from the wall. They were positioned at a height of 11.5 cm, so that rat would rear in order to press a lever and only hind paw would touch to contactor probes. Levers move generic push-button switches placed outside the chamber. Approximately 25 gram-force is adequate to turn the switches on. LEDs are aligned 2 cm above the levers. A 4.5-cm high cylinder with a hole for water delivery is used as the water receptacle and it is located at the center of the wall. The water reward ($\sim$7-8 μL) is delivered by actuating a solenoid valve (p) for a very short time ($\sim$10 ms). When the valve is open, water drips through a hose (f) from the water reservoir placed outside the chamber.

An electrodynamical shaker (V201, Ling Dynamic Systems, Royston, Herts, UK) was used as the mechanical stimulator (i). This shaker is similar to those used in other experimental setups in Tactile Research Laboratory, Boğaziçi University [75, 100, 126]. It is a highly accurate and linear device for generating any mechanical waveform. Static position of the shaker, hence the static indentation [127], the shaker was placed on a laboratory jack (m) equipped with a micrometer dial indicator (1044SB, Mitutoyo Corporation, Japan) (n).

The plastic (VeroWhite+) adaptor (u) was designed in CATIA V5.19 (Dassault Systèmes, France) and manufactured with a 3D printer (Objet260 Connex, Stratasys Ltd., Eden Prairie, MN) in clean room of Center for Life Sciences and Technologies, Boğaziçi University. Two different types of adaptor were designed; one for carrying 2-mm diameter stainless steel contactor probes (s) and one with plastic contactor probes (Figure 2.16). Former design has holes threated for ISO M3 screws. Latter design was printed as a whole with contactor probes on it. Both of the adaptors are identical except the materials used for the contactor probes. Nevertheless, stiffness of the plastic probes is high enough to easily indent the skin as metal probes do. Furthermore, the vibrotactile stimulation system was calibrated for both adaptors (see Section 2.3.3). The adaptors were mounted on the shaker's armature with a ISO M6-threated screw

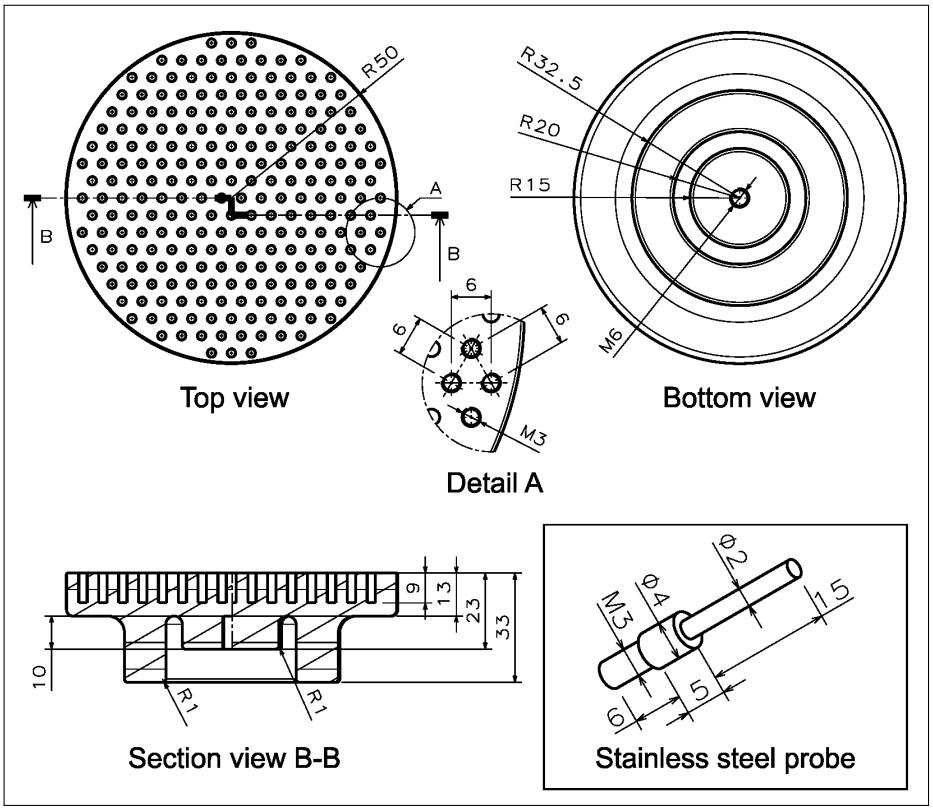

Figure 2.16 Technical drawing of multi-probe tip adaptor and individual stainless steel probes. R: radius, ∅: diameter, M: ISO Metric threating. A: detail view, B: cross-section view. Dimensions are in mm. (The figure was published in Devecioğlu and Güçlü, 2015 [125])

(v). The contactor probes have a flat surface for skin contact. The probes do not move individually; when the shaker vibrates, the adaptor and all probes move as a whole. Therefore, mechanical vibrations could be applied on the sole regardless of the freely behaving rat's position.

The chamber was placed in a light and sound-insulated box. Furthermore, during behavioral experiments, acoustic white noise was presented in the background at 90 dB SPL in order to mask environmental noises and any audible cues emitted by the shaker (b). All sessions were monitored and recorded by the infrared camera (a).

2.3.3 Electronics and control software

Figure 2.17 shows the flow chart of the setup. Off-the-shelf components were used to construct the interface circuits for the actuators and the sensors in the op-

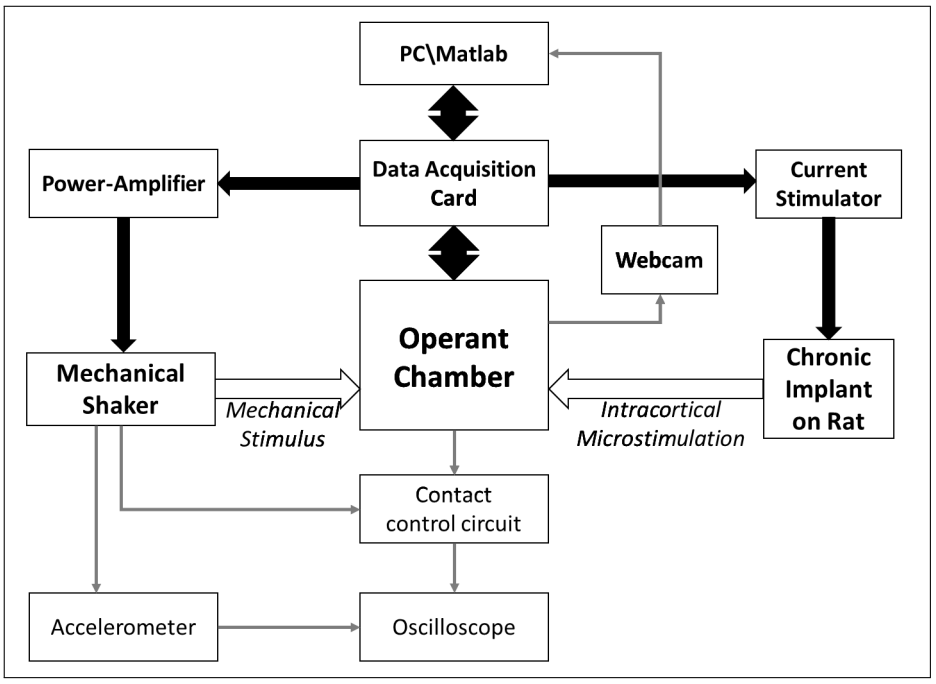

Figure 2.17 The flow diagram of the operant chamber. Operant chamber is controlled by a custom-made program prepared in MATLAB. A data acquisition card (DAQ card) provides digital input outputs for the sensors and actuators on the chamber and analog outputs for stimulus waveforms. Analog output for mechanical stimulation is amplified by a custom-made power-amplifier which drives the mechanical shaker. Contact control circuit measures the impedance between the ground plate of the chamber and the probes of the multi-probe tip adaptor providing an estimation of the contact surface. Its output voltage changes depending on the contact surface are monitored on the oscilloscope. The vibration of the multi-probe tip adaptor is monitored on the oscilloscope screen via an accelerometer located on the adaptor. A webcam is used to monitor the behavior of the animal in the chamber. The Waveform of intracortical microstimulation is supplied to a current source by the analog output of the data acquisition card. The current source delivered the current pulses into the cortex via microelectrodes (details are given in Chapter 3).

erant chamber. A commercial DAQ card (USB-6259, National Instruments, Austin, TX, USA) provided the digital inputs/outputs for the sensors and actuators and the analog output for the stimulus waveform. A custom-made power-amplifier (amplifier integrated circuit: TDA7296, ST Microelectronics, Switzerland) was used to amplify the analog output of the card and drive the shaker. The entire mechanical stimulation system was calibrated with a Fotonic sensor (MTI-2100, MTI Instruments, Albany, NY). The sensor has a probe consisted of optical fibers for light emission and detection. The probe was aligned with a single contactor probe in the vertical axis. The light emitted from the probe is reflected by the surface and the amount of light detected by the probe is converted into an instantaneous voltage by the device. Therefore, the calibration was performed in a dark environment. The stimulator was calibrated

at different amplitude levels for a given frequency of sinusoidal displacements. The peak-to-peak voltage of the waveform generated by the Fotonic sensor was measured by and oscilloscope (calibration factor: 0.07128 μm/mV). Straight lines were fitted to the calculated displacements as a function of the output by the USB-6259 card.

A custom program with a graphical user interface (GUI) prepared in MATLAB 2008a (The MathWorks, Natic, MA, USA) was used to control the vibrotactile system and acquire data from the chamber (Figure 2.18). The MATLAB scripts were published online (see [125] and http://web0.boun.edu.tr/burak.guclu/burak/TRL/index_files/Page967.htm). The program requires the task to be chosen first. Then, depending on the task, the parameters for the stimulus and the procedure are specified by the user. The status of each lever and LED and the water receptacle are shown on the maze

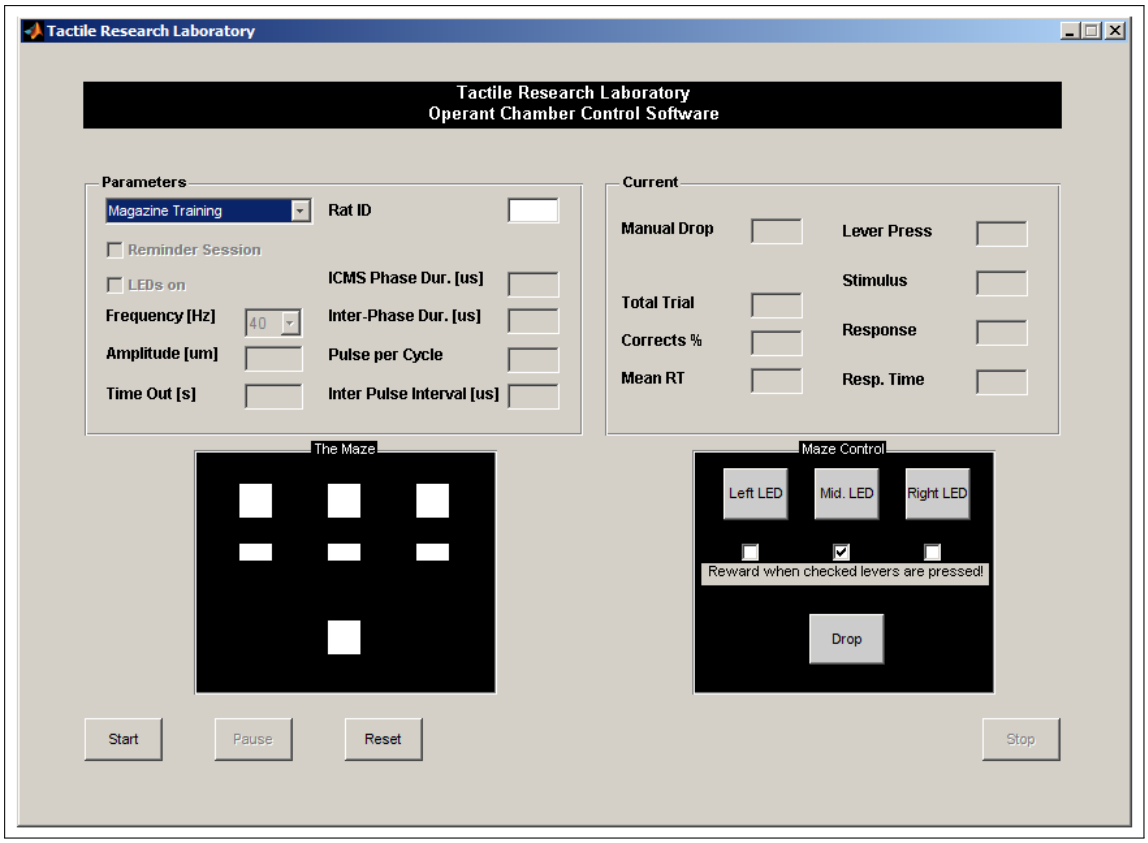

Figure 2.18 The graphical user interface of MATLAB program used to control operant chamber and generate stimulus waveforms. When the program is lunched first time, the experimenter choses which task to run. Depending on the task, different sets of parameters can be determined for the task and the stimulus waveforms. The current status of the session and instantaneous performance of the rat are shown in the *Current* box. *The Maze* box displays the instantaneous state of levers, LEDs and the water receptacle. The *Maze Control* box enables experimenter to control state of LEDs, to determine which levers to be activated and to deliver manual water rewards. (The figure was published in Devecioğlu and Güçlü, 2015 [125])

box of the GUI. The current status of the session and the performance of the rat are also displayed. At the end of each session or when the experimenter stops a session, the behavioral responses are recorded and simple statistics (e.g., accuracy and mean response time) are calculated.

2.3.4 Behavioral training

After arrival of animals from vivarium to Institute of Biomedical Engineering, they were let to rest and habituate for at least two days. During this period, food and water were ad libitum. Furthermore, rats were provided with 20-min daily free exploration sessions in the operant chamber. The water deprivation usually started on Saturday night and the trainings were performed in 1-h sessions during the weekday. Rats were provided ad libitum water after the final session of the week.

The training schedule consisted of 5 subsequent tasks (Figure 2.19);

- Magazine training session
- Task-A: The simple operant conditioning
- Task-B: Visually guided side-lever press
- Task-C: Visually guided tactile detection
- Task-D: Tactile detection

In the very first session, rats learned where to get water, and then, they associated the reward signal (sound duration: 0.3 s, frequency: 2.3 kHz, intensity: 90 dB SPL) with the reward on the water receptacle. Rats which consistently responded (i.e., approaching to water receptacle and drinking water) to the reward signal were carried onto Task-A. In Task-A, rats were trained to press the middle lever in order to get water. The association between the lever and the reward was established step-by-step:

- First, reward was presented manually each time the rat pointed its nose toward the middle lever. When this behavior became consistent, reward rate decreased

to force the rat to sniff or touch the lever.

- Next, the actions of sniffing, touching with whisker or nose and touching with forepaws followed each other as rewarding rate decreased when the rat performs an action consistently. When the rat consistently touched the lever with its forepaws, it was forced to press the middle lever by decreasing the rate of rewarding.

- Finally, the manual rewarding was stopped when the rat consistently pressed the middle lever.

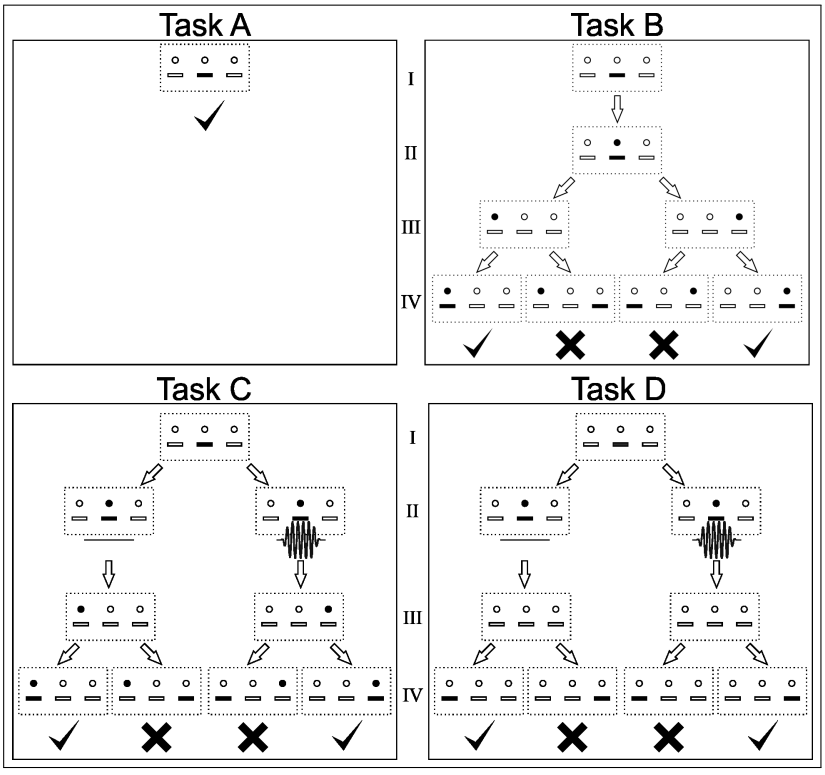

Figure 2.19 The flow diagrams of the behavioral training tasks. Levers are represented with small rectangles and LEDs are represented with small circles. A filled rectangle indicates the lever is depressed and a filled circle shows a lit LED. Different stages of each task are indicated by Roman numerals. After magazine training, rats were further tested in four consecutive tasks. Task-A, Simple operant conditioning: Each time the middle lever is depressed, the water reward is delivered (I). Task-B, Visually guided side lever pressing: A trials is started by depression of middle lever (I) and the middle LED was turned on for 0.6 s (II). Then, one of the side LEDs were turned on (III). The reward is presented if the lever below the lit LED is depressed (IV). Otherwise, no reward is given and the error signal occurred. Tack-C, Visually guided vibrotactile detection task: This task is similar to Task-B except a vibrotactile stimulus is presented for right-lever trials (II). Task-D, Vibrotactile detection task: Side LEDs are disabled. The reward is presented if right lever is depressed for stimulus condition and if left lever is depressed for no-stimulus condition. Otherwise, no reward is presented and the error signal occurred. (The figure was published in Devecioğlu and Güçlü, 2015 [125])

Rats performing ≥100 lever presses in a 1-h session were carried onto Task-B. In Task-B, rats were trained to initiate a trial by pressing middle lever and to respond on one of the side levers depending on which side LED was on (Figure 2.19). Beginning of a new trial was signaled by turning on the middle LED for 0.6 s. After this period, one of the side LEDs was turned on. The reward was presented if the rat pressed the lever below the lit LED. If the rat pressed the lever on the wrong side or did not responded within 60 s, the reward was not presented and an error signal (sound duration: 1 s, frequency: 3.5 kHz, intensity: 105 dB SPL) occurred. The attempts of pressing any side lever before 0.6-s interval was completed were not counted, but the trial continued and a response was expected from the rat. The trials in which rat did not respond with in 60 s were not recorded but repeated. Each session consisted of 100 trials where right and left trials were randomized and counter-balanced. At the end of each session, percentage of correct rates and mean response time were recorded. Rats completing two consecutive sessions with a correct rate of ≥85% were carried on Task-C.

In Task-C (Figure 2.19), the rats actually performed the same task as in Task-B, but they were presented with a high-level vibrotactile stimulus (Figure 2.20) for the first time (see Task-D for stimulus parameters). This step was necessary in order to habituate rats to this novel mechanical stimulus applied to their hindpaws and to continue performing the task without any disruption. The stimulus was presented during the period where the middle LED was turned on for 0.6 s in trials where the right LED would be on. Although a rat might ignore or facilitate the presence of the vibrotactile stimulus, rewarding strategy was same as in Task-B; reward if the rat pressed the lever under the lit LED. The rats completing a 100-trials session with an accuracy ≥85% were carried onto Task-D. 4 rats among those able to attend Task-C were presented with a high-level auditory stimulus instead of the vibrotactile stimulus. This experiments were performed to compare the performances of rats in auditory and tactile training.

The Task-D was a forced-choice yes/no detection task. As in previous tasks, the rat started a trial by pressing the middle lever. Right after, the middle LED was turned on and the stimulus was presented or not. In vibrotactile experiments, the stimulus was a burst of 40-Hz mechanical sinusoidal vibrations (zero-to-peak amplitude: 46 dB ref 1μm, rise and fall times: 50 ms, stimulus duration measured between half-power point:

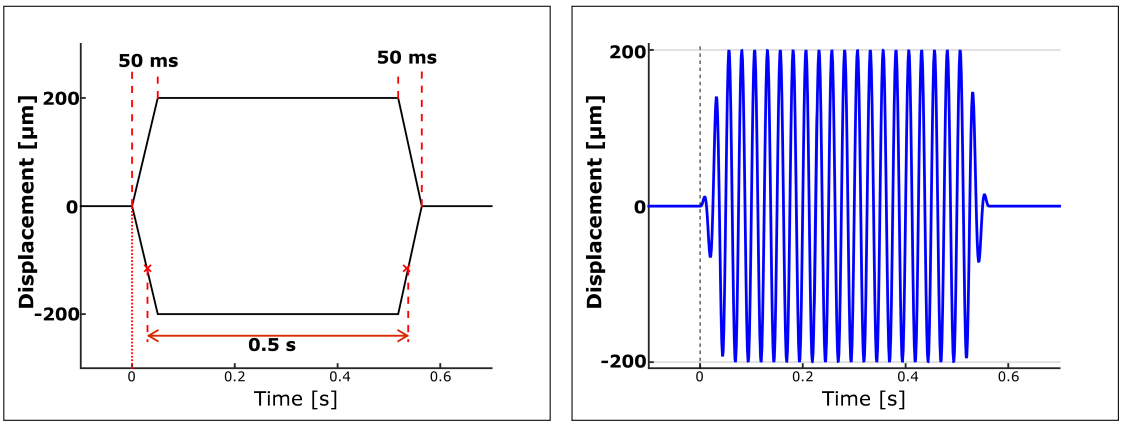

(a) (b)

Figure 2.20 Package of vibrotactile stimulus. (a) The vibrotactile stimuli began and ended as cosine-squared ramps. Rise and fall times were 50 ms and the duration between half-power points was 0.5 s. (b) A burst of 200-μm zero-to-peak amplitude, 40-Hz mechanical sinusoidal vibrations was used for training.

0.5 s) (Figure 2.20). In the auditory experiments, it was an 16-kHz tone presented at 85-dB SPL and had the same package as the mechanical stimulus. The right lever was associated with stimulus condition and the left lever was associated with no-stimulus condition. In order to get a reward, the rat had to press right lever if the stimulus was presented (successful detection, hit) and to left lever if the stimulus was not presented (correct rejection). Misses (pressing left lever for stimulus condition) and false alarms (pressing right lever for no-stimulus condition) were not rewarded and false responses were indicated with the error signal. The rat had to respond within 20 s, otherwise the trial was canceled and the error signal occurred. These trials were repeated later. Task-D was continued until the rats' behavioral performances reached the criteria for psychophysical experiments or until they did not show any improvement within 10 sessions. The criteria for moving in psychophysical experiments (*Experiment I*) were as following;

- The average of the percentage of accuracies in the last five sessions had to be >80% and did not show an improving trend (tested with *Kendall's* τ test) [128].
- Conditional probabilities (hit rate, *p(h)*, and false alarm rate, *p(f)*) had to be with in mean±0.1.

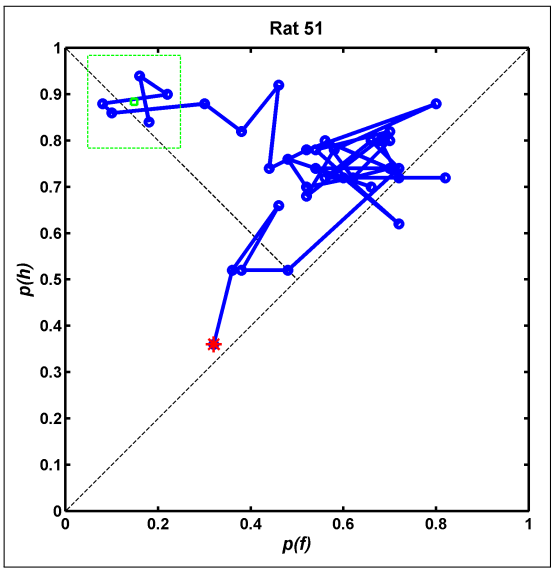

Figure 2.21 Visualization of learning on receiver operant characteristic graph. $p(h)$ and $p(f)$ were plotted on ROC to understand how the response strategy changed during learning and whether the rat had a stable response strategy as an indicator of learning. Red asterisk sign indicates the first session. Green open circle is the mean of $p(h)$ and $p(f)$ for last 5 session and the green rectangle is the ± 0.1 of mean. Rats' conditional probabilities were expected to accumulate in this green area.

If a rat's performance was still increasing, it was further tested until its accuracy showed no trends according to *Kendall's* τ test. Receiver operant characteristics (ROCs) were plotted based on conditional probabilities recorded in successive sessions to visualize the second criterion (Figure 2.21).

2.3.5 Experiment I: Vibrotactile psychophysical testing

14 rats successfully completed Task-D were further tested in psychophysical experiments where their sensitivity to vibrotactile stimuli at different frequencies were measured (Table 2.2). In psychophysical experiments, the rats performed the yes/no detection task as in Task-D, but they were tested with 6 amplitude levels (3-200 μm) at 3 different frequencies (40 Hz, 60 Hz and 80 Hz). Only three rats (Rats 38, 39 and 40) were tested at 20 Hz, 40 Hz, and 80 Hz. Each condition was tested 4 times in random days. In a given day, 6 amplitude levels were tested for a single frequency. Each amplitude level was tested in a different session consisted of 50 stimulus condition and 50 no-stimulus condition. Order of the amplitude levels were randomized and each

session was interleaved with a 20-trials reminder session where the rat was presented with training conditions and expected to perform an accuracy $\geq$85% in order to proceed to next test session. At the end of each session corrected hit rates were calculated from $p(h)$ and $p(f)$ using equation 2.2 [106].

$$p(h) = p^*(h) + p(f)[1 - p^*(h)] \tag{2.2}$$

where $p^*(h)$ is the corrected hit rate. Equation 2.2 defines the empirically observed hit rate, $p(h)$, as the sum of the rate of hits when the stimulus is actually above the threshold, $p^*(h)$, and the rate of hits due to the response bias although the stimulus is actually below the threshold (Figure 2.22) [106]. Corrected hit rates were plotted and fitted with a sigmoid curve (equation 2.3) to obtain psychometric functions.

$$p^*(h) = \frac{1}{1 + e^{(a-A)/b}} \tag{2.3}$$

where A is the zero-to-peak amplitude of the vibrotactile stimulus in dB ref 1μm, a is the 50% detection threshold and b is related to the slope of the sigmoid at a.

The amplitude levels corresponding to 50% detection probability were estimated from psychometric functions. Since sample sizes were not large enough, effect of frequency on 50% detection thresholds were tested with non-parametric Kruskal-Wallis

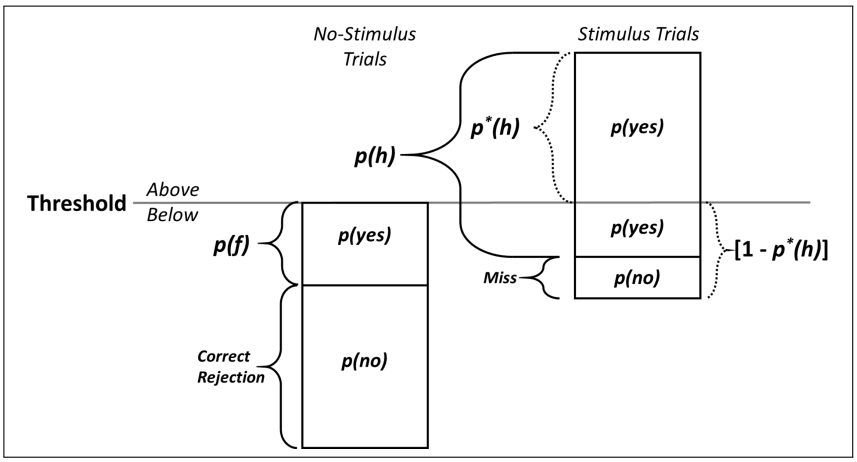

Figure 2.22 Illustration of how conditional probabilities are shaped based on threshold theory. $p(yes)$: reporting stimulus (i.e., pressing right lever), $p(no)$: reporting no-stimulus (i.e., pressing left lever). (Adapted from Gescheider, 1997 [106])

test. Wilcoxon ranksum test with Bonferroni correction was used for post-hoc analysis.

2.4 Results

2.4.1 The vibrotactile system

The stimulus package shown in figure 2.20 was used to calibrate the vibrotactile stimulation system consisted of the DAQ card (USB-6259), the power-amplifier and the mechanical shaker. The gain of the power-amplifier was set to a constant value. Stimuli were generated in MATLAB. Calibration were done in the amplitude range of 0.05-100 μm and the frequency range of 15-100 Hz (Figure 2.23). Straight lines were fitted to data points. Goodness-of-fits (R^2) were >0.99. When the shaker was driven with frequencies >100 Hz, it emitted sound which required masking with higher intensity levels of white-noise. Therefore, high frequencies were not used. Amplitude levels beyond the calibrated range were extrapolated from the fitted lines.

Figure 2.23(b) shows the zero-to-peak displacements produced by the shaker for a given amplitude setting (DAQ card output: 0.05 V_p). As seen from the figure, the displacement produced by the shaker decreases as the frequency increases. This trend

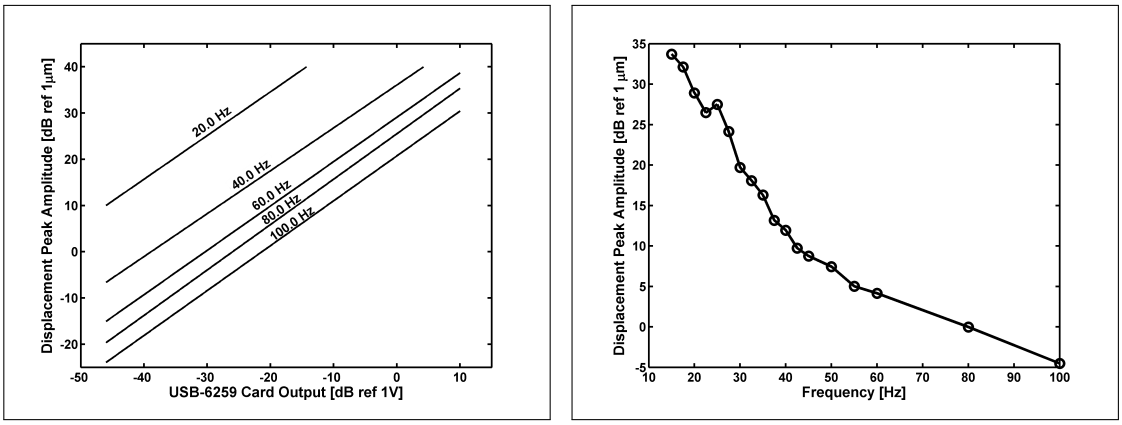

(a) (b)

Figure 2.23 Calibration graphs of the vibrotactile system. (a) Calibration was done in the amplitude range of 0.05-100 μm and the frequency range of 15-100 Hz. The system is linear for a given frequency. (b) Frequency response of the system. The downward trend at higher frequencies is mostly due to the mechanical response of the shaker. (The figures were published in Devecioğlu and Güçlü, 2015 [125])

is mostly related to the mechanical response of the electrodynamic shaker. Therefore, higher DAQ card output levels are required to generate a given displacement at higher frequencies.

2.4.2 Behavioral training schedule

52 rats (14 females and 38 males) out of 59 successfully completed the magazine training and Task-A (Table 2.1). Some rats associated to press middle lever with reward and achieved >100 lever press counts in their first session in Task-A (Figure 2.24). A minimum of eight session was required for a few rats to succeed this criterion. The rate of association was strongly depended on rat's motivation to act and explore the chamber. Interestingly, 3 rats rejected to get water during magazine training although they waited near the water receptacle. 4 rats failed to press middle lever, although they were responding to reward signal and drink water. Some of these established the association between the middle lever and the reward to some extend; for example, they started to sniff and/or touched the middle lever but couldn't press it. On the other hand, some rats did not interested in levers other than their very first time in the chamber.

In Task-B, 41 rats (13 females and 28 males) could reached >85% accuracy. The fastest learner completed 100 trials in its first session and achieved >85% accuracy criterion in next session. On the other hand, the training took up to 16 sessions for a few rats to reach the behavioral criterion. 2 rats learned to initiate a trial by pressing middle lever and to responded on a side lever, but their responses were mostly independent of visual cues. For this reason, they couldn't reach the criteria. Others mostly continued to press middle lever by ignoring visual cues and they did not interested in side levers.

Table 2.1
Rats which failed in the first two tasks. Age: the age that the rat started training. −: The rat couldn't achieve the criteria, ++: The rat successfully completed the task

Rat ID	Sex	Age	Task-A	Task-B
1	M	4	++	−
10	M	4	−	
13	M	5	++	+
15	M	5	−	
16	M	5	++	+
17	M	5	−	
28	M	6	−	
29	M	6	++	−
31	F	4	−	
35	F	4	++	−
48	M	3	−	
54	M	4	−	
57	M	5	++	−
58	M	5	++	−
61	M	4	++	−
62	M	6	++	−
63	M	6	++	−
64	M	6	++	−

Among those 41 rat successfully completed Task-B, 37 rats were tested in tactile version of Task-C (Table 2.2) and 4 rats were tested in auditory version (Table 2.3). The presence of vibrotactile stimulus disrupted one rat's performance; it continued to perform task, but couldn't achieve 85% criteria. All other rats continued to perform the task without any disruption.

In Task-D, absence of visual cues disturbed the behavior of only one rat in auditory group. This rat couldn't complete a 100-trial session without visual cues.

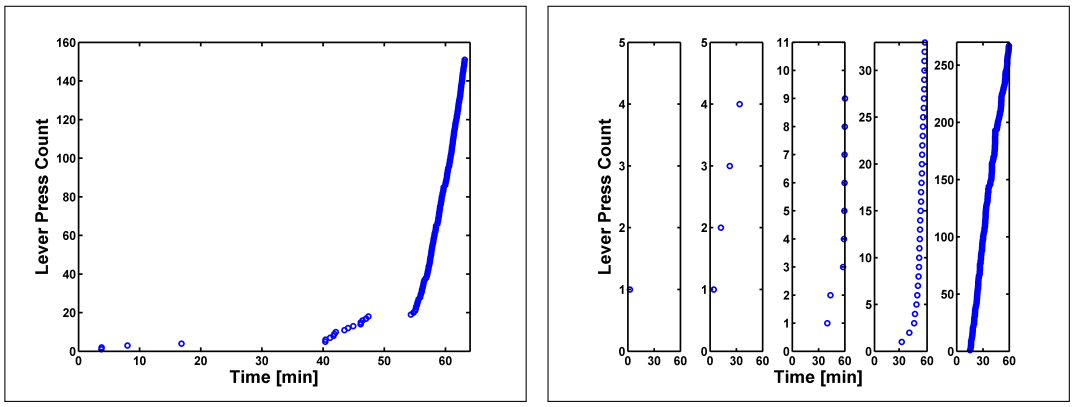

(a) Rat 51 (b) Rat 12

Figure 2.24 Learning Task-A: Simple operant conditioning. Rat 51 learned to press middle lever to get water reward in a 64-min session whereas it took 5 sessions for Rat 12 to achieve >100 lever press counts in a session.

All other rats continued perform the task but usually responded randomly in the first few sessions (Figure 2.25, also see Appendix A). 22 rats out of 36 in tactile group completed Task-D with accuracies >70% (Table 2.2). Among these, 16 rats (2 females and 12 males) achieved an accuracy >85%. From auditory group, all 3 rats performed accuracies between 70-85%.

All training schedule required a maximum of 7 weeks whereas some rats completed all training steps in 2 weeks.

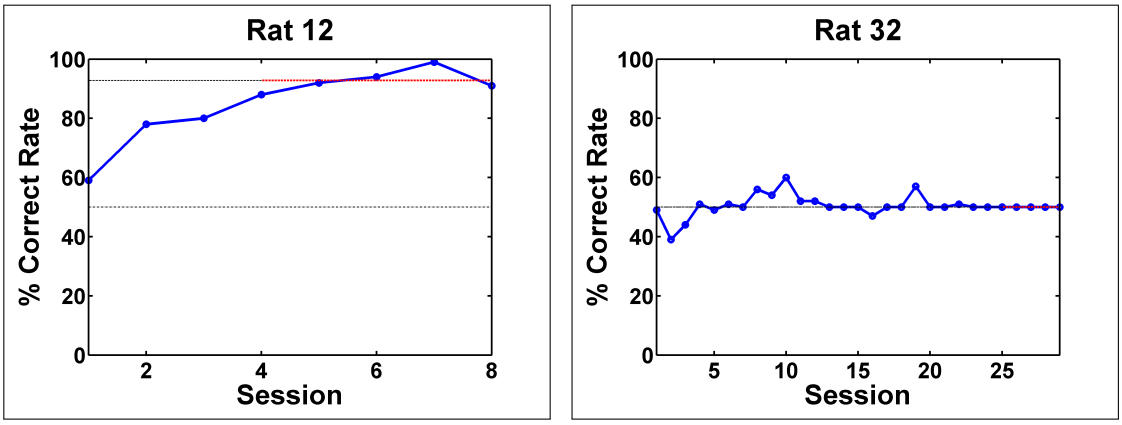

Figure 2.25 Development of vibrotactile operant conditioning in rats: Percentage correct rates. Rat 12 associated the stimulus condition with right lever and no-stimulus condition with left lever within 8 sessions, whereas Rat 32 performed at chance level even after 29 sessions.

Table 2.2: Rats tested in vibrotactile experiments. The percentage of correct rate is given for Task-D. Age: the age that the rat started training. −: The rat couldn't perform the task, +: The rat could perform the task but couldn't achieve the criterion, ++: The rat successfully completed the task, N/A: the rat was not tested in psychophysical experiments.

Rat ID	Sex	Age	Task-A	Task-B	Task-C	Task-D	Experiment I
4	M	7	++	++	++	80.0%	N/A
7	M	4	++	++	++	86.8%	N/A
8	M	4	++	++	++	77.6%	N/A
9	M	4	++	++	++	57.6%	N/A
11	M	4	++	++	++	75.6%	N/A
12	M	5	++	++	++	92.8%	N/A
14	M	5	++	++	+		
30	F	4	++	++	++	86.2%	N/A
32	F	4	++	++	++	50.0%	N/A
33	F	4	++	++	++	52.2%	N/A
34	F	4	++	++	++	56.0%	N/A
36	F	6	++	++	++	55.2%	N/A
37	F	6	++	++	++	82.9%	N/A
38	F	4	++	++	++	85.4%	++
39	F	4	++	++	++	84.7%	++
40	F	5	++	++	++	87.0%	++
41	F	5	++	++	++	65.2%	N/A
42	M	4	++	++	++	68.6%	N/A
43	M	4	++	++	++	62.2%	N/A
44	F	5	++	++	++	90.2%	++
45	F	5	++	++	++	56.2%	N/A

Continued on next page

Table 2.2 – *Continued from previous page*

Rat ID	Sex	Age	Task-A	Task-B	Task-C	Task-D	Experiment I
46	F	5	++	++	++	53.2%	N/A
47	M	3	++	++	++	80.6%	N/A
49	M	3	++	++	++	61.8%	N/A
50	M	3	++	++	++	63.8%	N/A
51	M	3	++	++	++	86.8%	N/A
52	M	3	++	++	++	64.8%	N/A
53	M	3	++	++	++	50.8%	N/A
55	M	4	++	++	++	90.0%	++
56	M	4	++	++	++	87.6%	++
59	M	4	++	++	++	91.4%	++
60	M	4	++	++	++	74.4%	N/A
65	M	6	++	++	++	95.6%	++
66	M	7	++	++	++	88.4%	++
67	M	7	++	++	++	89.4%	++
68	M	7	++	++	++	91.6%	++
69	M	7	++	++	++	86.6%	++

Table 2.3
Rats tested in auditory version of Task-C and -D. The percentage of correct rate is given for Task-D. Age: the age that the rat started training. −: The rat couldn't perform the task, ++: The rat successfully completed the task.

Rat ID	Sex	Age	Task-A	Task-B	Task-C	Task-D
18	M	5	++	++	++	81.6%
19	M	7	++	++	++	79.6%
20	M	7	++	++	++	−
21	M	7	++	++	++	72.0%

2.4.3 Receiver operant characteristics

In order to understand how the respond strategy was shaped during learning in Task-D, $p(h)$ and $p(f)$ of successive sessions were plotted in ROC graphs (Figure 2.26, also see Appendix A). Since the rats mostly responded to one of the side levers independent of the condition of the stimulus in the first few sessions, $p(h)$ and $p(f)$ were either too low (i.e., mostly responding to the left lever) or too high (i.e., mostly responding to the right lever). As the rats associated the no-stimulus condition with the left lever and the stimulus condition with the right lever, data points approached to the top left corner of the ROC graph (i.e., high $p(h)$ and low $p(f)$) (Figure A.6). Accumulation of data points in a narrow region is an indicator of the stabilized response strategy, and furthermore, it may show the maximum level of learning that can be achieved by the rat. On the other hand, random responses caused data points to accumulate at the center of the ROC (Figure A.4).

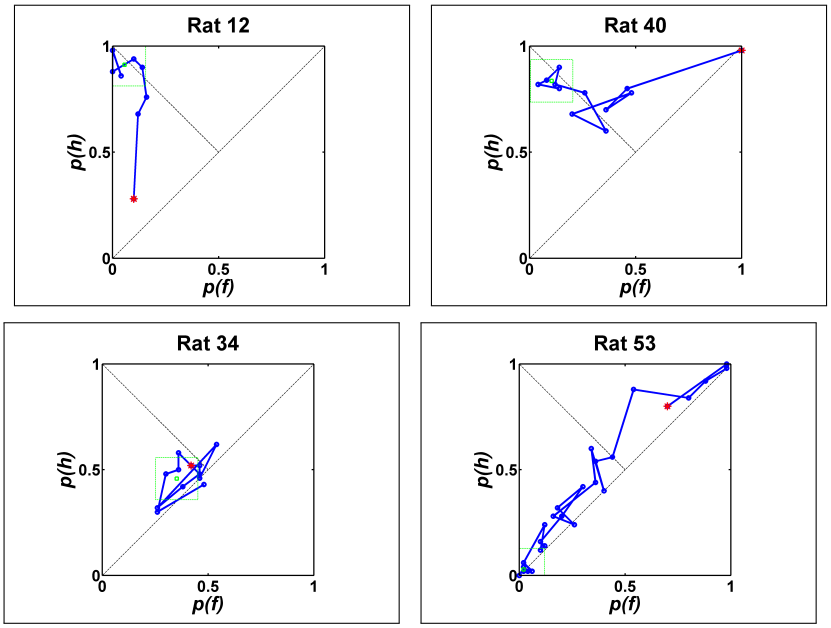

Figure 2.26 Development of vibrotactile operant conditioning in rats: Receiver operant characteristics. Rat 12 and 40 performed responses biased to left and right, respectively. Then their data points approached top left corner of the ROC which indicates that they successfully associated the levers with the condition of the stimulus. Rat 34 performed random responses in almost all of the sessions. Rat 53 started with a response strategy biased to right lever and its bias shifted to the left lever by time. Yet, it couldn't learn Task-D.

2.4.4 Vibrotactile sensitivity of freely behaving rats

$p^*(h)$ values were fitted with sigmoid curves to construct psychometric curves for each frequency (Figure 2.28). All R^2 values but 6 were >0.70. Those 6 fits had R^2 values between 0.55-0.70. An obvious effect of the frequency is the shift of curves to the lower intensity levels as the frequency increased. Therefore, for a given intensity level, a 80-Hz vibration is more likely to be detected than those at lower frequencies.

Likewise, 50% detection threshold levels decreased as the frequency increased (Figure 2.27). The mean (± standard error) threshold levels were 41.763 (±0.91) dB ref 1 μm for 20 Hz, 24.357 (±1.52) dB ref 1 μm for 40 Hz, 20.009 (±1.09) dB ref 1 μm for 60 Hz and 17.101 (±0.85) dB ref 1 μm for 80 Hz. Effect of frequency on threshold levels was significant ($p < 0.001$, Kruskal-Wallis test). Post hoc test revealed

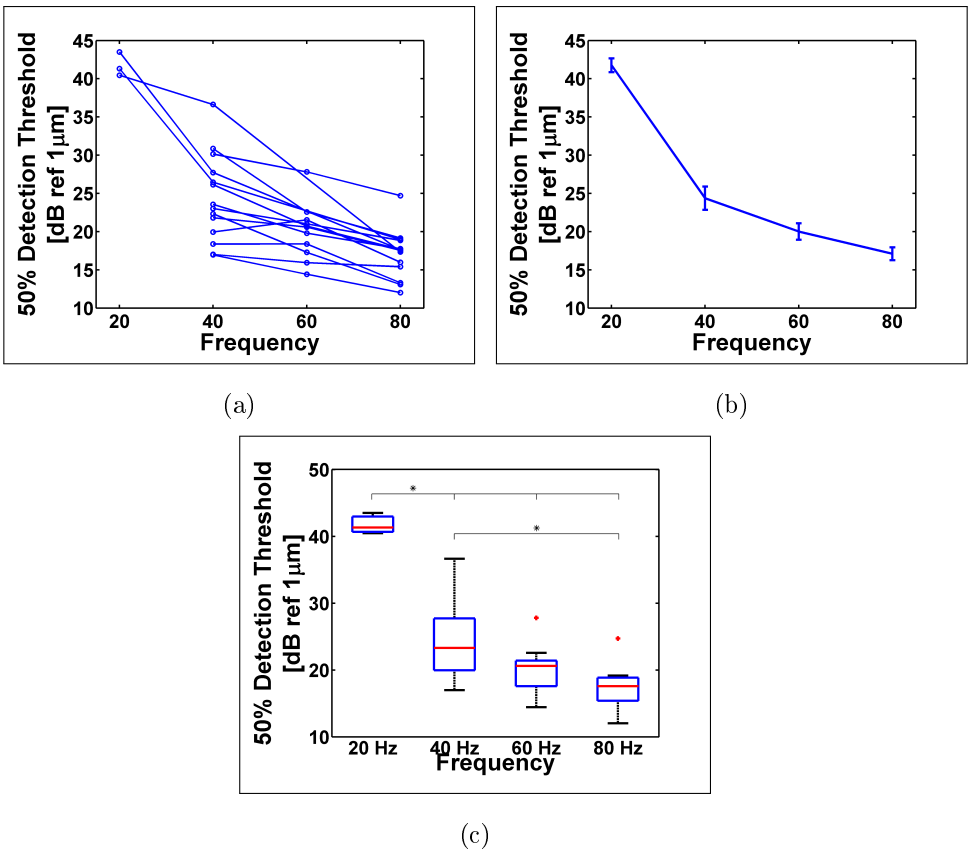

Figure 2.27 Sensitivity of rats to vibrotactile stimulation of their glabrous skin. (a) 50% detection thresholds of each rat at different frequencies. (b) Mean detection thresholds. Vertical lines shows the standard error. (c) Box plots showing the significant differences between frequencies. Significance level: $p = 0.05$.

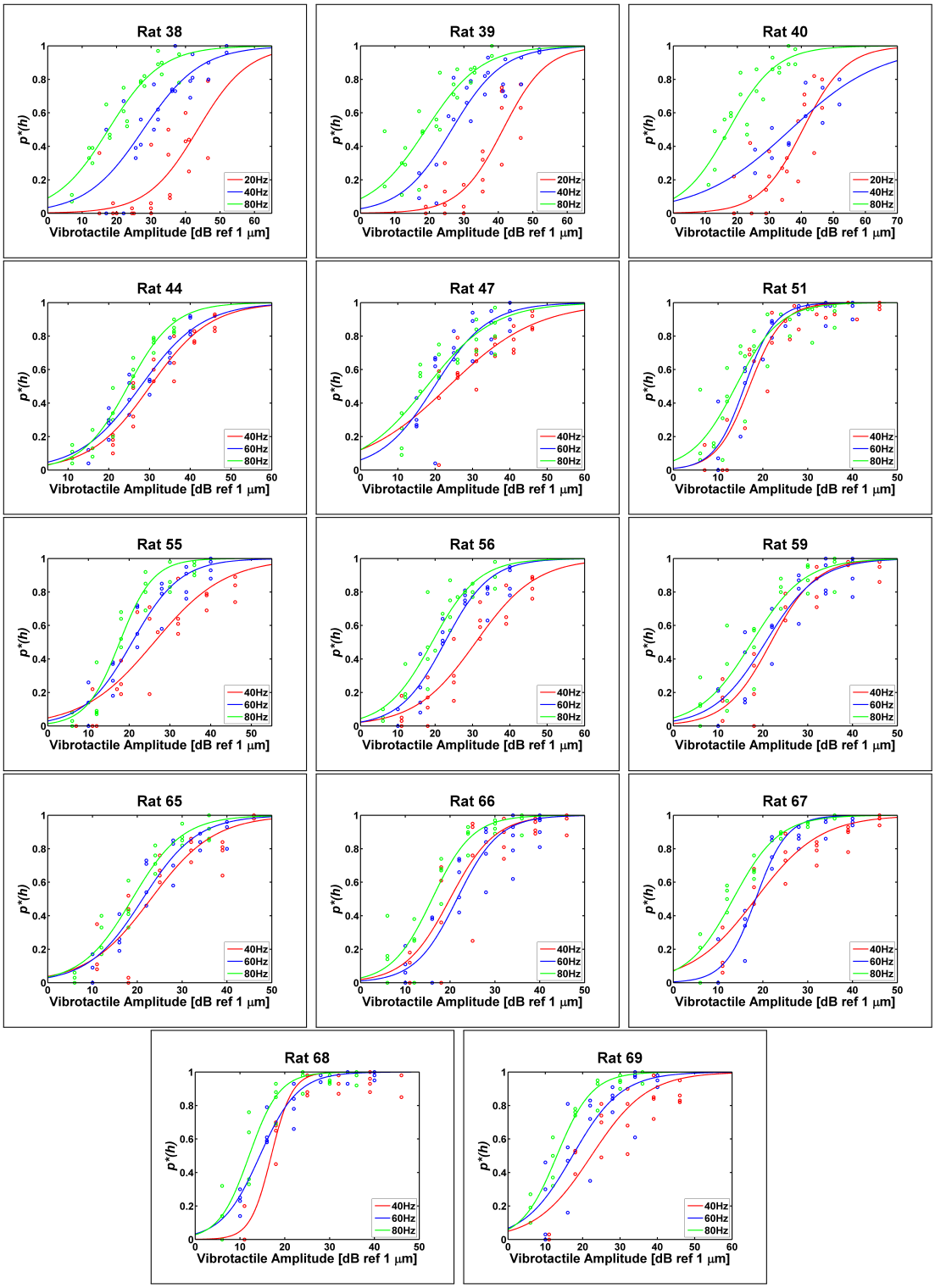

Figure 2.28 Vibrotactile psychometric curves. Data points (open circles) from each frequency is fitted with separate sigmoid curves (solid lines).

significant differences between frequencies (Figure 2.27(c)): Detection thresholds at 20 Hz were significantly higher than those at higher frequencies (20 Hz-40 Hz: $p = 0.018$,

20 Hz-60 Hz: $p = 0.033$, 20 Hz-80 Hz: $p = 0.018$) whereas detection thresholds at 40 Hz were higher than only those at 80 Hz ($p = 0.007$) (p values were adjusted according to Bonferroni correction).

2.5 Discussion

2.5.1 Technical limitations and improvements

A major improvement to the setup could be replacing the levers with retractable ones. With the help of these levers, first two tasks could be completed faster, because the lever presented other than the interested one might be distractive. Task-A and Task-B could be redesigned with such levers. In Task-A, only one of the levers present in the chamber and the rat could be trained to depress the presented lever to get water reward. This would make it easier for rat to adapt in Task-B. In addition, Task-B could be redesigned such that: (1) Only middle lever is presented for task initiation. (2) When the rat initiated a trial by depressing the middle lever, the middle lever is retracted after 0.6 s and (3) a side LED is turned on before side levers are presented in the chamber. Furthermore, this paradigm could be used in other training levels too. Retracted middle lever would prevent a rat chronically implanted with electrodes to snag its headstage or the cables connected to the headstage to the middle lever.

Although the rats differing in sex and size pressed the levers easily, many others just sniffed or touched to them. It is possible to use pressure or touch sensors for those rats. This might increase the sample size for the further training stages. Furthermore, if the forepaws are targeted for mechanical stimulation, a nose-poke sensor could be used instead of the middle lever.

In behavioral tasks, the control of the stimulus is critical [109]. A Fotonic sensor with a resolution of $\sim$30 nm to calibrate the vibrotactile stimulation system. In addition, the equipment used in this study is similar those used in neurophysiological experiments on anesthetized animals [64, 75] and human psychophysics experiments [98, 126]. However, the skin-contactor coupling held constant in these experiments since the human subjects are restrained or the animals are already anesthetized. The

effect of static indentation on responses of mechanoreceptive fibers and psychophysical thresholds is a well-known fact [129]. Therefore, it would be difficult to test the psychophysical responses of unrestrained rats at low intensity or difference levels with the current design. For this reason, high-level stimuli were used in this study and the static indentation (0.5 mm) was adjusted before each session. Furthermore, the mechanical impedances of the mechanical shaker and the probes were high enough to produce skin indentations set by the experimenter on the software. However, the loads generated by the animals, if any, were not controlled. These voluntary loads may have changed the skin-contactor coupling, and hence, effected the responses in some trials. Since each condition was tested in multiple trials, the behavioral responses (i.e., correct rates and conditional probabilities) may be expected to converge on an average value in long-term. The ROCs support this idea as the conditional probabilities accumulate in a region which might be showing the maximum level of association.

The multi-probe structure of the stimulating system, the stimulation of the glabrous skin was ensured regardless of the rat's location in the chamber. At least 3-4 probes were in contact with rat's one paw depending on the size of the paw. With the help of the circuit measuring the impedance change between the stimulating probes and the animal, the contact was clarified but measuring the stimulation area was not the focus of this study. However, it is possible to estimate the contact area using the impedance changes in each trial. This information may be used to study spatial summation in tactile psychophysical channels [130]. In addition, the circuit may be further developed to scan each probe separately in order to find the exact stimulation location on the skin.

2.5.2 Comparison with whisker stimulation

As the humans explore their environment with their hands and use touch for social interactions, the rats use their whisker to obtain a vivid model of their environment and interact with other rats. The importance of each individual whisker is represented by the size of cortical area reserved for them. The information mediated by each vibrissa is processed by a different cortical column called *barrel* [131]. Fur-

thermore, vibrissae are supplied by a complex sensorimotor network enabling rat to perform active touch on objects by moving individual whiskers [60]. Therefore, with such an elaborate organ, rats perform very well in tasks where their whiskers are stimulated [42, 44, 46].

On the other hand, the cortical representation of the entire hindpaw is smaller than the barrel field. Furthermore, according to the results of limited studies on cortical process of glabrous inputs in rats, computational capability of this region is inferior to the vibrissal system [132]. This might be one reason for why only 1/3 of the animals attended in vibrotactile detection task could perform correct rates >70%. On the other hand, 16 rats out of 36 had correct rates >85%. In the literature, rats performing correct rates >90% in a detection task based on whisker stimulation were reported. However, to my knowledge, there is not any comprehensive study reporting how many of the rats tested in such experiments could achieve that high accuracies.

It should be noted that some rats showed minor improvements while others performed at chance level after extensive training. Furthermore, the rats trained in auditory detection task could perform correct rates <85%. More importantly, most of the animals failed in Task-A and Task-B. Animals acquired from Vivarium's standard stock where the animals are bred in cages with minimal sensory stimulant. Environmental enrichment is an important factor in development of sensory systems [133]. Therefore, environmental enrichment targeting the somatosensory system may be helpful for improving animals performance during training. Furthermore, albinism, inbreeding and domestication have been shown to blunt learning and memory [134]. Wild rats captured from their environment would probably perform better than those bred in laboratory environment.

2.5.3 Vibrotactile sensitivity of rats

In humans, the sense of touch is conveyed by four psychophysical channels [105]. Although it is not clear whether the rats have these psychophysical channels or not, it is a known fact that they have mechanoreceptive fibers similar to those found in humans [71, 75]. In this thesis, mechanical vibrations were applied to the rat glabrous

skin at frequencies between 20-80 Hz. The stimulation probably activated many RA fibers mediated by Pacinian corpuscles and Meissner corpuscles because these afferents are sensitive to vibrations [70, 71, 74, 75]. However, contribution of other mechanoreceptive afferents should not be totally ignored.

Absolute spike threshold of RA and SAII fibers does not change too much between 20-80 Hz, but threshold of SAII fibers are higher than RA fibers ($\sim$4 times) [75, 90]. The threshold of SAI fibers are higher compared to RA fibers and increase as the frequency increase [90]. On the other hand, thresholds of PC fibers are considerably low compared to other fibers and decreases as the frequency increases. Therefore, different sets of mechanoreceptive afferents were activated during vibrotactile experiments. It is very likely that the detection probabilities at different amplitude levels during psychophysical testing were determined by the most sensitive mehcanoreceptive afferents at a given frequency. However, there is not a direct way to compare the thresholds of mechanoreceptive afferents with psychophysical thresholds. In literature, extensive studies were presented comparing neural thresholds with psychophysical thresholds [135, 136]. However, how the neural information from different submodalities contributes to the perception is still in debate [137, 138].

On the other hand, the 50% detection threshold of rats decreased as the frequency increased. The decreasing trend of detection thresholds is consistent with the literature [105, 139]. However, threshold levels measured in this study were higher than those reported by Mountcastle et al., 1972, who used method of constant stimuli to determine change of tactile sensitivity (50% detection threshold) with frequency in monkeys and humans. However, there are some methodological differences between the study of Mountcastle et al. and the current thesis. First of all, they tested primates whereas I used rats. Although both species have similar mechanoreceptive afferents, innervation density of these afferents would differ between species. Furthermore, the mechanical properties of the skin is an import factor on determining the thresholds of mechanoreceptive afferents [75]. Second, they restrained the subjects whereas the rats accompanied in the presented study are freely behaving. In humans, active or passive movements of the limb increases the vibrotactile detection thresholds in P-channel [140]. Therefore, voluntary movement of the rats would effect the detection thresholds. Finally, central saliency of glabrous touch in two species is probably different, because

primates are developed to use their hands to interact with their environment whereas rats use their whiskers or forepaws. Therefore, the psychophysical experiments might be conducted for forelimb stimulation for more comparable results. Nevertheless, the experiment presented here would help us to understand central processing of glabrous touch in awake freely behaving animals.

2.6 Conclusions

In this study, a novel vibrotactile operant conditioning chamber is presented. It enables stimulation of hindpaw glabrous skin of awake freely behaving rats with arbitrary waveforms. I used this chamber to train rats in a forced-choice yes/no detection task based on vibrotactile cues from their glabrous skin. Rats behavioral performances were comparable to those reported in whisker literature. However, only 16 rats out of 55 could completed vibrotactile detection task with correct rates >85%. Therefore, the number of animals planned for training should be at least 3 times the required sample size. I further tested the sensitivity of freely behaving rats with method of constant stimuli at four different frequencies. The decreasing trend of 50% detection thresholds was consistent with the literature whereas the thresholds were higher than those reported for monkeys and humans in the literature.

3. OPERANT CONDITIONING OF FREELY BEHAVING RATS WITH INTRACORTICAL MICROSTIMULATION IN HINDPAW REPRESENTATION OF PRIMARY SOMATOSENSORY CORTEX

3.1 Introduction

After the discovery of bioelectricity by Luigi Galvani in 1771 [141, 142], electricity have been widely used to poke the nervous system in order to reveal its functions in human behavior. In 1870s, Eduard Hitzig connected electrical batteries to the brains of soldiers with head injuries to *heal* them. In the same years, Gustav Fritsch observed muscle twitches when he electrically stimulated the cortex of dogs. In 1920s, Penfield started to study brains of epileptic patients with electrical stimulation [38]. With extensive studies, he mapped the sensory and motor regions in patients who were conscious during the surgical operations [93]. During his studies, the patients reported localized cutaneous or proprioceptive sensations when he electrically stimulated certain cortical regions (e.g., primary somatosensory cortex). Although, electrical stimulation of deep brain regions (called deep brain stimulation, DBS) is clinically used for the treatment of symptoms related to movement disorders (e.g., Parkinson's disease) [143] and depression [144], electrical stimulation of sensory cortices has recently attracted researchers in order to close the loop in brain-machine interfaces (BMIs), including neuroprosthetic devices [145, 146]. This enthusiasm also triggered many other studies on behavioral consequences of sensory ICMS [116, 147].

In this chapter, I studied the behavior of rats implanted with microelectrodes in a yes/no detection task based on ICMS trains delivered to the hindpaw representation in their SI. Therefore, I would like to present some background information on nervous tissue, electrode-tissue interfaces and electrical stimulation of the nervous tissue.

3.1.1 Nervous Tissue

According to the neuron doctrine, the nerve cells (or neurons) are the fundamental units for the structure and the functioning of the nervous system [142]. A generic neuron consists of three distinct structures; dendrites, the cell body and the axon (Figure 3.1) [148]. Dendrites are the input organelles of the neuron. They receive information from presynaptic neurons and transmit it towards the cell body (or soma). The soma is the control center as in all other cell types. It contains metabolic organelles, such as the nucleus and the endoplasmic reticulum, where the protein synthesis occurs. The axon is the output organelle of the neuron. It conducts the information coming from dendrites to the next neuron via axon terminals. However, the neurons may vary in shape and size depending on their function and location. For example, the pyramidal cells have many dendritic projections and a single axon projection from soma (multipolar cells). On the other hand, the sensory fibers conveying touch information from the skin has a single axonal projection which receives signals from mechanoreceptors in the skin at the one end and transmits the information to the next neuron at the other end.

The neurons conduct information as electrical currents from dendrites to the axon terminals where the electrical signals are transduced into chemical signals (Fig-

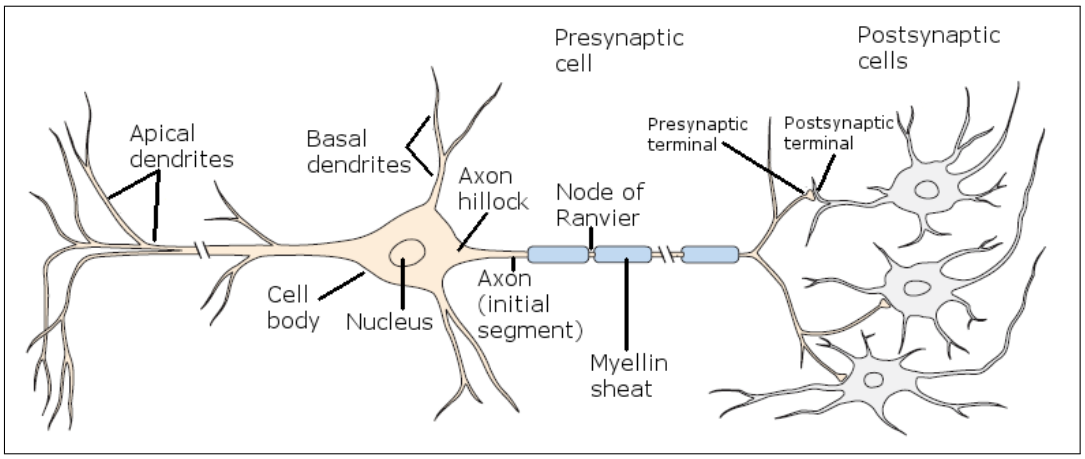

Figure 3.1 A generic nerve cell has three distinct regions: dendrites, the cell body and the axon. Dendrites receive information from presynaptic cells. The cell body contains the nucleus and other organelles required for protein synthesis. Axon transmits the information to the next cell via axon terminals. (Adapted from Figure 2-1 in Kandel et al., 2012 [148])

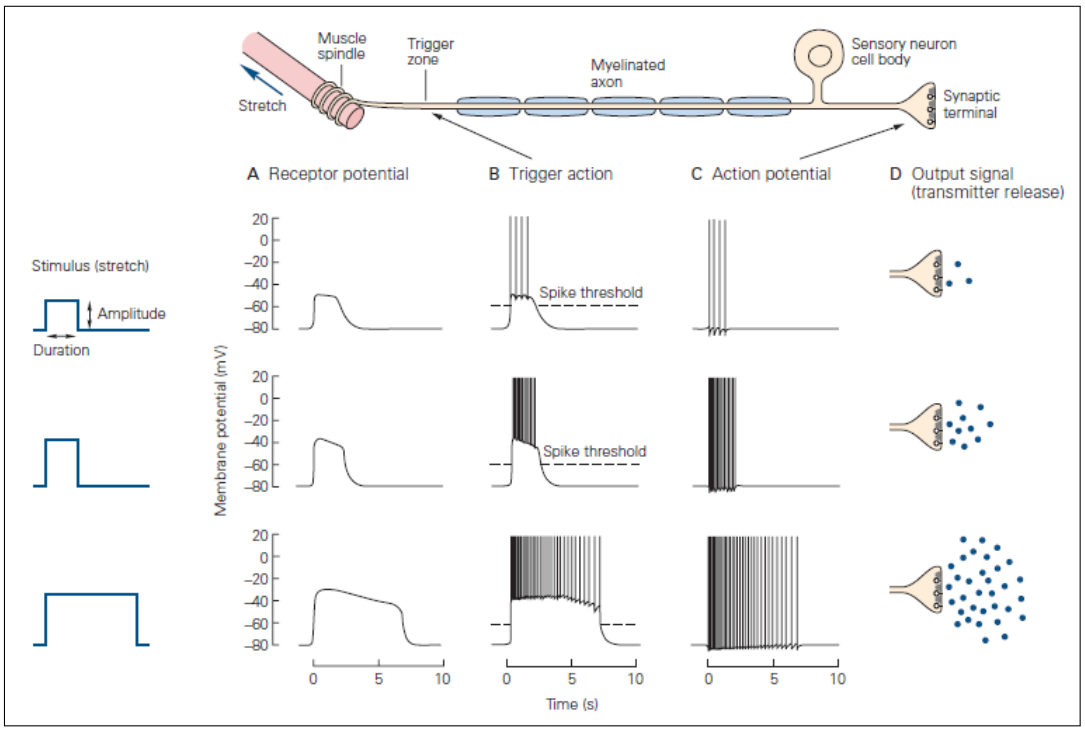

Figure 3.2 Signaling in the nerve cells. The information is propagated as electrical signals called action potentials on the axon. At the axon terminal, these electrical signals are transduced into chemical signals called neurotransmitters. [148]

ure 3.2) [148]. The communication between two neurons occurs with these chemicals called neurotransmitters. When a presynaptic neuron releases neurotransmitters from its axon terminal into the synaptic cleft, the dendrites of the postsynaptic neurons transduce chemical signals back into electrical signals. Transmission of information in electrical and chemical forms depends on the ion channels located within the cell membrane [149]. In equilibrium, inside of the nerve cell is more negative with respect to the extracellular environment due to the distribution of ions (Figure 3.3(a)) [150]. This resting membrane potential is around -65 mV. When the nerve cell is excited by either an electrical or chemical signal, ion channels open and cause a redistribution of ions between inside and outside of the cell (Figure 3.3(b)). This redistribution causes the membrane potential to drift away from its equilibrium. Ion channels can vary in their gating mechanism and selectivity to different ions. For example, voltage gated ion channels detect the potential changes on the membrane and allow the flow of ions through the cell membrane [149]. This type of channels generally accompanied during electrical transmission on the cell membrane. On the other hand, ligand gated ion

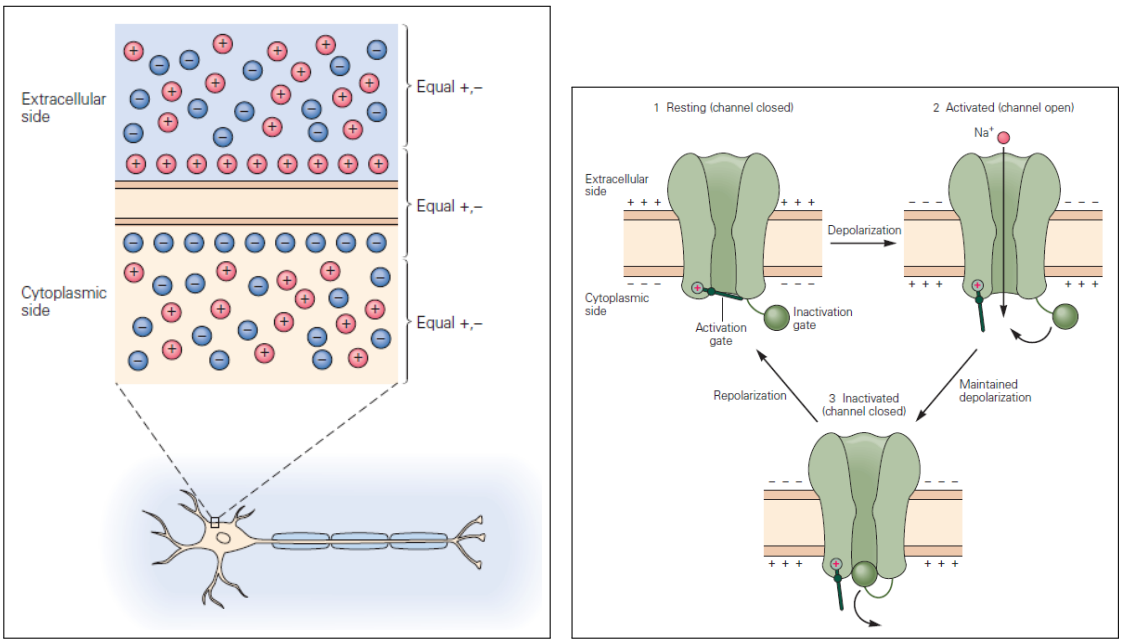

(a) (b)

Figure 3.3 Distribution of ions at resting state and functioning of ion channels. (a) At resting state, the inside of the cell is more negative due to the distribution of ions. [150] (b) When an ion channel is activated, it allows the flow of ions through the cell membrane. Then, they could be inactivated to stop ion flow. [151])

channels allow flow of ions in the presence of specific chemical compounds such as neurotransmitters. These type of ion channels are generally located in the synaptic cleft. Ligand gated ion channels on postsynaptic neuron detect neurotransmitters released by presynaptic neuron and change their state allowing flow of ions causing a change in the membrane potential. Some ion channels can be activated by mechanical stimuli (such as stretch of the cell membrane) or protein phosphorylation.

As mentioned previously, the chemical signals from a presynaptic neuron are transduced into electrical signals on the postsynaptic cell membrane. This electrical deflections in membrane potential are called postsynaptic potentials (Figure 3.4(a)). A postsynaptic potential can be either an increase (depolarization) or decrease (hyperpolarization) in membrane potential. The postsynaptic potentials that are more positive than the resting membrane potential are called excitatory postsynaptic potentials (EPSP). On the other side, the postsynaptic potentials that are more negative than the resting membrane potential are called inhibitory postsynaptic potentials (IPSP). These postsynaptic potentials spread from where they are initiated and travel through

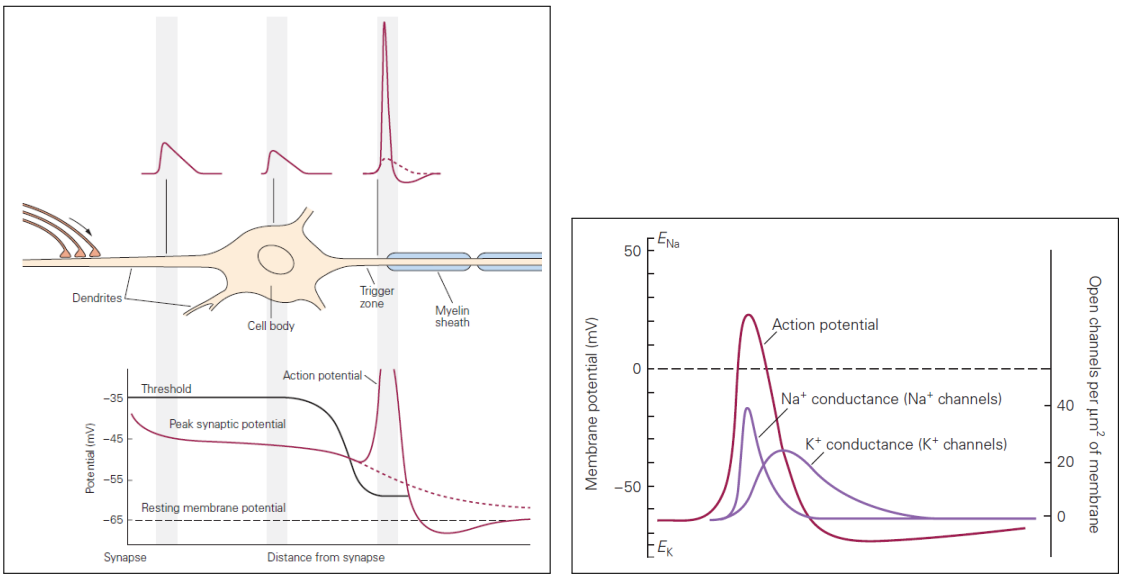

(a) (b)

Figure 3.4 Postsynaptic potentials and generation of action potential. (a) Postsynaptic potentials propagate through the cell membrane and reaches the axon hillock. If the net depolarization is high enough an action potential can be triggered. [152]. (b) Action potentials are generated by the sequential activation of Na^+ and K^+ channels. Opening of Na^+ channels cause the rush of Na^+ into the cell and the membrane potential increases. At some point, membrane potential starts to decrease, because K^+ channels are open and Na^+ channels are being inactivated. Adequate K^+ flow out the cell to reverse the effects of Na^+ influx. Finally, delayed inactivation of K^+ channels cause the hyperpolarization of the cell membrane. The membrane potential returns back to its resting state by active transport of ions between intracellular and extracellular environments. [151])

the cell membrane. Finally, they are summed up at the axon hillock which is the initial segment of the axon. If the net polarization is high enough, a brief electrical pulse called action potential (AP, or spike) is generated and transmitted through the axon (Figure 3.4(a)). Therefore, EPSPs increase the chance of generation of an AP, whereas IPSPs decrease the probability.

Action potentials are formed and transmitted by sequential activation of Na^+ and K^+ channels (Figure 3.4(b)). In the resting state, Na^+ and Cl^- ions are high in concentration outside the cell whereas concentrations of K^+ and organic anions (A^-) are high inside the cell [149]. When the net depolarization at the axon hillock exceeds a threshold, voltage gate Na^+ channels open and Na^+ rushes into the cell [151]. The sudden increase in Na^+ concentration in the cell cause the inside of the cell to be more positive (around +20 mV) with respect to the outside. At some point, the rate of depolarization decreases by inactivation of Na^+ channels and activation of K^+

channels. Activated K^+ channels cause the outward flow of K^+. Consequently, the membrane potential starts to decrease (repolarize). The repolarization is followed by a hyperpolarization of the cell membrane because of delayed inactivation of K^+ channels. After a while, the membrane potential returns its resting state by active transportation of ions between intracellular and extracellular space. The total duration of an AP is approximately 1 ms. After an AP is generated, the cell enters the refractory period lasting 5-10 ms where it is not possible to generate a second AP. The refractory period ends as the K^+ channels close and inactivated Na^+ channels recover.

Under normal circumstances, APs are initiated at the axon hillock and they propagate through the axon down to the axon terminal. It is also possible to initiate APs at any point on the axon by means of electrical stimulation. When an electrode located near the axon is electrically polarized, it depolarizes the cell membrane and causes voltage gated ion channels to open [153]. Consequently, an AP might be triggered if adequate number of ion channels are activated. The successful initiation of an AP by electrical stimulation requires an adequate amount of charge transfer between the electrode and the tissue.

3.1.2 Electrode-Tissue Interface

Different electrode types have been used to establish an interface between the neural tissue and an external device depending on the purpose of the application. Cuff-electrodes, for example, are used for recording and/or stimulating purposes on peripheral nerve bundles [154] whereas penetrating electrode arrays (e.g., Utah or Michigan arrays) are popular for recording from or stimulating ensembles of cortical neurons [155]. A single electrode is not adequate to record or stimulate the biological environment. Therefore, at least two electrodes are used: the electrode that is interested in study is called the active electrode and the other is the reference electrode for completing the electrical circuit.

When an electrode get in contact with body, which is an electrolytic environment, the ions inside the body are redistributed around the electrode (Figure 3.5(a)) [153]. A double layer is formed on the electrode surface by the redistribution of metal

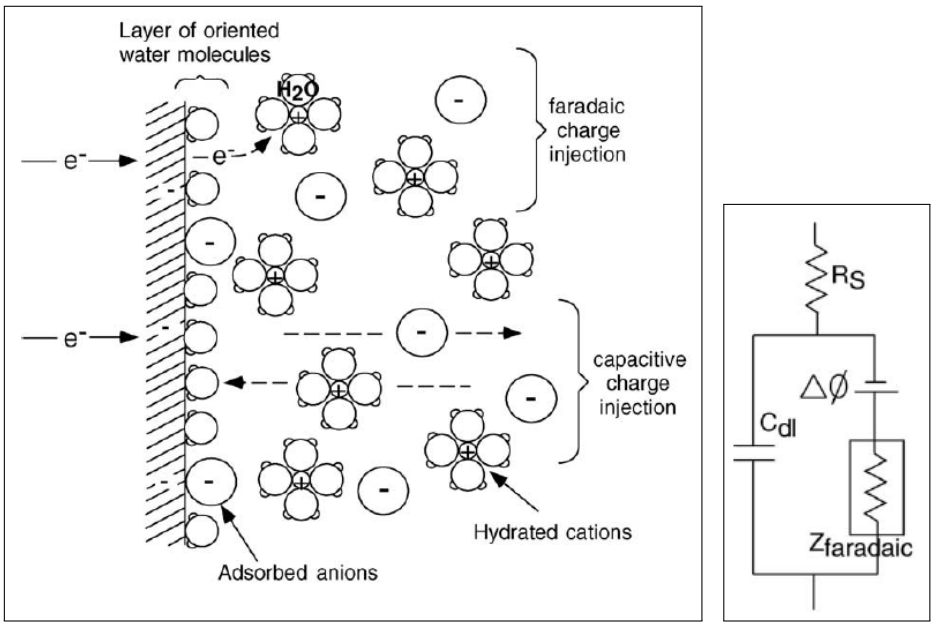

(a) (b)

Figure 3.5 Electrode-electrolytic interface. (a) When an electrode is immersed in an electrolyte, ions in the electrolyte are oriented around the electrode surface and forms a double layer structure. (b) The interface between the electrode and the electrolyte can be modeled with capacitive and resistive components. R_s is the impedance of the electrolytic, $\triangle\phi$ is the resting membrane potential, C_{dl} represents the capacitive charge transfer and $Z_{faradaic}$ represents the Faradaic charge transfer. [153]

ions, adsorption of some anions to the electrode surface and orientation preferences of polar molecules on the electrode surface (e.g., water molecules). This double layer structure behaves like a capacitor and keeps the interface at a constant electrical potential in equilibrium where there is no net charge transfer between environments. However, this potential may vary with the redistribution of ions in the tissue or current injection into the tissue by applying electrical loads between the working electrode and the counter electrode. For example, if the working electrode is located at a close proximity to an axon, redistribution of ions during action potential generation would cause this potential to drift away from its equilibrium and we could record the neural activity in this way [156]. On the other hand, when an electrical charge is applied between electrodes, a charge transfer occurs between the electrodes and the tissue causing the interface potential to shift from its equilibrium.

The charge transfer may occur through two different mechanisms; Faradaic charge transfer or non-Faradaic charge transfer [153]. Non-Faradaic (capacitive) charge transfer does not penetrate the double layer structure on the electrode surface but

only cause the redistribution of ions around interface; the electrode attracts oppositely charged ions and repels similarly charged ions. On the other hand, in Faradaic charge transfer, the charge carriers (electrons) in the electrode are transfered to the ions located near the interface. This may cause some reactions resulting in oxidation of some chemicals while reducing others and forming new compounds [153]. The products of these reactions may accumulate by time and might be damaging for the neural tissue if they are not reversed back into their initial forms. A reaction can be reversed if the direction of the charge transfer is reversed (e.g., inverting the polarity of electrodes). Yet some reactions are not reversible and continue to accumulate in the tissue. The reversibility of a reaction is determined by the material of the electrode and how far the potential of the interface is drifted away from its equilibrium [153].

In most cases, the electrical stimulation of neural tissue starts with the capacitive charge redistribution, and then, the Faradaic charge transfer occurs, because a high level of charge transfer might be required in order to obtain the desired effect (e.g., triggering action potentials on the axon or a behavior in the subject) [153]. Therefore, a stimulating neural interface can be demonstrated with parallel non-Faradaic (capacitance) and Faradaic (impedance) components in series with resistance of the electrolytic medium as measured between two electrodes (Figure 3.5(b)). In non-Faradaic charge transfer, the Faradaic impedance is infinitive and the interface is consisted of a capacitance. On the other hand, during Faradaic charge transfer, Faradaic impedance is low low enough to allow flow of electrons between two media. Therefore, if Faradaic reactions might not be avoided, then stimulation techniques and material of the electrode has to be chosen carefully for minimizing the damage to the tissue and the electrode.

3.1.3 Electrode Material

A stimulating electrode is expected to meet the following requirements [153];

- *Biocompatibility*: The material of the electrode should not be toxic for the tissue nor cause necrosis. In addition, it should minimize the foreign body response.

- *Mechanical flexibility*: The electrode should maintain its mechanical integrity during implantation. On the other hand, its flexibility is important not only for itself to withstand movements but also for minimizing the mechanical damage to the tissue.

- *Charge transfer efficiency*: The electrode should be able to deliver the required amount of charge for, for example, triggering spikes without causing Faradaic reactions.

- *Corrosion resistance*: The material should not corrode during Faradaic charge transfer.

- *Long term stability*: Impedance of the electrode and insulating properties should not vary in time.

Many materials have been reported as biocompatible, such as titanium, nickel-titanium alloy, platinum, platinum-iridium, polyimide and silicone [153]. On the other hand, copper, iron, silver and germanium are toxic and not used in electrodes. Although an electrode known to be biocompatible is placed in the nervous tissue, it would cause an immune response called foreign body response (FBR). Indeed, this reaction is due to the damage given to the tissue during insertion of the electrode and the rigid structure of the electrode compared to the tissue [35, 157]-[160]. FBR might be minimized by coating electrodes with drug-loaded nanoparticles slowly releasing their anti-inflammatory content into the tissue [158, 159] or by using flexible electrodes reducing the mechanical stress on the tissue [35, 160, 161].

The reversible charge storage capacity (CSC) of an electrode defines the capability of reversing the reactions occurred during Faradaic charge transfer [153]. Therefore, a high CSC is desired especially for chronic stimulation. Platinum, iridium, alloys of these two and iridium oxide provides a CSC value. Furthermore, these materials are resistive against corrosion.

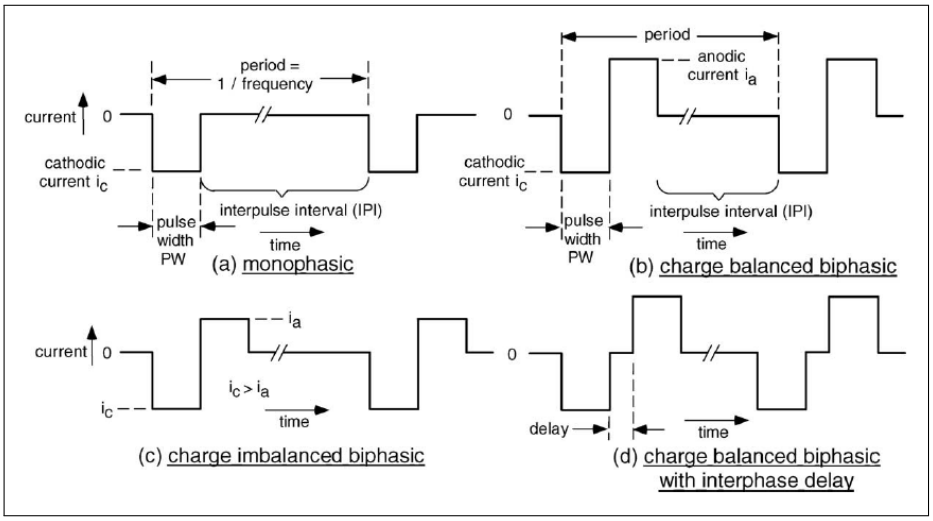

Figure 3.6 Waveforms used for electrical stimulation. (a) Monophasic stimulation: This method generally does not used, because it cause too much tissue damage due to non-reversed Faradaic reactions. (b,c) Charge-balanced and charge-imbalanced biphasic stimulation are used to reverse the Faradaic effects injected in the first phase. However, the second phase also reverses the physiologic effects of the first phase that is necessary for AP generation. (d) Placing a delay between two phases helps AP generation. [153]

3.1.4 Electrical Stimulation of the Nervous System

Current-controlled charge injection is the most widespread method used in electrical stimulation of nervous system [153]. In this method, the charge is delivered to the tissue by current pulses. The current level (measured in ampere) is monitored and kept constant during the pulse. Either monophasic or biphasic pulses have been used in the literature (Figure 3.6). In monophasic stimulation, either negative (cathodic) or positive (anodic) pulses are delivered to the tissue. However, this cause accumulation of products of Faradaic reactions, because these reactions are not reversed (see Section 3.1.2). On the other hand, both consecutive cathodic and anodic pulses are delivered to the tissue in the biphasic stimulation. In this way, some of the Faradaic reactions occured during the first phase might be reversed. Yet, this may reduce the efficiency of the stimulation in triggering spikes compared to the monophasic stimulation [153], because the second phase may reduce the effects of first phase by reversing the flow of some ions in the medium. In order to prevent this, the amount of current delivered in the second phase can be reduced (charge-imbalanced biphasic stimulation). Alternatively, a brief delay can be placed between the first phase and the second phase in order

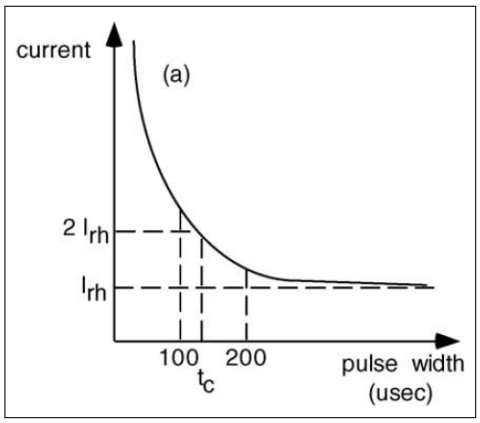

Figure 3.7 Current intensity-duration curve. The current intensity required to generate an AP decreases as the stimulus duration increases until the current intensity reaches a minimum called rheobase, I_{rh}. t_c is the chronaxy. [153]

to let the effects of first phase take place. This two methods can also be combined.

On the other hand, efficiency of current pulses to trigger APs decreases as the distance between the electrode and the neuron increases [153]. The relationship between the extracellular potential (V_e) created by electrical stimulation, the current level (I) and the distance (r) is shown by equation 3.1. Therefore, it is harder to elicit APs on neurons away from the electrode, unless the current level is not increased. However, increasing the current level behind a limit is not desired because of the possible damage to the tissue (see Section 3.1.2).

$$V_e = \frac{I}{4\pi\sigma r} \tag{3.1}$$

where σ is the conductivity of extracellular fluid.

The duration of the current pulse is important as well as the current intensity. There is a relationship between the duration a current pulse and its intensity in order to elicit an AP [153]. The required current intensity decreases as the duration increases until a minimum is reached for the current intensity which is called *rheobase* (Figure 3.7). This relationship can be defined by Lapicque (equation 3.2) or Weiss equations (equation 3.3) [162].

$$I_{stim} = \frac{I_{rh}}{1 - 2^{-\tau/\tau_{ch}}} \tag{3.2}$$

$$I_{stim} = I_{rh}\left(1 + \frac{\tau_{ch}}{\tau}\right) \tag{3.3}$$

where I_{stim} is the stimulation intensity, I_{rh} is the rheobase, τ is the stimulus duration, τ_{ch} is the chronaxy (the duration at which I_{stim} becomes twice the I_{rh}).

3.2 The Aim

In this chapter, it was aimed to train rats implanted with microelectrodes in a yes/no detection task based on microstimulation of hindpaw representation in primary somatosensory cortex (SI). Furthermore, I tested their sensitivity to intracortical microstimulation (ICMS) at different frequencies in psychophysical experiments. Psychometric curves obtained in these experiments were also used in Chapter 4 where we proposed a model for translation of vibrotactile stimuli into ICMS trains.

3.3 Materials and Methods

3.3.1 Animals

18 Wistar albino rats (8 females and 10 males) were implanted with microelectrodes (Table 3.1, also see Section 3.3.3). These rats were previously tested in vibrotactile experiments. However, 12 of these rats (4 females and 8 males) could be tested in following experiments, because some rats either couldn't recover from surgery or removed their implants. Among those 12 rats, 9 rats had completed vibrotactile detection task (Task-D) with accuracies >80%. Three female rats (Rats 32-34) had performed at chance level in Task-D but they were further tested in ICMS experiments.

As in vibrotactile experiments, water deprivation was used to motivate rats in behavioral tasks (see Section 2.3.1). Water was only available in the operant chamber while rats were performing the task. Rats were kept at >80% of their normal weights. Additional water was provided if their weight decreased more than 20%. Food was ad libitum in both home cages and the operant chamber.

All experiments were approved by the Boğaziçi University Institutional Ethics Committee for the Local Use of Animals in Experiments.

3.3.2 Apparatus

The operant chamber presented in Section 2 was used in the following experiments. Waveforms of ICMS were prepared in MATLAB and supplied to an analog stimulus isolator (Model 2200, A-M Systems, Sequim, WA, USA) via the analog output of the DAQ card. The analog stimulus isolator was used in voltage-controlled current supply mode to generate the current pulses. Impedances of implanted microelectrodes were measured with a microelectrode impedancemeter (Omega-Tip-Z, World Precision Instruments, Sarasota, FL, USA). Von Frey hairs were used to stimulate the skin for mapping cortical RFs during and after microelectrode implantation. Plexon's PBX preamplifier (Plexon Inc., Dallas, TX, USA) was used to amplify spikes from the headstage (E2b, Plexon Inc.) attached to the microwire arrays. A custom-made microelectrode amplifier was used to amplify spikes from single electrodes. Spikes were visualized on an analog oscilloscope and a speaker was used to hear neural activity.

3.3.3 Surgery and Microelectrode Implantation

Surgical anesthesia was induced with intraperitoneal (IP) injection of 65 mg/kg ketamine and 10 mg/kg xylazine. Pedal withdrawal and eye blinking reflexes were controlled during the surgery to determine anesthesia level and to supply additional doses (1/3 of the induction dose) if necessary. Rats were placed on a thermostatically controlled heating pad (TCAT-2LV, Physitemp Instruments, Clifton, NJ, USA) and rectal temperature was kept at 37 °C. Atropine (0.05 mg/kg, IP) was injected in order to reduce bronchial and oral secretion and to prevent bradycardia. Furosemide (2 mg/kg, IP) and mannitol (0.2 g/kg, IP) were used to prevent brain edema and decrease intracranial pressure. Diclofenac (5 mg/kg, subcutaneous (SQ)) was injected before the surgery and repeated in every 4 h to relief the pain. Cephalexin (15 mg/kg, SQ) was

injected in every 12 h to prevent any infections. Analgesic and antibiotic injections continued for the first 3 days of the surgery. After all injections were done, animals were placed on a stereotaxic frame and the scalp was open. Bregma and lambda were located and craniotomy sites were determined based on a rat brain atlas [163].

Five rats (Rats 30, 32-34 and 69) were implanted with single Teflon-insulated tungsten microelectrodes (diameter: 80 μm, blunt-tipped). Other rats were implanted with Teflon-insulated platinum/iridium (90/10%) microwire arrays (array size: 4×4, distance between wires: 250 μm, microwire diameter: 25 μm,) (Plexon Inc., Dallas, TX, USA). A 2×2 mm craniotomy was open on the hind limb representation in SI for both single electrode and electrode array implantations. Dura was removed carefully. For the rat implanted with single electrodes, a hole on the forelimb representation in the agranular lateral cortex was open for implanting the control electrode [96]. Stainless steel screws were mounted on the skull for securing the implant and connecting the ground wire of the electrodes. Before inserting electrodes, the cortex was mapped with a single microelectrode while the skin was tapped (Figure 3.8). Microwire array was positioned so that most of the electrodes were on the cortical regions with RFs on the hindpaw glabrous skin. Some of the electrodes were intentionally positioned out of the sensory region as control electrodes for ICMS experiments. Electrodes were positioned at a depth where amplitudes of spikes elicited by tapping of hindpaw glabrous skin were the highest. After insertion of the electrodes, each electrode's RF was mapped using von Frey hairs. Muscle projections of the electrodes were also mapped by injecting single cathodic current pulses (pulse width: 600 μs, 40 μA). Any observable muscle twitches were mapped. The electrodes were fixed with dental acrylic. The scalp was sutured and antibiotic ointment was applied. Rats were kept on heating pad until they started to move, and then, they let to recover in their home cage for at least one week. Impedances and RFs of electrodes were controlled periodically. RF checks performed once in a week. Impedance measurements were done before and after each ICMS session. Before ICMS experiments, one of the electrodes was chosen as sensory ICMS channel. This electrode had a proper RF on the sole of hindpaw and showed the strongest multiunit response for tapping on its RF compared to other electrodes. Another electrode which was unresponsive to touch and elicited vibrissal or forelimb muscle twitches when electrically stimulated was chosen as the control electrode.

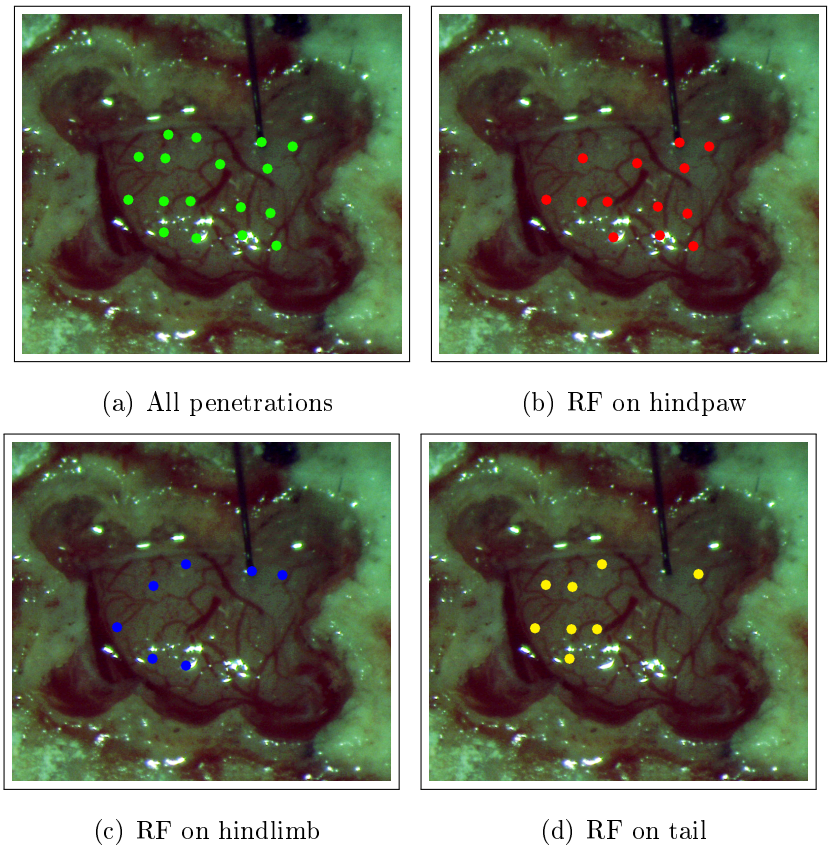

(a) All penetrations (b) RF on hindpaw

(c) RF on hindlimb (d) RF on tail

Figure 3.8 RF mapping of cortex before electrode implantation. (a) All penetrations performed for mapping cortex. (b) Penetrations where tapping of hindpaw glabrous skin elicited spikes. (c,d) Locations responsive to hindlimb and tail tapping, respectively.

3.3.4 Operant conditioning with ICMS

Rats were conditioned to perform a detection task based on ICMS (Task-E) as in Task-D (see Section 2.3.4). There was not any additional task between Task-D and Task-E except vibrotactile psychophysical experiments. In brief, the rat initiated a trial by pressing middle lever. The middle LED was turned on for 0.6 s. During this period the ICMS was presented or not. The rat was rewarded if it pressed right lever for stimulus condition and left lever for no-stimulus condition. Otherwise, no reward was presented and the error signal occurred.

The ICMS was a train of biphasic charge-balanced current pulses (cathodic phase leading, phase duration: 600 μs, inter-phase interval: 53 μs) presented at 40 Hz for 0.5 s (Figure 3.9). The intensity level was initially kept low ($\sim$20μA) and increased if the rat did not show any improvements in its performance. The charge intensity

delivered in a single phase was ranged between 24-60 nC for single microelectrodes and 12-90 nC for microwire arrays.

At the end of each session, percentage correct rate and conditional probabilities ($p(h)$ and $p(f)$) were recorded. The criteria for moving in psychophysical experiments with ICMS (*Experiment II*) were as following;

- The average of the percentage of accuracies in the last five sessions had to be >85% and did not show an improving trend (tested with *Kendall's* τ test).
- Conditional probabilities (hit rate, *p(h)*, and false alarm rate, *p(f)*) had to be with in mean±0.1.

If a rat's performance was still increasing, it was further tested until its accuracy showed no trends according to *Kendall's* τ test. Receiver operant characteristics (ROCs) were plotted based on conditional probabilities recorded in successive sessions to visualize the second criterion.

Rats were further tested in an additional session where the ICMS was delivered to the control electrode located in the agranular cortex (see Section 3.3.3). Percentage

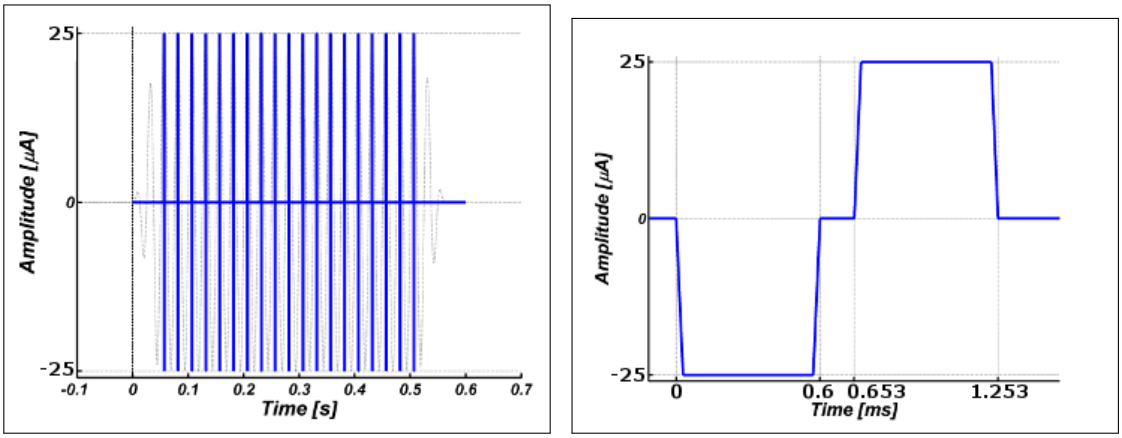

(a) (b)

Figure 3.9 ICMS package. (a) ICMS consisted of burst of current pulses delivered at 40 Hz. Dashed sinusoidal line is shown for comparison of vibrotactile and ICMS packages. (b) Current pulses were biphasic and charge-balanced. Cathodic phase was leading. Phase duration was 600 μs and inter-phase interval was 53 μs.

correct rate was recorded at the end of session to compare with somatosensory ICMS sessions.

3.3.5 Experiment II: Psychophysical testing with ICMS

9 rats successfully completed Task-E were further tested in psychophysical experiments where their sensitivity to ICMS trains at different frequencies were measured (Table 3.1). Experiment II was similar to the Experiment I (see Section 2.3.5). 6 amplitude levels (1.4-150 μm) were tested at 3 different frequencies (40 Hz, 60 Hz and 80 Hz). Each condition was tested 4 times. At the end of each session corrected hit rates were calculated from $p(h)$ and $p(f)$ using equation 2.2. Corrected hit rates were plotted and fitted with a sigmoid curve (equation 2.3) to obtain psychometric functions. The amplitude levels corresponding to 50% detection probability were estimated from psychometric functions. Since sample sizes were not large enough, effect of frequency on 50% detection thresholds were tested with non-parametric Kruskal-Wallis test.

3.4 Results

3.4.1 Condition of microelectrodes

Figure 3.10 shows the location of microwire array in the cortex and tactile RF of each electrode on the array in Rat 51. The figure shows the RFs on the day of implantation. In most cases, the amplitudes of the spikes drastically decreased in one week and sometimes lost (Figure 3.11). In those cases, RFs were mapped based on the compound neural activity while tapping the skin. Only in one rat (Rat 51), I observed the RFs shifted from hindpaw to the upper extremities, such as forepaw. These were the electrodes not used for ICMS stimulation. However, these changes didn't effect the behavior of the rats in behavioral experiments (see Section 3.4.2).

Electrode impedances were periodically measured at 500 Hz. The electrode impedances decayed over a time and stayed relatively stable until the end of exper-

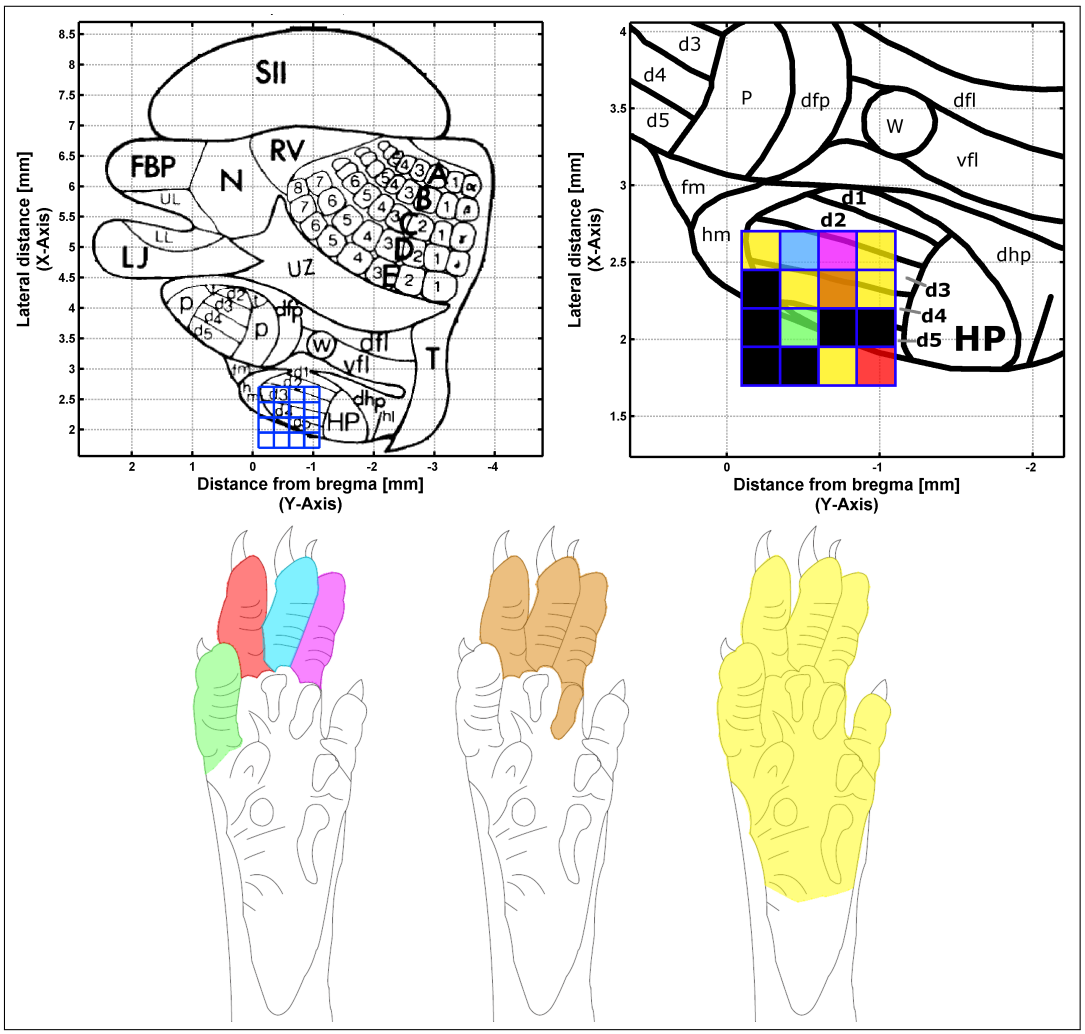

Figure 3.10 Implantation of microwire arrays in hindlimb representation of SI and RF mapping. Location and RF structures of microwire array in SI of Rat 51. Top left figure shows the structure of somatosensory cortex in rats [95] and the location of array (blue square). Right top figure shows a close up illustration of electrode location. Tactile RFs are color-coded. Black indicates no spikes related with tactile stimulation were observed. FBP: furry buccal pad, N: nose, RV: rostral small vibrissae, A-E: rows of barrels (barrel cortex), UL: upper lip, LL: lower lip, LJ: lower jaw, UZ: zone unresponsive in anesthetized recordings, p: palm, t: thumb, d2-5: digits of forepaw, dfp: dorsal forelimb, w: whiskers on wrist, dfl: dorsal forelimb, vfl: ventral forelimb, T: trunk, fm: forelimb muscle, hm: hindlimb muscle, d1-d5: digits of hindpaw, HP: hindpaw, dhp: dorsal hindpaw, hl: hindlimb.

iments. Figure 3.12 shows the change of impedances over time for pre-stimulus and post-stimulus (after an ICMS session) conditions in 2 rats. The effect of ICMS on impedances of microwire electrodes varied rat to rat. In 4 rats (Rats 44, 47, 51 and 56), the post-stimulus impedances were significantly lower than their pre-stimulus conditions (paired t-test, $p<0.01$). On the other hand, ICMS had no significant effects on impedance in Rats 55, 65 and 68. Only int Rat 67, post-stimulus impedance values were significantly higher than pre-stimulus impedances (paired t-test, $p<0.01$). Since

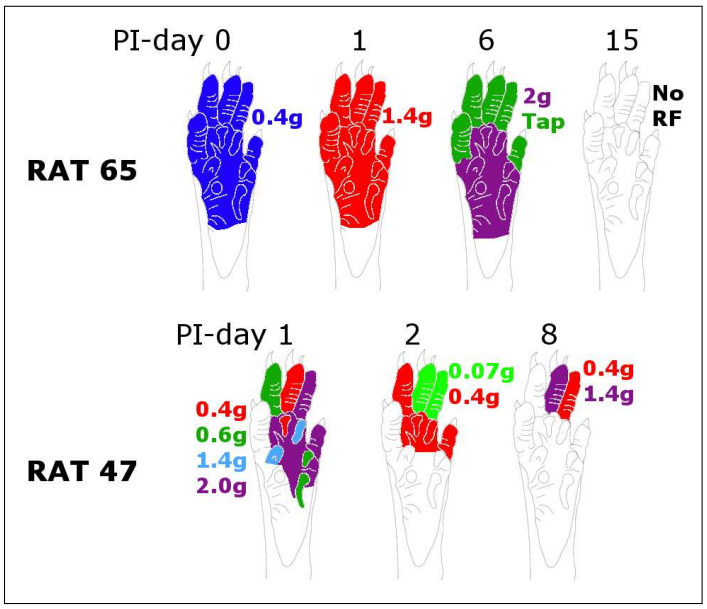

Figure 3.11 Change of RF structures in Rat 65 (electrode #:4) and 47 (electrode #:1). The skin was stimulated with different von Frey hairs with different gram-forces. RF and force of von Frey hair were color coded. PI-day: postimplantation day.

the impedance values were too low for single microelectrodes, post-stimulus impedance measurements were not done.

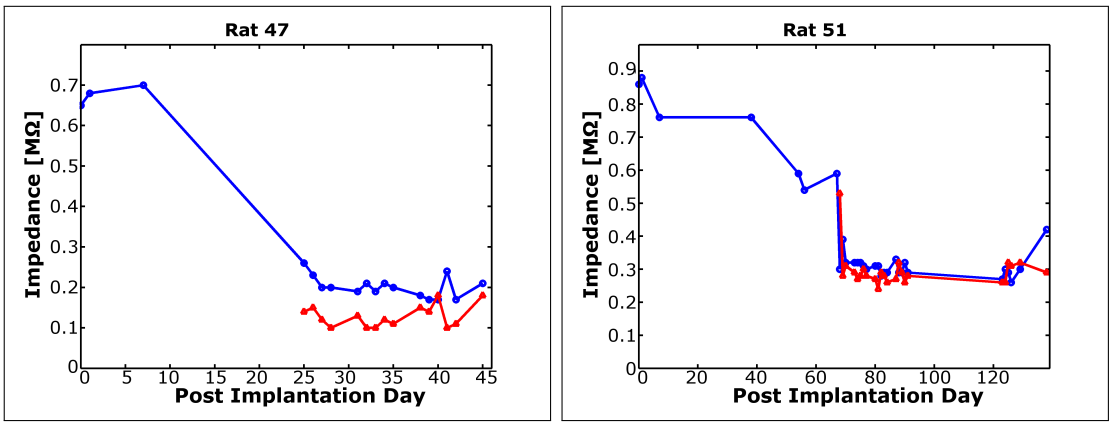

Figure 3.12 Change of electrode impedances. Blue data points shows pre-stimulus impedances. Red data points show post-stimulus impedances.

Table 3.1
Rats tested in ICMS experiments. Task-D: Vibrotactile detection task. Task-E: ICMS detection task. Experiment II: ICMS psychophysical testing. +: Missing repetitions due to implant drop, ++: The rat successfully completed the task. N/A: data is not available either due to behavioral criterion or implant drop.

Rat ID	Sex	Task-D	Task-E	Experiment II
30	F	86.2%	*Removed its implant.*	
32	F	48.6%	93.6%	N/A
33	F	52.2%	96.4%	N/A
34	F	56.0%	*The rat didn't perform.*	
38	F	85.4%	*Removed its implant.*	
39	F	85.9%	*Poor perfomance in Task-D after surgery*	
40	F	86.6%	*Died in surgery.*	
44	F	90.2%	94.0%	++
47	M	80.6%	90.0%	+
51	M	86.8%	95.4%	++
55	M	90.0%	90.2%	+
56	M	90.0%	94.6%	++
59	M	92.0%	*Died in surgery.*	
65	M	95.6%	93.0%	+
66	M	88.4%	*Died in surgery.*	
67	M	89.4%	92.2%	++
68	M	91.6%	89.6%	++
69	M	86.6%	86.9%	++

3.4.2 Behavioral training with ICMS

Some rats successfully completed vibrotactile experiments (i.e., Task-D) couldn't be tested in ICMS detection task (Task-E), because some died in implantation surgery and others removed their implants (Table 3.1). All rats but one tested in ICMS detection task performed accuracies >85% (Table 3.1, Figure A.9). Only Rat 34 did not perform the task with head-cable attached to the electrodes. On the other hand, Rats

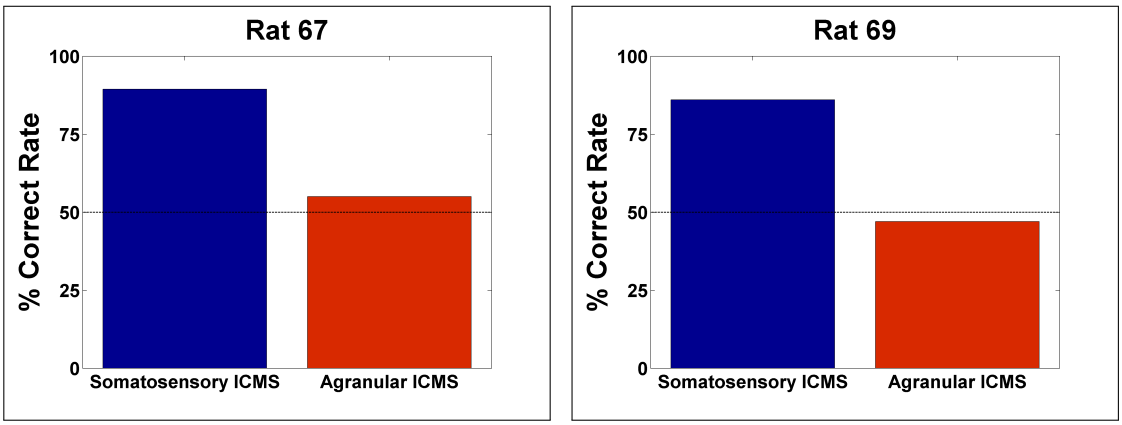

Figure 3.13 Accuracies in ICMS control sessions. Rats performed correct rates >85% in somatosensory ICMS but their accuracy was at chance level (∼50%) when ICMS delivered to the control electrode placed in agranular cortex.

32 and 33 who performed at chance level in Task-D had correct rates >90% in Task-E. The rats acquired the ICMS detection task within a maximum of 22 sessions. ROC curves were similar to those obtained in vibrotactile experiments (Figure A.10). Rats were more likely to start Task-E with no-bias in their responses. 7 rats started from a point close to the center of the ROC. On the other hand, Rat 32 was started with a bias for reporting stimulus while Rats 56 and 67 had a bias for reporting no-stimulus in their first few sessions. Only Rat 33 started with a high $p(h)$ and low $p(f)$ compared to others and performed 99% correct rate in its 4th session (Figure A.9). In control sessions where the ICMS delivered to the control electrode placed in agranular cortex, rats performed at chance level (∼50%) (Figure 3.13). Therefore, rats were utilizing the elicited sensations by ICMS in SI rather than using other cues due to the spread of the current.

3.4.3 Sensitivity of rats to ICMS

Figure 3.14 shows the psychometric curves for ICMS detection at frequencies 40 Hz, 60 Hz and 80 Hz. For a given current intensity, detection probability increased as the frequency increased. Generally, this trend was more obvious for the amplitude levels close to the upper asymptote of the sigmoid curve. 50% detection thresholds showed a decreasing trend almost for all rats (Figure 3.15(a)). Two rats (Rats 67 and

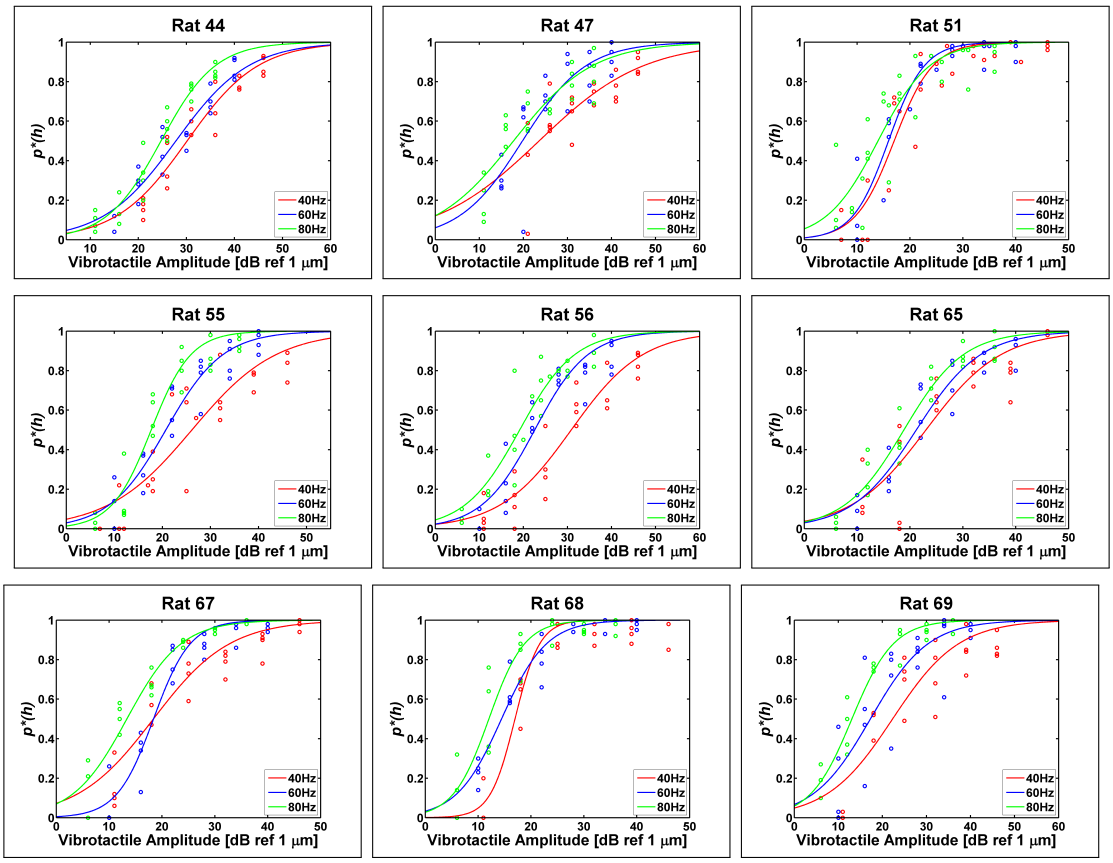

Figure 3.14 ICMS psychometric curves. Data points (open circles) from each frequency is fitted with separate sigmoid curves (solid lines). Red: 40 Hz, blue: 60 Hz, and green: 80 Hz.

68) had similar thresholds for 60 and 80 Hz whereas detection threshold of Rat 51 was higher at 80 Hz with respect to 60 Hz. In average, the detection thresholds were 22.48 ($\pm$2.51) dB ref 1μA for 40 Hz, 19.34 ($\pm$2.46) dB ref 1μA for 60 Hz and 18.23 ($\pm$2.25) dB ref 1μA for 80 Hz (Figure 3.15(b)). However, this decreasing trend was not statistically significant (Kruskal-Wallis test, $p > 0.05$).

3.5 Discussion

3.5.1 Receptive fields and impedance of microelectrodes

Receptive field structures of microelectrodes changed dramatically in the first few weeks. This is most probably related to the foreign body response of the tissue

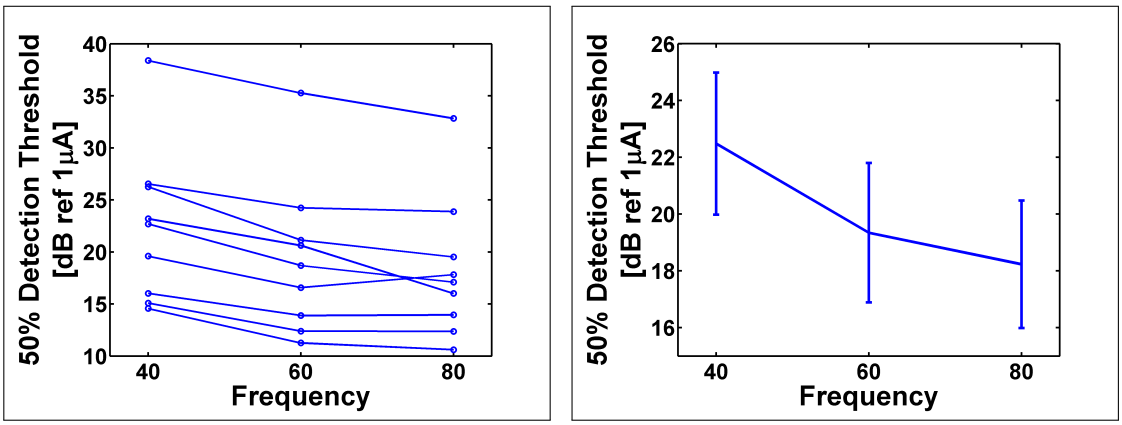

(a) (b)

Figure 3.15 Sensitivity of rats to ICMS. (a) 50% detection thresholds of each rat at different frequencies. (b) Mean detection thresholds. Vertical lines shows the standard error.

in addition to the effects of ICMS [160]. The decline in the spike amplitudes and loss of activity are known phenomenons in the literature even in the absence of microstimulation [160]. Due to the initial damage given to the tissue during implantation and consequent damages during the movement of the tissue relative to the implants, an immune response occurs by the accumulation of glial cells (i.e., astrocytes) around the electrode [160, 164]. By time, astrocytes may form a capsule around the electrode reducing the signal quality. Furthermore, the cortical atrophy may occur [165]. On the other hand, in the literature, it has been shown that low current levels ($\sim$5 μA) do not have detrimental effects on the cortical receptive fields or responsiveness of cortical neurons to tactile stimulation [166]. In addition, Rajan et al. reported that ICMS stimuli up to 100 μA caused no damage or minimal damages to the tissue [165]. However, they did not reported the condition of neural activity. Even a minimal scar tissue at the tip of electrodes may reduce the amplitudes of spikes by interrupting electrode-tissue interface. Despite all, the performance of the rats does not show any obvious changes in behavioral experiments as reported in the literature [165, 167].

The initial changes and the later stability of the electrode impedances were consistent with the literature [168, 169]. The initial increase in the impedance for the first few days is assumed to be representation of acute response of the glial tissue to the damage given during insertion of the electrodes [168]. The effect of ICMS was differential in the experiments presented here. It caused decrement of impedances in some

rats or caused no effects on other. Only in one rat, post-stimulus impedance values were higher than pre-stimulus conditions. Nevertheless, impedances usually recovered to their pre-stimulus values before the next session. Chen et al. reported a decrement in post-stimulus impedance values for all the conditions they tested [168]. However, the rate of decrement was varying depending on the charge per phase delivered by the stimulus and was not always significant. They reported higher intensity levels caused higher decrements in the impedance at the beginning of the experiments, but this effect decreased by the time as the impedance levels are stabilized. However, this decrement in the effect of ICMS was due to the rate of impedance recovery between sessions. The ability of the impedance values to recover their pre-stimulus conditions seems to be decreases as the stimulus regime accompanies high charge deliveries. This might be the reason why I did not see decrements in some rats where the impedance levels might be reached this minimum level. On the other hand, electrical stimulation may also cause changes in properties of the electrode such as the insulation. However, it should be noted that this minimum impedance value has nothing with the functioning of the electrodes from a behavioral point of view, because rats continued to perform the tasks with no obvious decline in their behavioral performances.

3.5.2 Operant conditioning with ICMS

Compared to Task-D, rats acquired the Task-E faster. Their previous experience in Task-D might contribute to a faster association in Task-E. Nevertheless, two rats which performed poorly in Task-D achieved high correct rates within very short time. Electrical stimulation elicits highly regular and periodic firing patterns in the cortex [147, 170]. On the other hand, natural stimulation cause irregular responses in the cortical neurons [132, 171]. Therefore, ICMS might present a more salient sensation compared to the natural one [172].

The rats trained to detect ICMS in SI were further tested in additional sessions where the ICMS was delivered to a control electrode which was located outside the SI. In these sessions, rats performed at chance level ($\sim$50%). These results were consistent with the literature [116]. Rousche et al. trained rats to detect ICMS stimulis delivered

to their auditory cortex. The rats performed poorly when the ICMS was presented to visual cortex. Therefore, the rats associates the specific artificial sensations elicited by ICMS rather than utilizing cues due to the spread of the current on the cortex.

I used a longer phase duration (600 μs) compared to literature where phase durations of 200-250 μs were usually used [36, 116, 169, 173]. The reason was that; the output of the current source rose exponentially and couldn't reach the desired current level within 200 μs due to the capacitive effects of the stimulation system (custom-made electrode channel distributor box and the head cable). 600 μs was adequate to see the plateau on the current pulse. Increasing the phase duration is shown to cause a decrement in the current levels required for detection [111, 170]. On the other hand, the total charge delivered to the tissue increases with increasing phase duration. Koivuniemi and Otto reported that the relationship between the phase duration and the detection threshold was highly linear [111]. According to their findings, with a 600 μs phase duration, a 30 nC of charge intensity was required for a detection probability of 0.5. However, during ICMS conditioning in Task-E, the maximum charge intensities were between 24-60 nC for single electrode implanted rats and 12-90 nC for microwire array implanted rats. It should be noted that, 90 nC was used only for one microwire implanted rat as an extreme case while charge intensities were $<$24 nC for other rats. Furthermore, the current levels required to elicit behavioral responses were highly variable from rat to rat. Electrode properties (e.g., diameter, exposed area and material) and electrode location (e.g., the depth and the proximity to neurons) are important factors for determining the behavioral effects of an ICMS regime [111]. In addition, in the literature, it is shown that even in the same animal implanted with microelectrode arrays, different electrodes may yield different sensitivities to ICMS [167].

3.5.3 Sensitivity of rats to ICMS

Rousche et al. applied ICMS trains (biphasic, cathodic phase leading, phase duration: 250 μs, frequency: 150 Hz) into the auditory cortex of rats performing a detection task similar to Task-E. They reported 50% detection thresholds ranging from 16.7-69.2 μA in rats with a mean of 42.4 μA. These thresholds were higher than

the mean detection threshold (∼8 μA) obtained in Experiment II (see Section 3.4.2). However, the differences might be attributed to the electrode properties (electrode diameters: 50 μm for Rousche et al. and 25 μm for this thesis) when the charge densities are regarded and the differences in cortical organization [174].

Detection thresholds showed a decreasing trend with increasing stimulus frequency which is consistent with the literature [111, 170]. Cortical neurons are suggested to integrate the ICMS-elicited activity over time, and consequently, the perceived intensity may increase with increasing frequency [175]. However, the increased sensitivity at higher ICMS rates may not be completely attributed to the temporal integration. Romo et al. showed that monkeys can discriminate frequencies of vibrotactile and ICMS stimuli [147]. Therefore, periodicity of ICMS affects the qualitative aspects of the perceived sensations (e.g., the intensity and the periodicity). Furthermore, ICMS detection thresholds were shown to plateau at frequencies >80 Hz in rat auditory cortex [111] and frequencies >250 Hz in monkey SI [170]. Although I did not test the frequencies >80 Hz, the small difference between the thresholds for 60 Hz and 80 Hz (relative to the difference between 40-60 Hz) may be attributed to such a plateau effect of the frequency. Yet, whether the detection thresholds for SI electrical stimulation in rats would plateau or not at higher frequencies has to be tested in further experiments.

Callier et al., 2015, reported improvements in ICMS detection thresholds of monkeys over time [167]. This improvement almost took 40 weeks, and then the thresholds were stabilized. They discussed whether this improvement was due to a better association in the task or any improvement in recognizing the elicited sensations by ICMS. My experiments were conducted in a shorter period of time compared to Callier et al.'s study and I did not observe any improvements in the performances of the rats during ICMS psychophysical experiments.

3.6 Conclusions

All rats tested in ICMS detection successfully performed accuracies >85%. Rats associated the task faster than they do in vibrotactile detection training. This might be attributed to their previous experience with vibrotactile experiments or increased

saliency of ICMS compared to vibrotactile stimulation. Furthermore, rats couldn't perform the task based on ICMS delivered to a different cortical region (i.e., agranular cortex). This is showed that somatosensory ICMS elicits associable discrete sensations. Detection thresholds showed a decreasing trend as the frequency increased which is consistent with the literature.

4. PSYCHOMETRIC CORRESPONDENCE BETWEEN THE SENSATIONS ELICITED BY VIBROTACTILE STIMULATION OF THE GLABROUS SKIN AND MICROSTIMULATON OF THE PRIMARY SOMATOSENSORY CORTEX IN RATS

4.1 Introduction

The brain consists of complex networks of functionally organized populations of neurons. This highly interconnected network structure establish the fundamentals of the behavior (i.e., perception, cognition and action). However, the integrity of the nervous system might be interrupted in some cases such as traumatic spinal cord injury or Parkinson's disease. In these cases, the brain can be coupled with external devices for therapeutic purposes using neural interfaces. In this way, the intents of the nervous system can be estimated, and based on these estimations, the external devices can be controlled [22]. Alternatively, activity of a particular neural population can be monitored and regulated by the external device if necessary [143]. In the literature, different neural interfaces have been proposed that is either unidirectional (from or to the nervous system) or bidirectional (from and to nervous system) depending on the application.

4.1.1 Neural Interfaces

A neural interface can be defined as the medium where the communication between the neural system (e.g., a single neuron or a population of neurons) and an external device (e.g., an amplifier or a robotic arm) occurs (Figure 4.1). The most common known neural interface is the brain-machine interfaces (BMIs). The principle of BMIs is to record neural activity and interpret the data to produce a desired

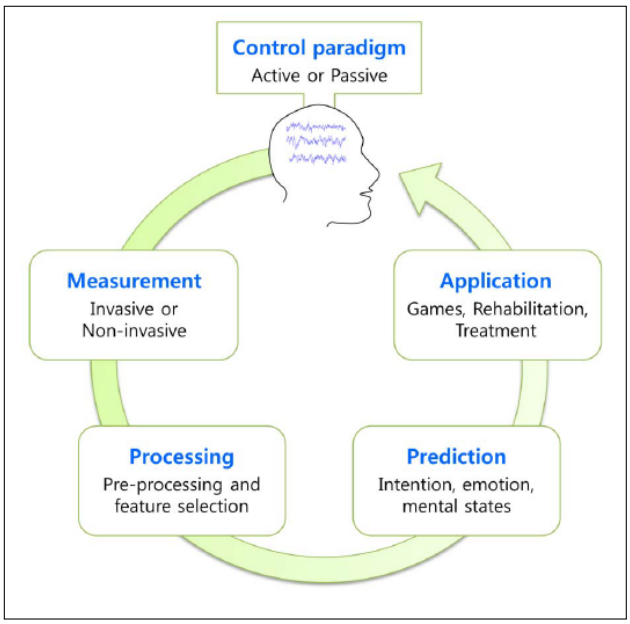

Figure 4.1 Neural interfaces. A neural interface is the medium where the communication between the nervous system and an external device occurs. [176]

outcome such as moving a cursor on the screen. The wide spread of BMIs promoted the use of different techniques in different applications varying in range from scientific experiments to gaming [146, 176].

There are different methods for recording neural activity in the brain varying in their temporal and spatial resolution and invasiveness [177]. The most common technique for capturing the brain activity is the electroencephalography (EEG), because it is non-invasive (not penetrating the body) and practical to apply [178]. In EEG, electrical signals produced by the population of neurons are captured from the surface of the scalp via surface electrodes. Therefore, the signals recorded in this way are very susceptible to electrical noise and artifacts due to muscle movements. In order to improve the signal quality (i.e., signal-to-noise ratio), EEG electrodes can be placed directly on the surface of the brain which is called electrocorticography (ECoG) [179]. Yet, the spatial resolution of these techniques are very low. In those applications requiring control of multiple degrees of freedom, the neural activity is recorded with penetrating electrodes in the form of action potentials (AP or spikes) [24]. The spike trains recorded from hundreds of neurons are supplied to a decoder which extracts the data required to drive an external device. However, this method is highly invasive and require professional care during and after the implantation operation.

Peripheral neural interfaces are also used to control external devices, such as robotic hands [37, 180]. Spike trains recorded from individual motor fibers or compound action potentials recorded from a bunch of neuron are used to control robotic hands. However, this method is requires invasive implantation of either cuff, intrafasicular or penetrating electrode arrays into the peripheral nerve bundles. On the other hand, it is not always necessary to implant electrodes in the nerve bundle to record neural activity, but muscles can be used to command external devices since they act like biological amplifiers [181]-[183].

Although neural interfaces are usually considered as one-directional devices (e.g., from brain to machine), an awareness has been raised to close the sensorimotor loop by implementing sensory feedback mechanisms in these application [146, 154, 177, 184, 185]. The idea is to feedback information from sensors placed on the external device into the sensory regions of the brain while driving these devices based on the brain's motor intentions. Thus, researchers aim to find a more efficient and naturalistic way to control external devices. Transcranial electrical stimulation (TES) or transcranial magnetic stimulation (TMS) are two non-invasive methods for modulating the neural activity in the brain [177, 178]. However, the stimulus, which is electrical current for TES and magnetic field for TMS, is not focal and effects a very broad region (e.g., the entire primary visual cortex) [178]. On the other hand, ECoG electrodes can be used to deliver electrical stimulus into a more local region [169], but their resolution can not reach to that of penetrating microelectrode arrays [186]. Optogenetic techniques can also be used to elicit artificial sensation [113]. However, their application in humans seems to be a long term outcome with many ethical debates on genetic modification of human nervous system. For peripheral nerve fibers, similar electrodes are used for both recording and stimulating [154, 157, 182, 187]. However, extra care has to be taken to prevent excitation of nociceptive (pain related) fibers. Furthermore, during the electrical stimulation of the nervous tissue (both the central regions and peripheral nerves), the current spreads through the tissue and may interfere with recording system. Therefore, artifacts due to stimulation has to be corrected in the recorded signal [155].

4.1.2 Motorized Neuroprostheses

Before the BMIs became that widespread, prostheses were designed as either passive devices only for aesthetic appearance or mechanically/electrically activated devices to enable particular movements (Figure 4.2) [188, 189]. Although these devices are still popular due to their availability, they may not satisfy the users [190].

With the improved insight into neural signals, more sophisticated functional prostheses have been emerging. Using myoelectric signals generated by a muscle group is the most practical method to control a motorized prosthesis (Figure 4.3) [19, 180, 181, 192, 193]. Activity of muscles, for example, in the stump (the remaining limb after amputation) can be used to drive actuators on the prosthesis either in an on-off manner (e.g., extend the fingers) or proportionally (e.g., position of fingers vs EMG intensity). For those subjects with more proximal amputation (i.e., from shoulder), chest muscles can be used to control the prosthesis by reinnervating them by nerve fibers previously serving the amputated limb (Figure 4.3) [183, 194]. In this way, the subject is enabled to move his/her chest muscles by thinking about moving his/her arm or fingers. The purpose of *targeted nerve reinnervation* is to amplify limb/hand-targeted neural signals on the muscles, and hence, to present the user with a more convenient way of prosthesis control. Currently, there are commercialized motor prosthesis

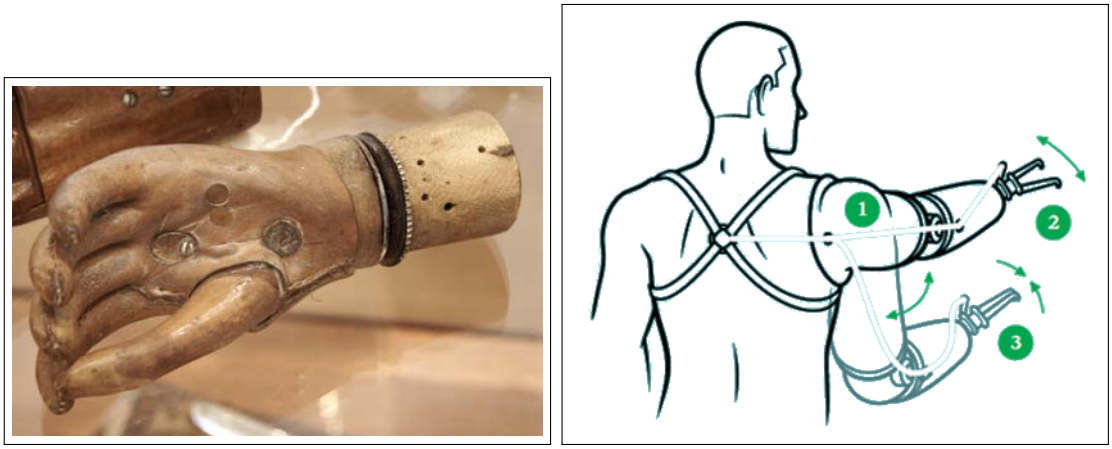

(a) (b)

Figure 4.2 (a) An passive hand prosthesis for aesthetic purposes used in 1500s [189]. (b) A body-powered prosthesis is controlled by the posture of the body [191]. A harness is used to control the position of the prosthesis.

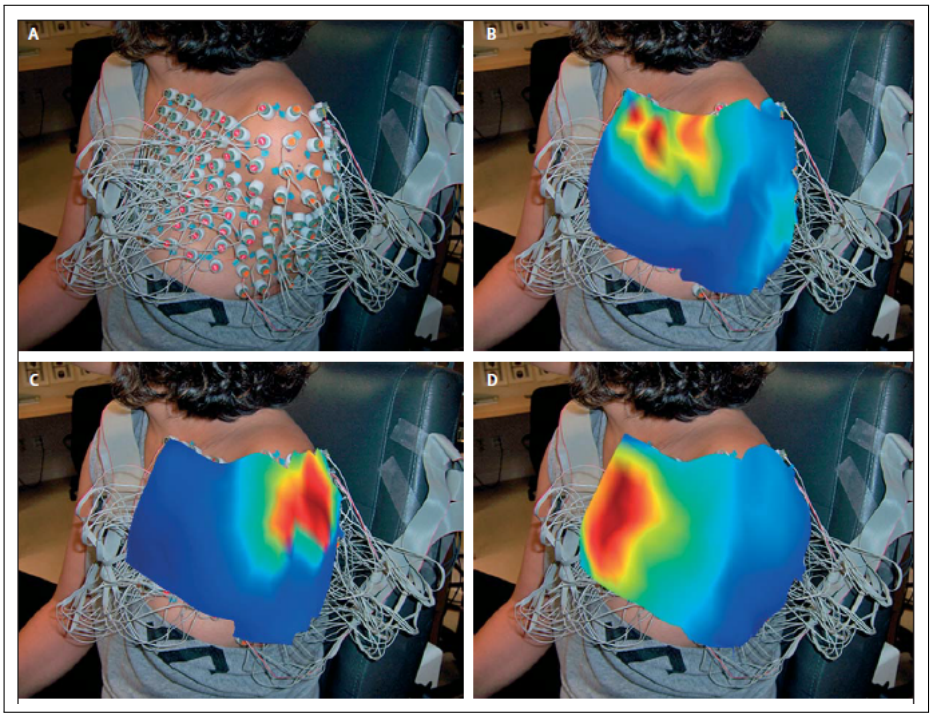

Figure 4.3 EMG-based prosthesis application. The subject underwent targeted nerve reinnervation operation and the efferents previously serving the amputated arm connected to nerve bundles innervating the chest muscles. EMG electrodes were placed on the chest and muscle activity is recorded. Depending on the activity pattern, an motorized prosthesis was controlled. [194]

using myoelectric signals to drive robotic hands [23]. Alternatively, peripheral nerve activity (i.e., compound events or action potentials) can be used to control prosthesis [37, 180]. Direct neural recordings from peripheral nerve fibers has the advantages of improved signal quality and feasibility for more sophisticated functions. Nevertheless, the invasiveness and the long-term applicability (e.g., condition of electrodes) of this technique are the two major disadvantages compared to EMG-based motor prostheses.

However, EMG-based motor prosthesis are not applicable for paralytics who may lose the control of the entire body. Although vision-based aid systems have been developed for these subjects [195], they have limited capacity for correctly interpreting the gestures of the users [196]. EEG based BMIs may provide slightly better solutions, but the susceptibility to noise is their greatest drawback. On the other hand, penetrating electrodes have been used for control of the robotic arms [20, 24] or the real limb by means of functional stimulation of the muscles or the spinal cord [197, 198]. Furthermore, BrainGate Co. (USA) currently studies BMIs with paralytic human subjects implanted with microelectrode arrays in their motor cortex (Figure 4.4) [24].

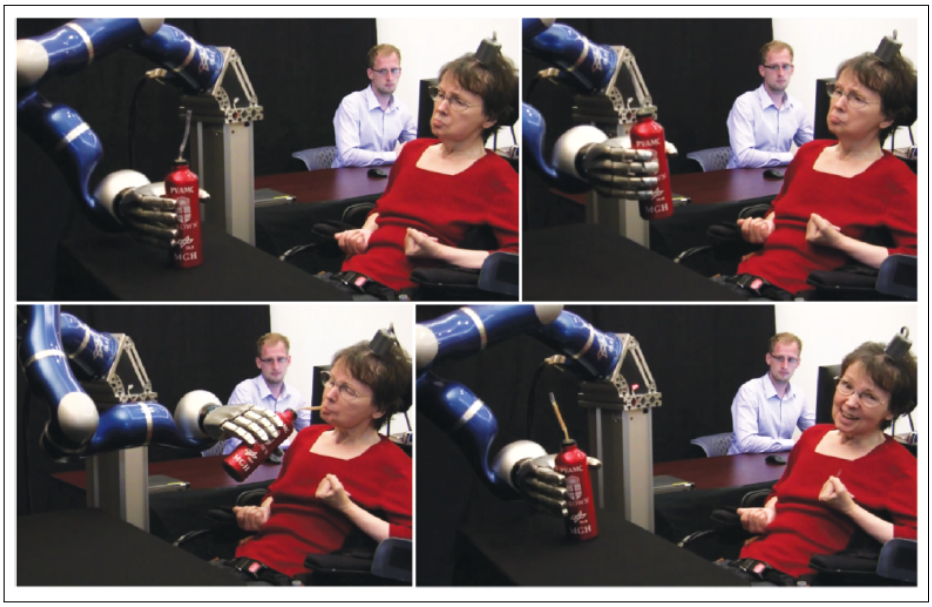

Figure 4.4 Cortical brain-machine interface. A paralytic patient was implanted with microelectrode array in her motor cortex. The neural activity is used to control the robotic arm with multiple degrees of freedom. [24]

They have successfully demonstrated the control of a robotic arm by neural ensembles recorded from a human subject.

4.1.3 Somatosensory Neuroprostheses

Although motorized prostheses significantly contribute to wellbeing of the amputees and paralytics, they lack the somatosensory feedback which is a must for precise control of the movements under normal conditions. Therefore, users depend on their vision in order to control these devices and the movements are slow and clumsy. According to a survey conducted by Lewis et al., motorized prosthesis users demand a sensory feedback from the device in the form of either tactile, temperature or electrical instead of observing or listening to their prosthesis [199]. Furthermore, not only for the satisfaction of the users but also for the improvements in motor planning and movement correction, multisensory feedback has a critical role [25]. Motor actions are build up and corrected based on sensory information. Brain knows the position and the posture of a limb in the space with respect to body with somatosensory information mediated by mechanoreceptors located in the muscles and the skin [26, 27]. In addition, any

contact with external world is signaled by the tactile afferents. In the absence of multisensory feedback from the body, our ability to recognize our own bodies is disrupted [200]-[203] as well as the ability to master tools [33].

Regarding the importance of somatosensory feedback, there is a great effort to implement sensory feedback mechanisms in functional prostheses. The principle behind the sensory neuroprostheses is to excite populations of functionally organized neurons. The cochlear implant developed in 1950s is the first demonstration of a sensory neuroprosthesis [142, 204]. In the cochlea, the auditory nerve fibers arranged so that nerve fibers sensitive to low-frequency sound waves are located close to the apex of the cochlea and fibers sensitive to high-frequency waves are located at the base. The cochlear implant electrically stimulates these nerve fibers via an electrode array placed along the cochlea. It generates patterns of electrical stimuli based on the quantitative aspects of the sound waves such as frequency components and the intensity. For example, it would deliver electrical stimulus to an electrode close to the apex when a low-frequency sound is received (for details see [204]). Nowadays, this technology is approved as a clinical application and used by hundreds of thousand people all over the world. Moreover, it encouraged the research on other sensory aid systems.

In literature, different indirect (mechanical or electrical stimulation of residual limb) and direct (electrical stimulation of peripheral or central nervous systems) tactile feedback methods have been proposed for prosthetic applications. In indirect feedback systems, as a non-invasive approach, feedback is achieved by stimulation of an intact body side with electrical stimuli or mechanical vibrations (Figure 4.5) [205, 206]. However, since the tactile feedback is supplied to an alternate body part (i.e. residual limb), subjects must be trained to associate and utilize these physiologically inconsistent signals [203]. There are two reasons behind this: (1) Population and distribution of receptors and their receptive field structures vary across the skin (i.e. glabrous vs. hairy skin) [27, 71], (2) Stimulation of residual body part would not evoke the sensation of being touched in, for example, the amputated hand, because different skin regions are represented by topographically distinct cortical areas in the primary somatosensory cortex (SI) [26].

On the other hand, electrical stimulation of residual peripheral nerve fibers via chronically implanted intraneural electrodes, as a direct sensory feedback technique,

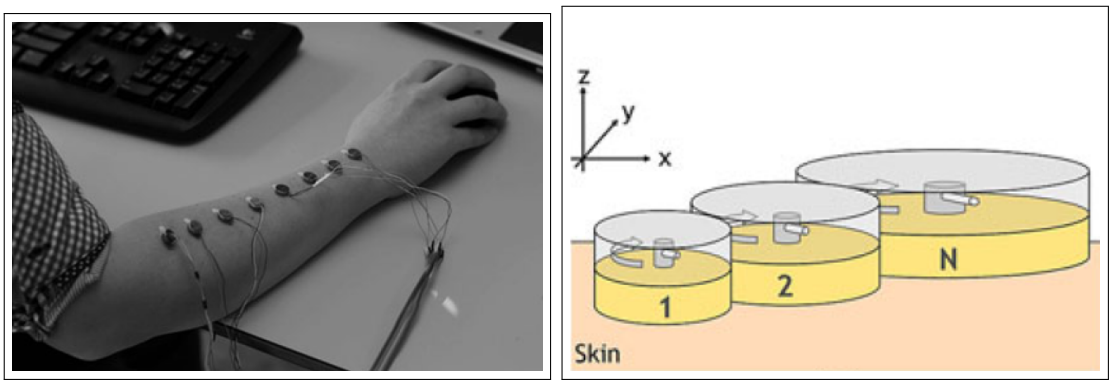

(a) (b)

Figure 4.5 Non-invasive tactile feedback systems. (a) Placement of surface electrodes or electric motors on the skin of intact limb for tactile feedback from prosthetic hand in a computer simulation [205]. (b) Use of electric motors that apply shear forces on the skin for tactile feedback.[206]

can elicit proprioceptive and/or tactile sensations (Figure 4.6) [37, 207, 208]. However, distribution of the motor and the sensory fibers serving different modalities in a nerve bundle is considerably heterogeneous. Stimulation of a nerve fiber in the bundle might unintentionally cause reflexes or pain sensation, even if the electrodes are placed in a nerve bundle with the highest tactile and proprioceptive fiber population. Furthermore, those indirect and direct feedback methods are not applicable for paralytic subjects since they might lose the control of and the sensations from their entire body.

Electrical stimulation of specific cortical regions is known to elicit sensation since studies on treatment of epilepsy in 1930s [38]. Recent studies adopted this technique to evoke artificial sensations comparable to natural ones. Romo et al. trained monkeys to discriminate two mechanical stimuli at different frequencies applied to their fingertip (Figure 4.7) [36, 209]. Then, they replaced one of the mechanical stimuli with current pulses injected into the area 3b of SI via microelectrodes. Monkeys could compare and discriminate the frequencies of mechanical and electrical stimuli with each other as good as they performed with two mechanical stimuli. This study shows that sensations evoked by ICMS is comparable to natural ones in means of frequency.

In addition, Rousche et al. studied the microstimulation of auditory cortex by training rats based on a detection task [116]. Rats that were trained to detect presence or absence of an auditory stimulus were chronically implanted with single microelectrodes in the auditory cortex and the visual cortex. When the auditory signal

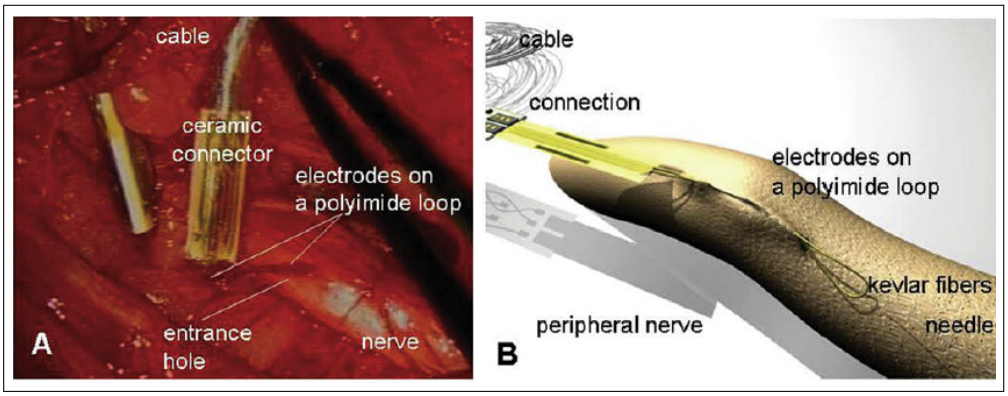

(a)

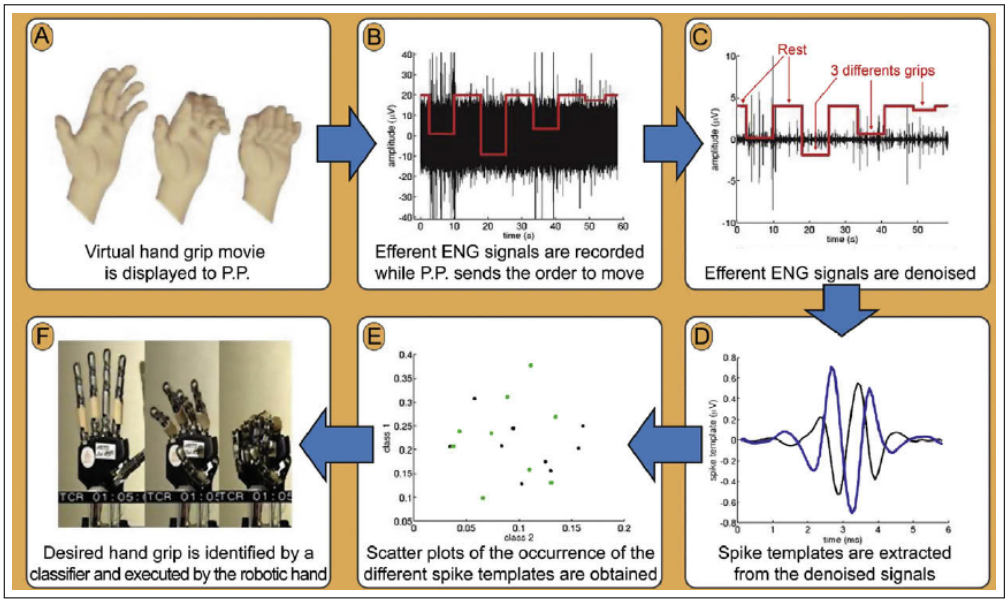

(b)

Figure 4.6 Peripheral neural interfaces. (a) Implantation of electrode array in nerve bundle. (b) Flow diagram of the prosthesis control system. [37]

was replaced with ICMS trains delivered to the auditory cortex, the rats were able to perform the detection. Rousche et al. also tested if the rats were using the cortical stimulation (i.e. spread of current to other cortical regions) as a cue instead of using the sensation that it created; they delivered electrical stimuli to the visual cortex of the rats instead of the auditory cortex. However, rats performed poorly (i.e., $p(h)\approx 0$) with visual cortex microstimulation.

Tabot et al. trained monkeys in a two-interval forced choice location discrimination task [186]. In this task, two mechanical stimuli (i.e., skin indentations) were applied to the different fingers. The monkeys were trained to indicate whether the

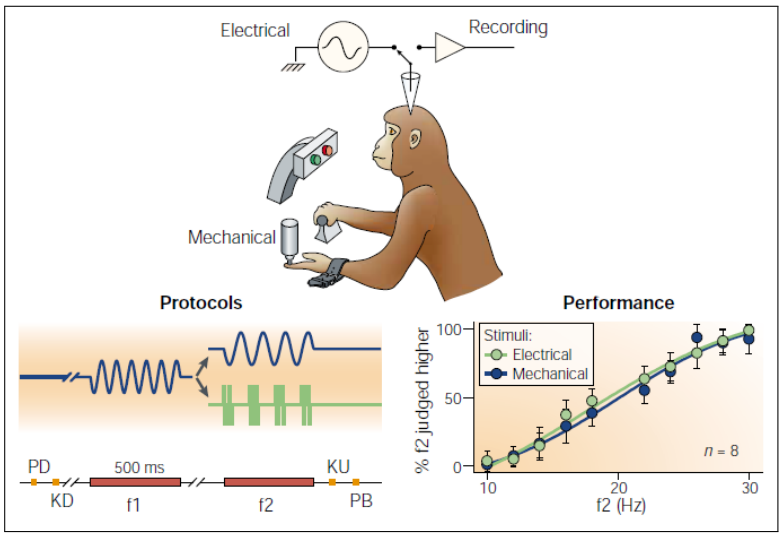

Figure 4.7 Frequency discrimination based on intracortical microstimulation. The monkey was implanted with microelectrodes and trained to discriminate frequency of vibrotactile and ICMS stimuli. They performed in vibrotactile vs ICMS discrimination as good as they did in vibrotactile experiments. [209]

second stimulus was lateral or medial to the first one. Then, one of the mechanical stimuli was replaced with ICMS trains applied through the electrodes with relevant cortical receptive fields. The monkeys were tested whether they could discriminate the perceived locations elicited by mechanical and ICMS stimuli. They performed poorer compared to pure mechanical discrimination, but their performances were above chance level.

These studies showed that ICMS elicits modality-specific and localized perceptions that is associated with relevant natural stimuli. Nevertheless, we still do not know how exactly the sensations elicited by natural and ICMS stimuli are similar. As a consequence, current research is focused on how the different aspects of ICMS (e.g., frequency, amplitude and duration) relate to the psychophysical aspects of the perception (e.g., detectability and discriminability).

4.1.4 Psychometric Equivalence Theory

The somatosensory cortex is has a functional organization where distinct neural populations receive and process different aspects of the sensory stimuli (see Section

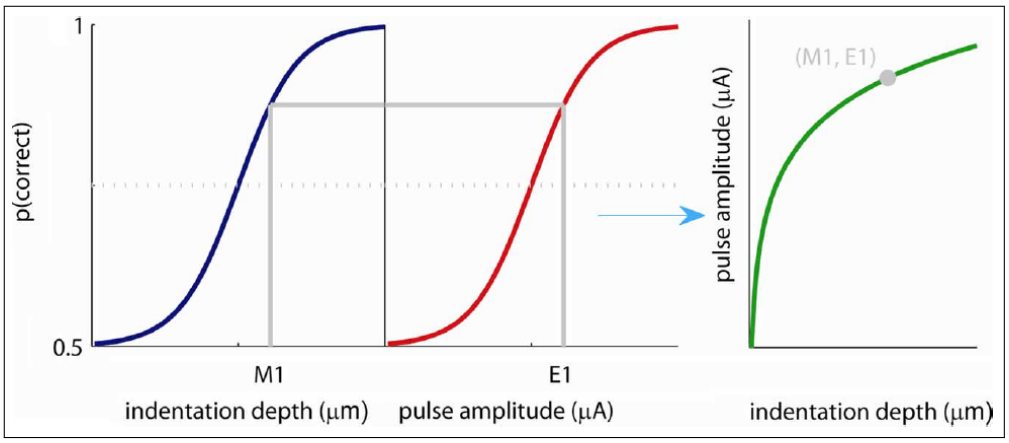

Figure 4.8 The construction of a *psychometric equivalence function*. In PEFs, Berg et al. matched the mechanical and electrical intensities with equal detectability. [173]

2.1.2). This highly organized structure is advantageous for delivering localized sensation by means of ICMS [186]. Therefore, we only have to, somehow, relate the quantitative aspects of ICMS to the qualitative aspects of the elicited perception.

According to psychometric equivalence theory, detection or discrimination rate of natural and ICMS stimuli can be used to model the correspondence between the sensations elicited by these stimuli [173, 186]. The theory proposes that a natural and an ICMS stimuli eliciting sensations with similar psychometric qualities (e.g., detectability) can be used interchangeably. The models based on this theory map the equally detectable/discriminable mechanical and ICMS stimuli (Figure 4.8). Thus, for a given natural stimulus setting and psychometric quality, ICMS parameters can be chosen from this map to elicit a sensation similar to that elicited by the given natural stimulus.

Berg et al. [173] and Tabot et al. [186] demonstrated the application of *psychometric equivalence functions (PEFs)* in a series of experiments where they combined ICMS in monkey with a sensorized robotic arm. Berg et al. trained monkeys to detect a mechanical indentations in a two-interval forced choice task. Monkeys reported in which interval they felt the stimulus. In psychophysical experiment following the training, they derived the psychometric functions for mechanical detection. Then, they replaced the mechanical stimulus with ICMS and derived the psychometric functions for ICMS detection. Finally, they substantiate the relationship between psychometric functions for both mechanical and ICMS detection tasks by means of PEFs (Figure

4.8). They assumed that a mechanical stimulus (e.g., skin indentation) and an electrical stimulus (e.g., current injection into SI) that are equally detectable (equal detection probabilities) elicit similar sensations and can substitute each other. These functions were used to convert mechanical stimulus applied to the robotic finger into ICMS trains delivered into SI of monkeys. Briefly, the mechanical indentations applied on the robotic finger were measured as force information and than converted to indentation on the sensor based on the sensor calibration. As the amount of indentation read on the sensor, ICMS intensities were simultaneously derived from PEFs. Amplitude of ICMS train delivered to the monkey was modulated based on these derivations. In this experimental setup, the monkeys achieved correct rates similar to those when mechanical stimuli applied to their fingers.

In series with Berg et al.'s study, Tabot et al. trained monkeys in a two-interval forced choice amplitude discrimination tasks. Two mechanical stimuli with different amplitudes were applied to the same finger of the monkeys. The monkeys were trained to determine whether the second stimulus was higher or lower in amplitude than the first one. Then, both mechanical stimuli were replaced with ICMS. Similar to Berg et al.'s study, they constructed PEFs and tested whether the monkeys could compare mechanical stimuli applied to the robotic finger with that applied to the real finger. In this experiments, the monkeys' performed as well as they did when the mechanical stimuli applied to their own finger.

Results of these studies are important in terms of how the sensations elicited by mechanical indentations and ICMS trains correspond to each other. However, they modulated the intensity of current pulses but ignored the effect of stimulation frequency on the sensation. Romo et al. showed that periodic electrical stimulation elicited flutter sensation that is comparable to vibrotactile stimuli in monkeys [147]. Therefore, the sensations elicited by mechanical indentations and electrical stimuli might not be same, but the monkeys used the ICMS amplitudes as a cue while ignoring the specific submodality of the sensation.

4.2 Aim

The aim of this study to develop a model (*psychometric correspondence function*, PCF) representing the behavioral correspondence between sensations elicited by vibrotactile stimulation of the glabrous skin and intracortical microstimulation (ICMS) of primary somatosensory cortex in freely behaving rats. I want to note that the word *correspondence* was used instead of *equivalence*, because we cannot exactly know whether the sensations elicited by natural and ICMS stimuli equal to each other, but we can only assume that they correspond to each other based on psychometric functions.

The particular novelty of the model is that the psychometric functions were constructed based on the frequency and the intensity of the stimuli. Therefore, the PCFs were used to estimate the ICMS intensity level for a given vibrotactile intensity and frequency. PCFs were validated in an additional behavioral detection task (Experiment III) with probe trials containing either a vibrotactile or ICMS stimulus. ICMS current levels were determined based on the PCF with respect to the vibrotactile amplitude levels and the test frequency. In Experiment III, I tested the hypothesis that vibrotactile and ICMS stimuli produce similar psychophysical detection probabilities.

4.3 Material and Methods

4.3.1 Animals

5 male rats (Rats 51, 56, 67-69) were tested in PCF validation experiments (Experiment III). As in previous experiments, rats were motivated with water deprivation. In addition, all available psychometric functions were presented for rats tested in vibrotactile and/or ICMS psychophysical experiments.

All experiments were approved by the Boğaziçi University Institutional Ethics Committee for the Local Use of Animals in Experiments.

4.3.2 Psychometric Functions

Corrected hit rates ($p^*(h)$) recorded in Experiment I and II were used to construct psychometric functions based on the frequency and the intensity of the stimuli (Figure 4.10 and 4.11). Equation 4.1 was used to fit data point.

$$p^*(h) = \frac{1}{1 + e^{-\frac{A - af^c}{bf^d}}} \tag{4.1}$$

where A is the intensity of the stimuli (i.e., zero-to-peak displacement in dB ref 1μm for vibrotactile stimuli or current level in dB ref 1μA for ICMS), f is the frequency of the stimuli, and a, b, c and d are the coefficients. Equation 4.1 is a sigmoidal function where af^c is the midpoint and bf^d is the parameter related to the slope at the midpoint. It should be noted that the mean and the slope of the sigmoid function varies depending on the frequency at different rates (c and d). With these surface functions it is possible to interpret the detectability of a stimulus at a given intensity and frequency between 40-80 Hz.

4.3.3 Psychometric Correspondence Functions

The PCFs were constructed based on the theory presented by Berg et al. and Tabot et al. [173, 186]. In addition, based on the findings of Romo et al. [147], it was assumed that periodic electrical stimulation elicits flutter sensations as vibrotactile stimulation of the skin did. Therefore, the vibrotactile and ICMS intensity levels with equal $p^*(h)$ were matched for each frequency using equations 4.2.

$$\left[p^*(h) = \frac{1}{1 + e^{\frac{af^c - A}{bf^d}}}\right]_E = \left[p^*(h) = \frac{1}{1 + e^{\frac{af^c - A}{bf^d}}}\right]_T \tag{4.2}$$

$$A_i, f_i, a, b, c, d \in R \qquad f_E = f_T$$

which can be rewritten as

$$A_E = \frac{b_E}{b_T} f^{d_E - d_T}(A_T - a_T f^{c_T}) + a_E f^{c_E} \tag{4.3}$$

where E and T are the indexes of ICMS and vibrotactile stimuli, respectively. For each rat a separate PCF was constructed (Figure 4.12). Equation 4.3 was used to determine the current level (dB ref 1μA) for a given vibrotactile intensity and frequency.

4.3.4 Experiment III: PCF Validation Experiments

PCFs were validated in an additional detection experiments (Figure 4.9). In this experiments, rats were presented with either a rewarded or an unrewarded trial. In a given session, 1/4 of the trials were unrewarded trials. Rewarded and unrewarded trials were randomized. A rewarded trial could be either a stimulus condition, where a vibrotactile stimulus with the amplitude level used in training was presented, or a no-stimulus condition, where no-stimulus was presented. Stimulus and no-stimulus conditions were randomized and counter balanced. In these trials, rats were rewarded for their correct responses (right lever press for stimulus condition and left lever press for no-stimulus condition). Otherwise, an error signal occurred. Rats' correct rates were always >85% in the rewarded trials.

In probe trials, either a vibrotactile or electrical stimulus was presented. 6 different vibrotactile amplitude levels were tested for a given frequency. Based on vibrotactile test amplitudes, ICMS intensities were calculated using PCFs. Each condition was presented 10 times. Vibrotactile and ICMS trials were randomized. Probe trials were not rewarded, but the responses were recorded.

5 frequencies (40 Hz, 50 Hz, 60 Hz, 70 Hz, and 80 Hz) were tested in random order at four repetitions. At the end of each trial hit rates were recorded for probe trials. For each frequency, the mean hit rates were calculated for each amplitude level for both vibrotactile and electrical stimuli. Kolmogorov-Smirnov statistic was used to test the null hypothesis that hit rates for vibrotactile and electrical stimuli have similar cumulative probability distributions. If the test fails to reject the null hypothesis, relevance of PCFs for a somatosensory neuroprosthetic application would be validated.

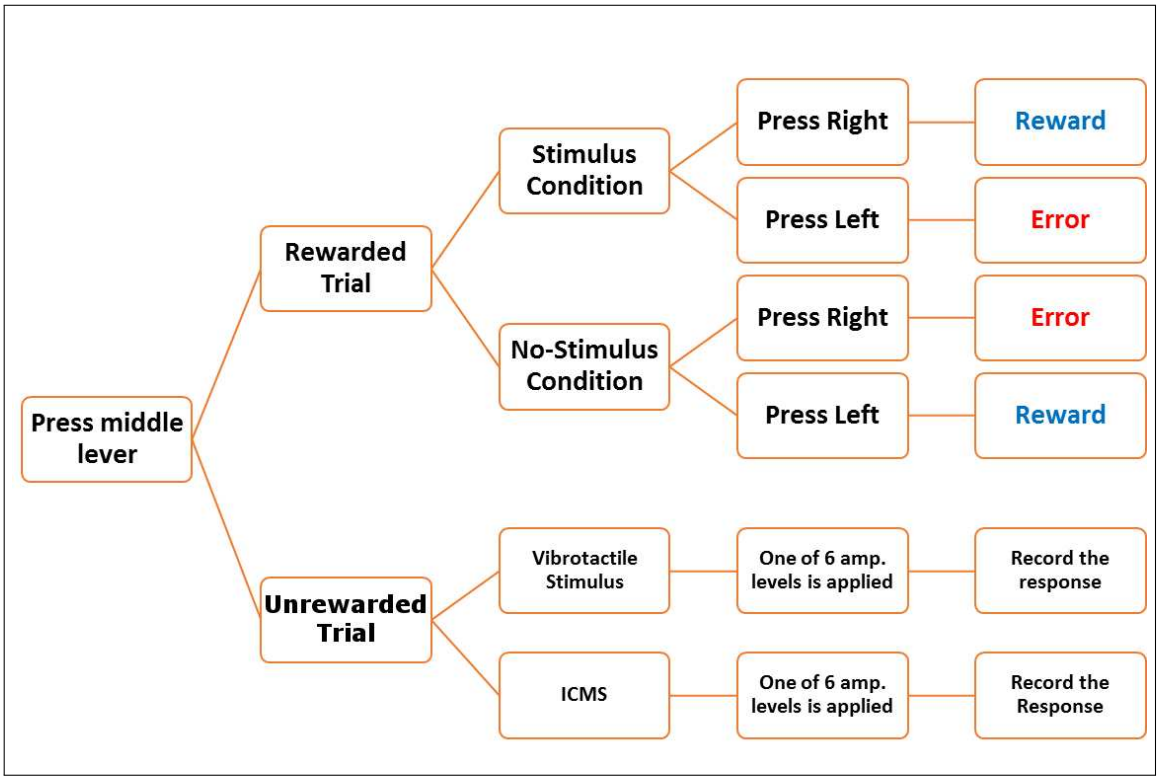

Figure 4.9 Flow diagram of Experiment III. When the rat pressed middle lever and initiated a trial, the trial was determined as either a rewarded or an unrewarded trial. If the trial was a rewarded trial, a vibrotactile stimulus with a suprathreshold amplitude level was presented or not. The rat was rewarded for pressing right lever if the stimulus was presented or pressing left lever if the stimulus was not presented. Otherwise, no reward was given and the error signal occurred. If the trial was an unrewarded trial, the either a vibrotactile or ICMS stimulus was presented. The intensity level was randomly chosen among 6 intensity levels. The response of the rat was recorded. No error or reward was presented.

4.4 Results

4.4.1 Psychometric Surface Functions

Table 4.1 shows the coefficients and R^2 values of psychometric fits for vibrotactile psychophysical experiments. All R^2 values but one are >0.75%. Only, Rat 47 has an R^2 of 0.69. Psychometric functions are shown in Figure 4.10. a and b coefficients varied extensively. On the other hand,a negative value for c shows the inverse proportionality for the midpoint of the curve with the frequency whereas a positive value for d indicates the inverse proportionality for the the slope of the curve at the midpoint with the frequency (see Equation 4.2). Therefore, since all c values were negative, the 50% detection threshold (af^c) was inversely proportional to the frequency for all rats.

Table 4.1
Psychometric function coefficients for vibrotactile experiments.

Rat ID	a	b	c	d	R^2
44	85.65	29.2	-0.2806	-0.3572	0.918
47	118.3	53.74	-0.4356	-0.4341	0.691
51	29.73	0.204	-0.1521	0.7476	0.839
55	209.9	447.7	-0.5548	-1.064	0.884
56	395.5	33.46	-0.6935	-0.3932	0.879
59	64.47	2.6	-0.2896	0.1893	0.861
65	65.85	24.13	-0.2822	-0.3336	0.888
66	53.6	11.19	-0.2515	-0.2043	0.809
67	89.1	41.17	-0.4112	-0.4993	0.873
68	97.78	0.5112	-0.4735	0.4551	0.919
69	367.7	84.87	-0.7553	-0.6460	0.816

In other words, detection threshold decreased as the frequency increased. This was expected as discussed in Section 2.5.3. On the other hand, some d values were positive indicating that the slope of the psychometric function at the midpoint decreased as the frequency increased. In other words, the standard deviation of the normal distribution of biological and psychological events related to the detection increased as the frequency increased.

Coefficients of the psychometric functions fitted for ICMS experiments are given in Table 4.2. Figure 4.11 shows the psychometric functions. Goodness of fits were relatively lower compared to vibrotactile experiments. As in vibrotactile psychometric functions, the 50% detection thresholds were inversely proportional to the frequency for all rats.

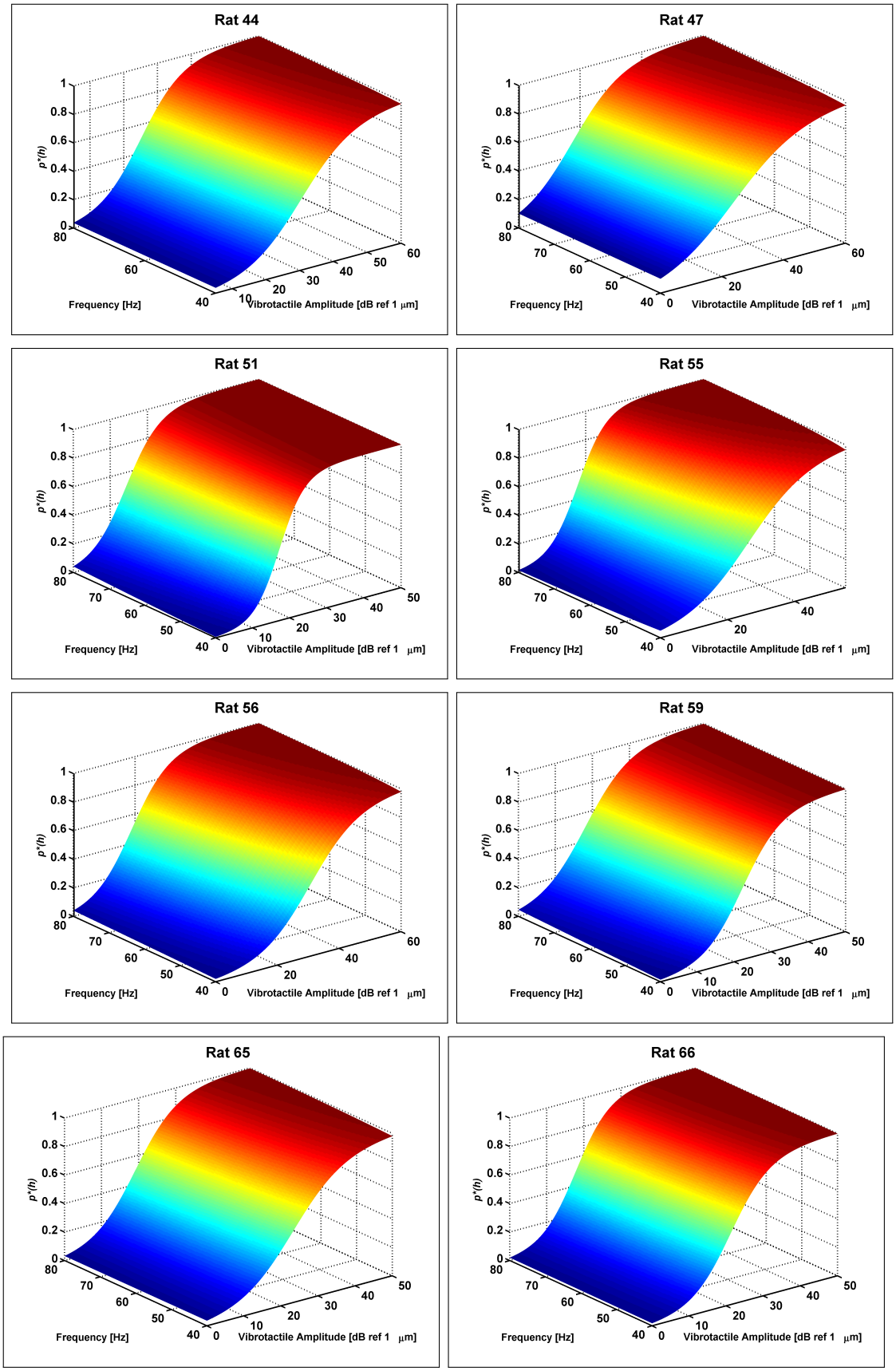

Figure 4.10 Psychometric surface functions for vibrotactile experiments. x-axis: zero-to-peak displacement in dB ref 1 μm, y-axis: frequency (Hz), z-axis: corrected hit rate, $p^*(h)$. *Continued on next page.*

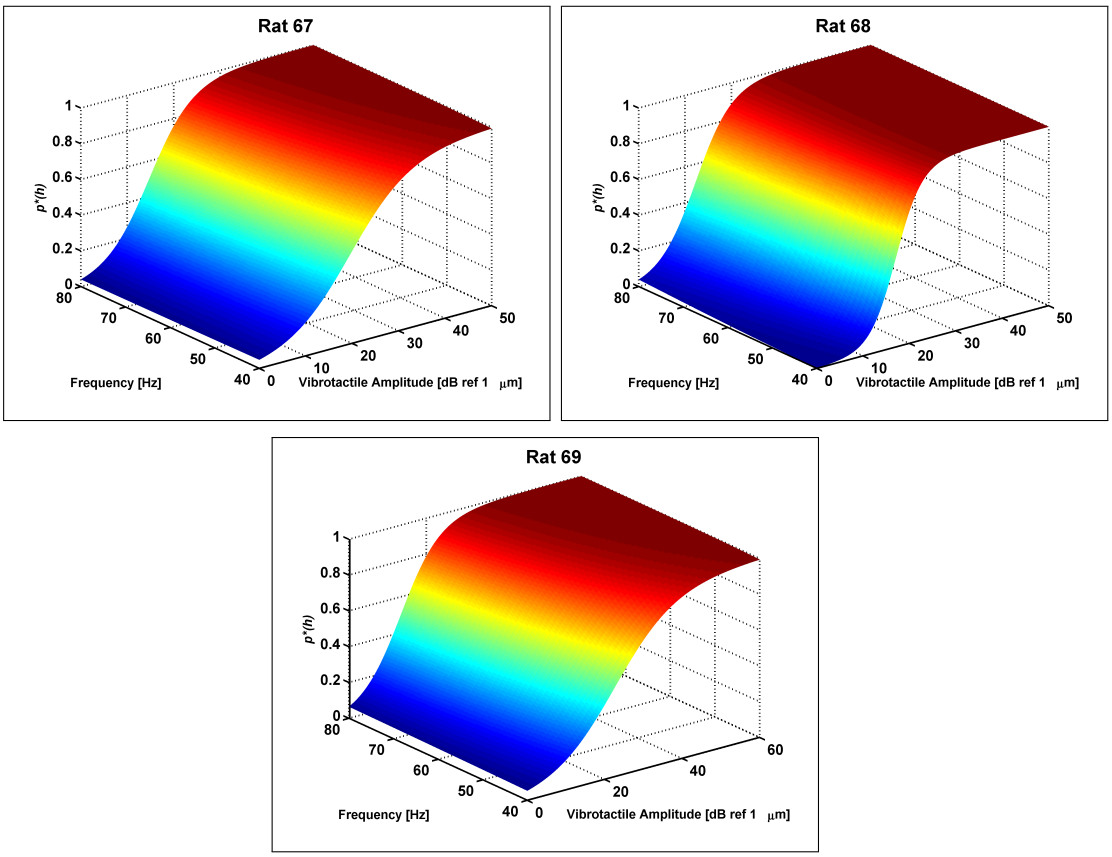

Figure 4.10 *Continued.* Psychometric surface functions for vibrotactile experiments. x-axis: zero-to-peak displacement in dB ref 1 μm, y-axis: frequency (Hz), z-axis: corrected hit rate, $p^*(h)$.

Table 4.2
Psychometric function coefficients for ICMS experiments.

Rat ID	a	b	c	d	R^2
44	102.3	48.78	-0.4105	-0.7451	0.882
47	130.7	54.39	-0.4420	-0.8350	0.882
51	36.39	3.378	-0.1750	-0.1104	0.691
55	121.0	3.002	-0.4451	-0.0287	0.668
56	87.87	5.627	-0.2240	-0.2126	0.729
65	99.37	0.847	-0.5229	0.2738	0.619
67	48.79	0.6972	-0.3221	0.2483	0.856
68	32.83	164.5	-0.2009	-1.1400	0.917
69	45.19	86.44	-0.1476	-1.0190	0.835

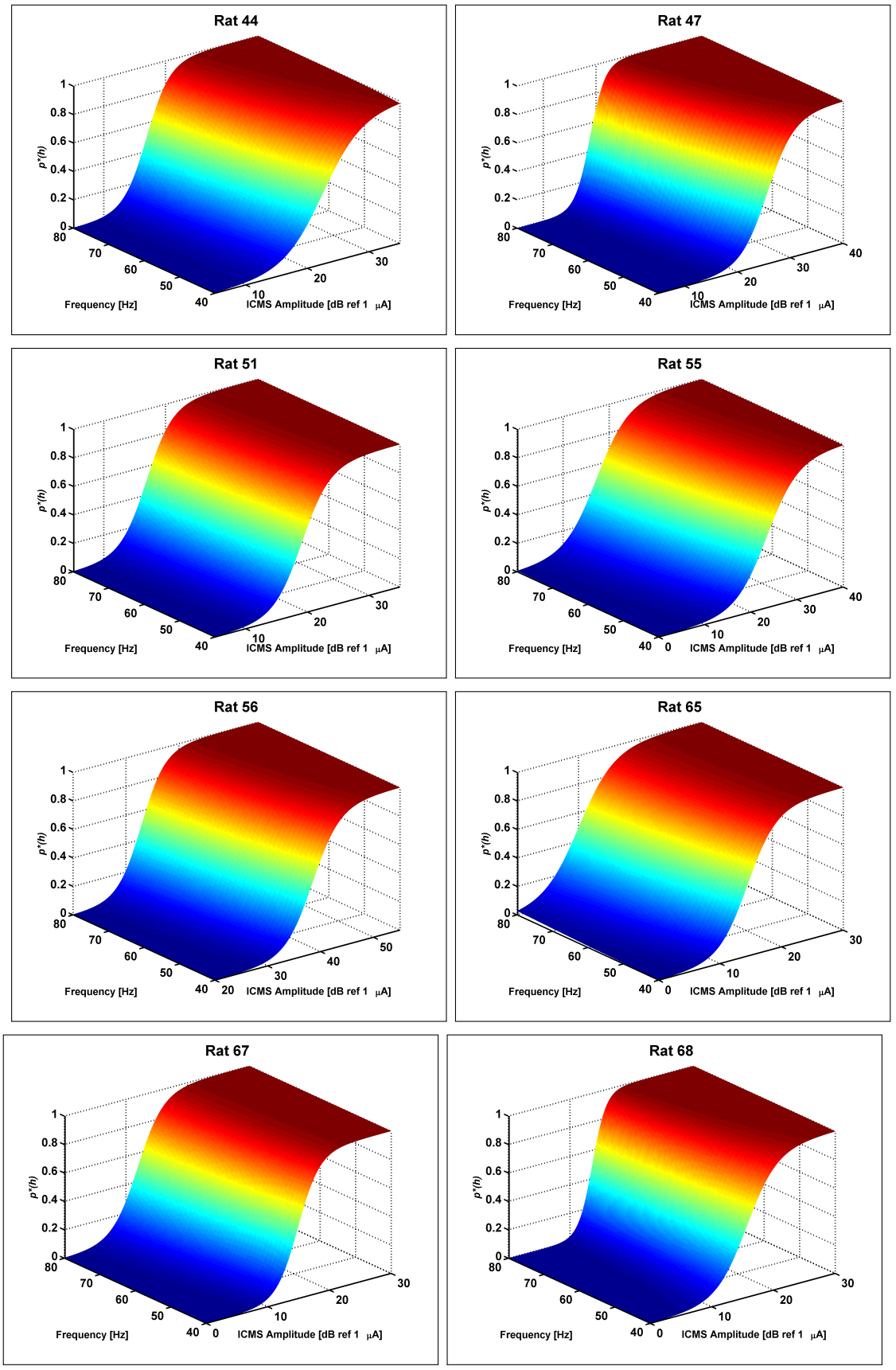

Figure 4.11 Psychometric surface functions for ICMS experiments. x-axis: current amplitude in dB ref 1 μA, y-axis: frequency (Hz), z-axis: corrected hit rate $p^*(h)$. *Continued on next page.*

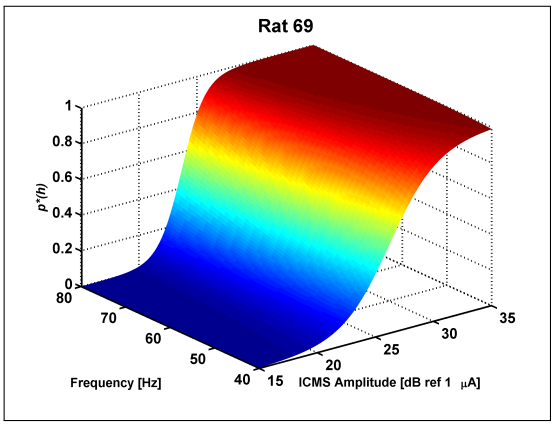

Figure 4.11 *Continued.* Psychometric surface functions for ICMS experiments. x-axis: current amplitude in dB ref 1 μA, y-axis: frequency (Hz), z-axis: corrected hit rate, $p^*(h)$.

4.4.2 Psychometric Correspondence Functions

For each rat, corresponding vibrotactile and ICMS intensities were calculated with Equation 4.3 using the coefficients given in Tables 4.1 and 4.2. Figure 4.12 shows the constructed PCFs. For a given frequency the relationship between the tactile and ICMS intensity is linear due to the nature of Equation 4.3. The shape of the PCF varied from rat to rat. For some rats, a given current intensity corresponded to higher displacement levels as the frequency increased (see Rats 44 and 47). For these rats, the z-intercept was decreased with increasing frequency while the slope did not vary too much. On the other hand, the frequency effected the slope for other rats. For example,

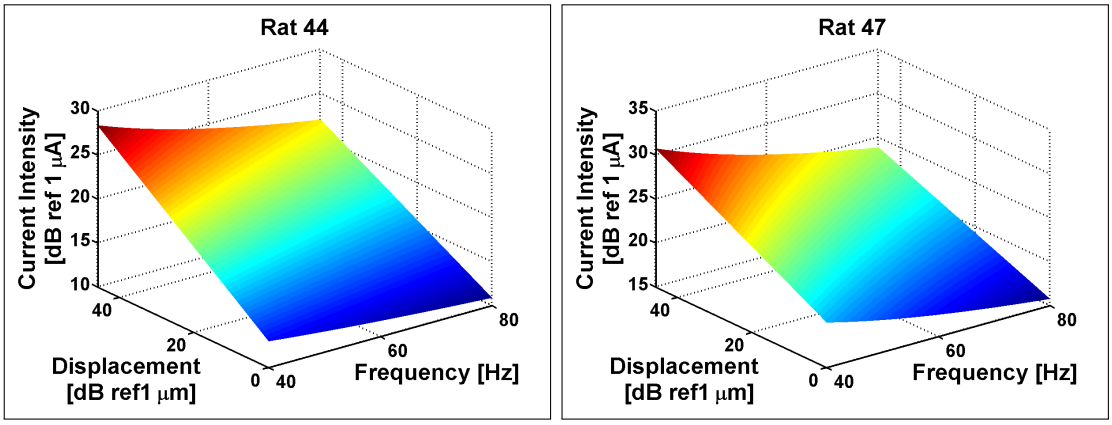

Figure 4.12 Psychometric correspondence functions. The functions give the current amplitude for a given frequency and displacement level. x-axis: frequency (Hz), y-axis: zero-to-peak displacement in dB ref 1 μm, z-axis: current amplitude in dB ref 1 μA. *Continued on next page.*

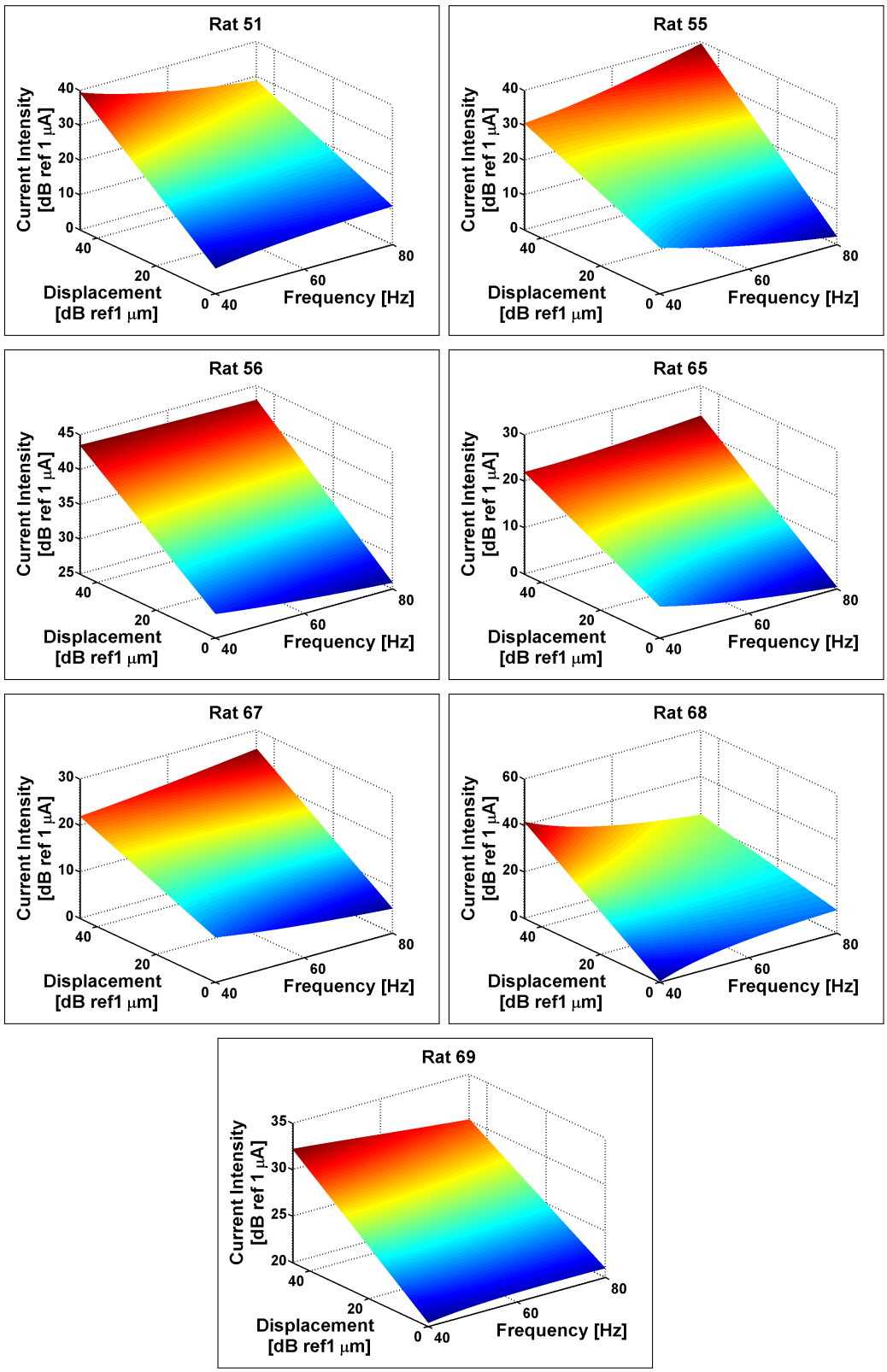

Figure 4.12 *Continued.* Psychometric correspondence functions. The functions give the current amplitude for a given frequency and displacement level. x-axis: frequency (Hz), y-axis: zero-to-peak displacement in dB ref 1 μm, z-axis: current amplitude in dB ref 1 μA.

the slope decreased as the frequency increased for Rats 51, 68 and 69 while it increased with increasing frequency for others.

4.4.3 Validation of PCFs

PCFs were tested at five frequencies including 2 intermediate frequencies (50 Hz and 70 Hz) at which rats were not tested before. Only Rat 51 could complete three sessions with 40 Hz, and then, it removed the implant. Figures 4.13-4.17 show the results of PCF validation experiments and Table 4.3 shows the results of Kolmogorov-Smirnov statistic. All rats performed similar psychophysical performances at vibrotacile and ICMS probe trials. Kolmogorov-Smirnov statistic failed to reject the null hypothesis that hit rates for vibrotactile and electrical stimuli have similar cumulative probability distributions (all p values >0.05). However, only Rat 69 performed poorly in ICMS probe trials at 60 Hz. This might be related to the electrode diameter (80 μm) which is thicker than the microwire electrodes (25 μm) implanted in other 4 rats. Most importantly, the PCFs successfully predicted the intermediate frequencies (50 Hz and 70 Hz) in which rats were not tested before.

Table 4.3
Results of Kolmogorov-Smirnov statistic for PCF validation experiments. Mean of hit rates recorded for each condition of mechanical and ICMS trials in Experiment III were used in Kolmogorov-Smirnov statistic to test whether they had similar cumulative probability distributions or not. Table gives the p values. N/A: Data is not available.

	Frequency				
Rat ID	40 Hz	50 Hz	60 Hz	70 Hz	80 Hz
51	0.810	N/A	N/A	N/A	N/A
56	0.810	0.810	0.810	0.318	0.810
67	0.810	1.00	0.810	1.00	0.318
68	0.810	1.00	0.810	1.00	0.810
69	1.00	0.810	0.077	0.318	0.318

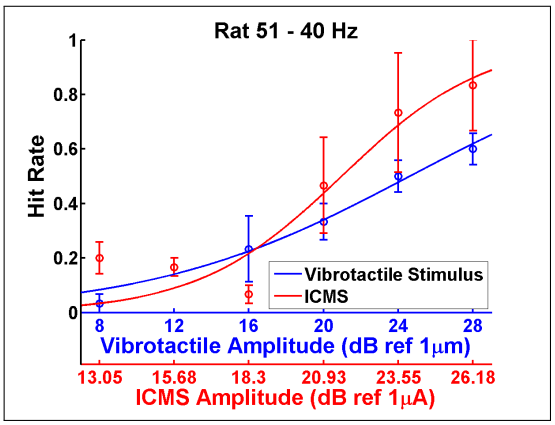

Figure 4.13 Psychometric curves obtained from PCF validation experiments: Rat 51. Data points are the mean of hit rates. Vertical lines represent the standard errors.

4.5 Discussion

4.5.1 Psychometric Functions

The psychometric functions were constructed with corrected hit rates. It is possible to use other psychometric parameters, such as hit rate or d' [39]. However, if the hit rate was used alone, the bias in response would be ignored. On the other hand, sensitivity indices do not have fixed asymptotes. For example, d' have been widely used in evaluation of psychometric functions [39]. d' depends on the how the conditional probabilities ($p(h)$ and $p(f)$) deviated from the mean of a normal population. For the extreme $p(h)$ and $p(f)$ values, such as 0 and 1, d' becomes either too high or too low since $z(0)$ and $z(1)$ are defined as negative and positive infinity, respectively. Although, d' can be limited at some maximum and minimum, psychometric functions would vary in their positive and negative asymptotes. For example, it is possible that a vibrotactile psychometric function may have an upper asymptote of 2 while the ICMS psychometric function may have an upper asymptote of 6. In this case, it is not possible to equate these two function to each other, because there is not any vibrotactile displacement level which has a sensitivity index greater than 2. Therefore, it was reasonable to use corrected hit rate since it accounts the response bias and asymptotes can be defined based on detection theory (i.e., 0 for no detection and 1 for 100% detection).

The psychometric data collected at three frequencies was fitted with a sigmoidal

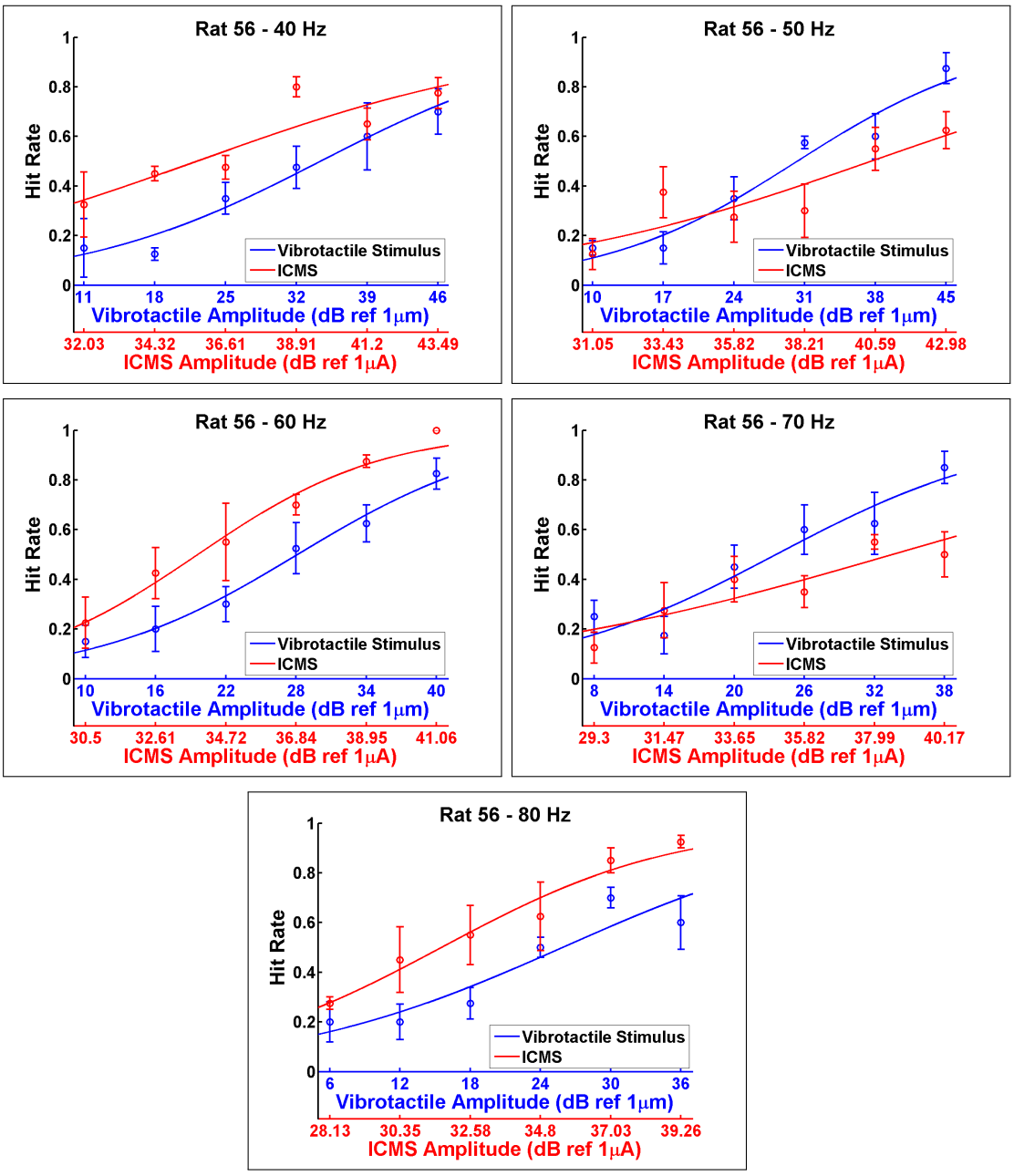

Figure 4.14 Psychometric curves obtained from PCF validation experiments: Rat 56. Data points are the mean of hit rates. Vertical lines represent the standard errors.

surface function (equation 4.1) based on the intensity and frequency information. The surface functions fit to the data well. Especially, psychometric functions of rats tested in Experiment III had R^2 values >0.69. These functions make it possible to interpret the rate of detection for other frequencies between 40-80 Hz and intensity levels which were not tested before.

On the other hand, model coefficients (a, b, c and d) showed a high inter-subject

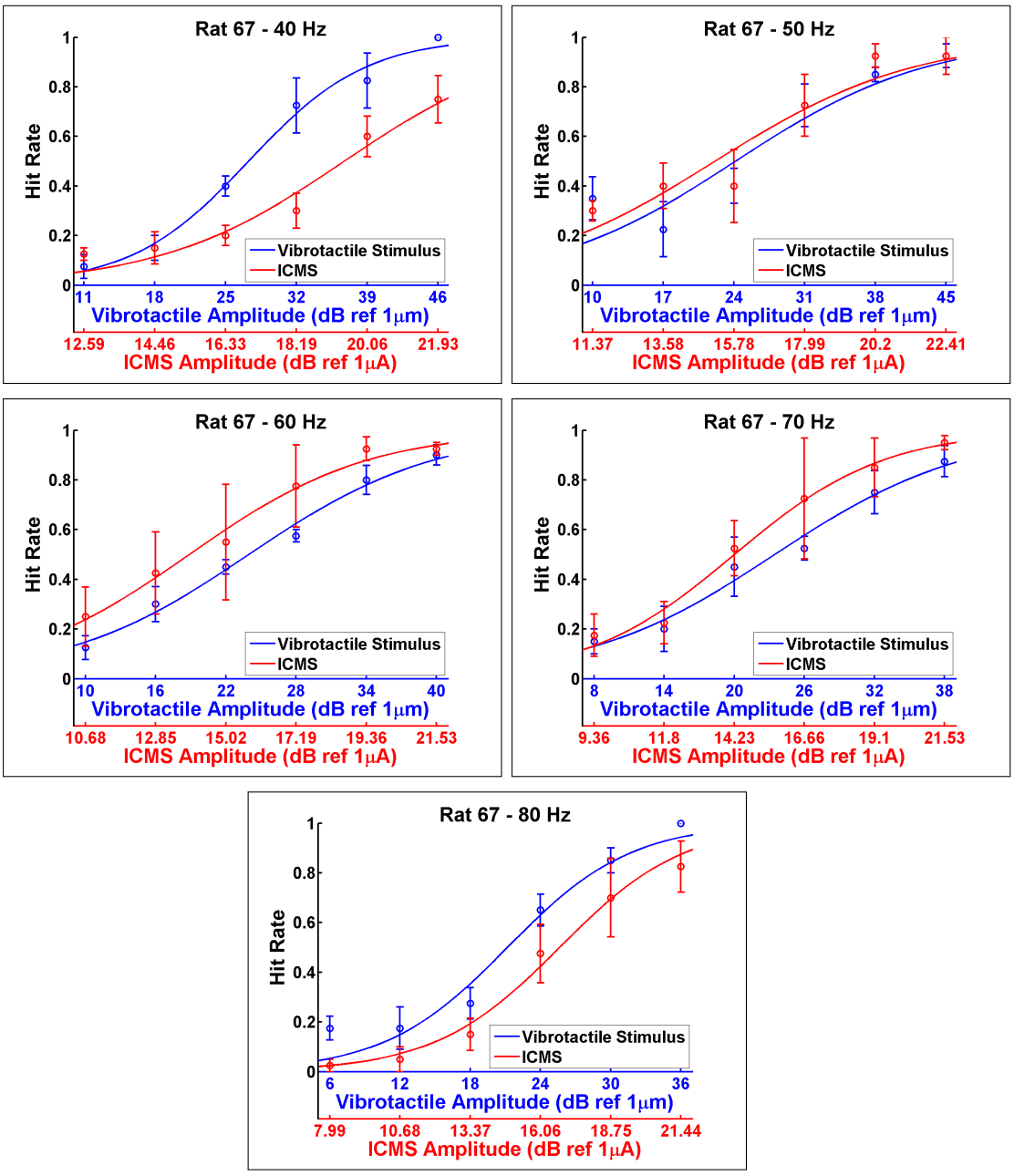

Figure 4.15 Psychometric curves obtained from PCF validation experiments: Rat 67. Data points are the mean of hit rates. Vertical lines represent the standard errors.

variation. Therefore, the model was not able to represent the physiological and psychological events during the detection of mechanical and ICMS stimuli. Yet, the model was used to fit psychometric data from mechanical and ICMS experiments in order to obtain psychometric correspondence functions for each individual separately.

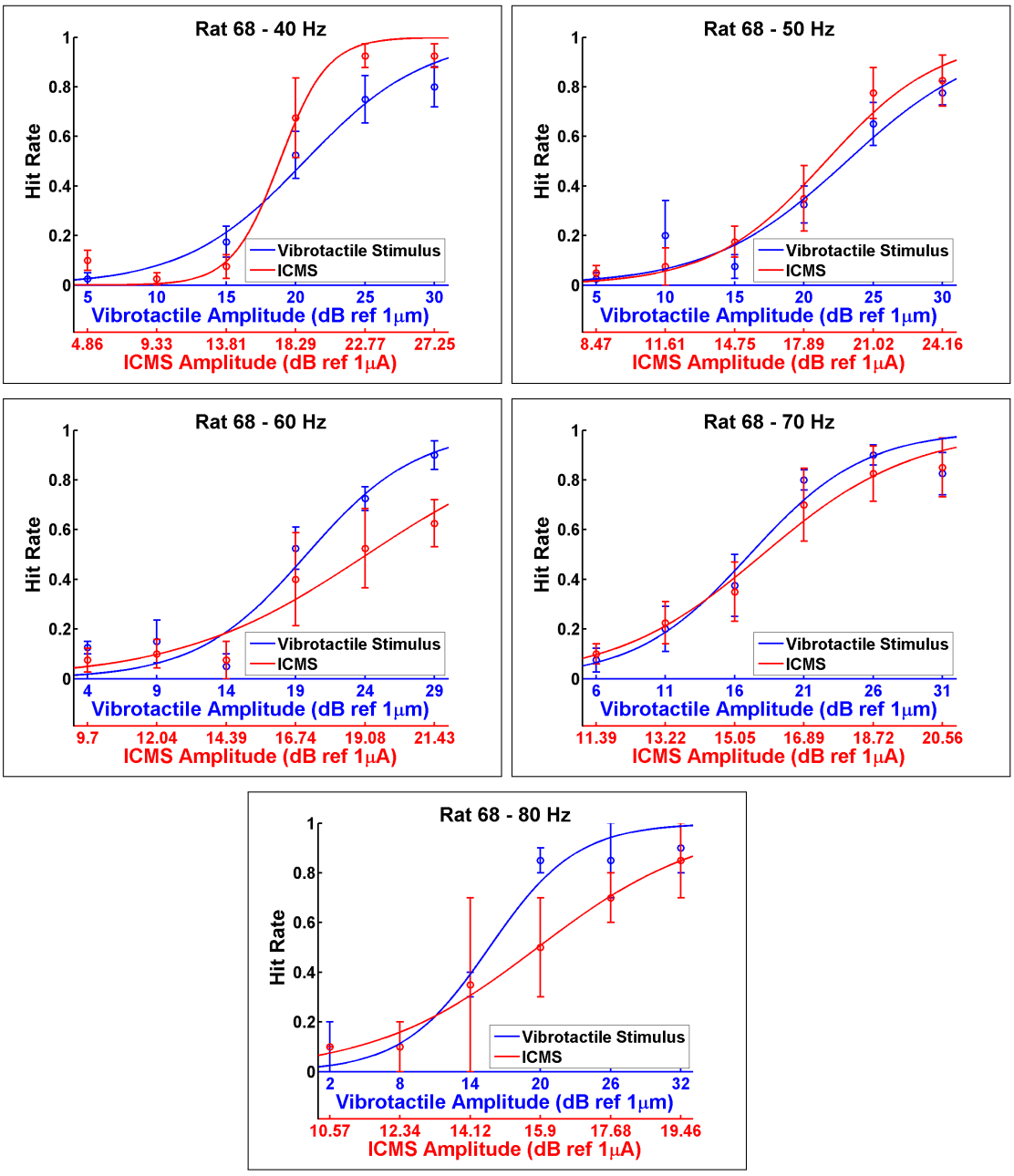

Figure 4.16 Psychometric curves obtained from PCF validation experiments: Rat 68. Data points are the mean of hit rates. Vertical lines represent the standard errors.

4.5.2 Psychometric Correspondence Functions

The psychometric correspondence functions were constructed based on corrected hit rates and they showed the linear relationship between vibrotactile and ICMS intensities for a given frequency. The effect of frequency on correspondence between the vibrotactile and ICMS stimuli varied from rat to rat. The intercept of the curve

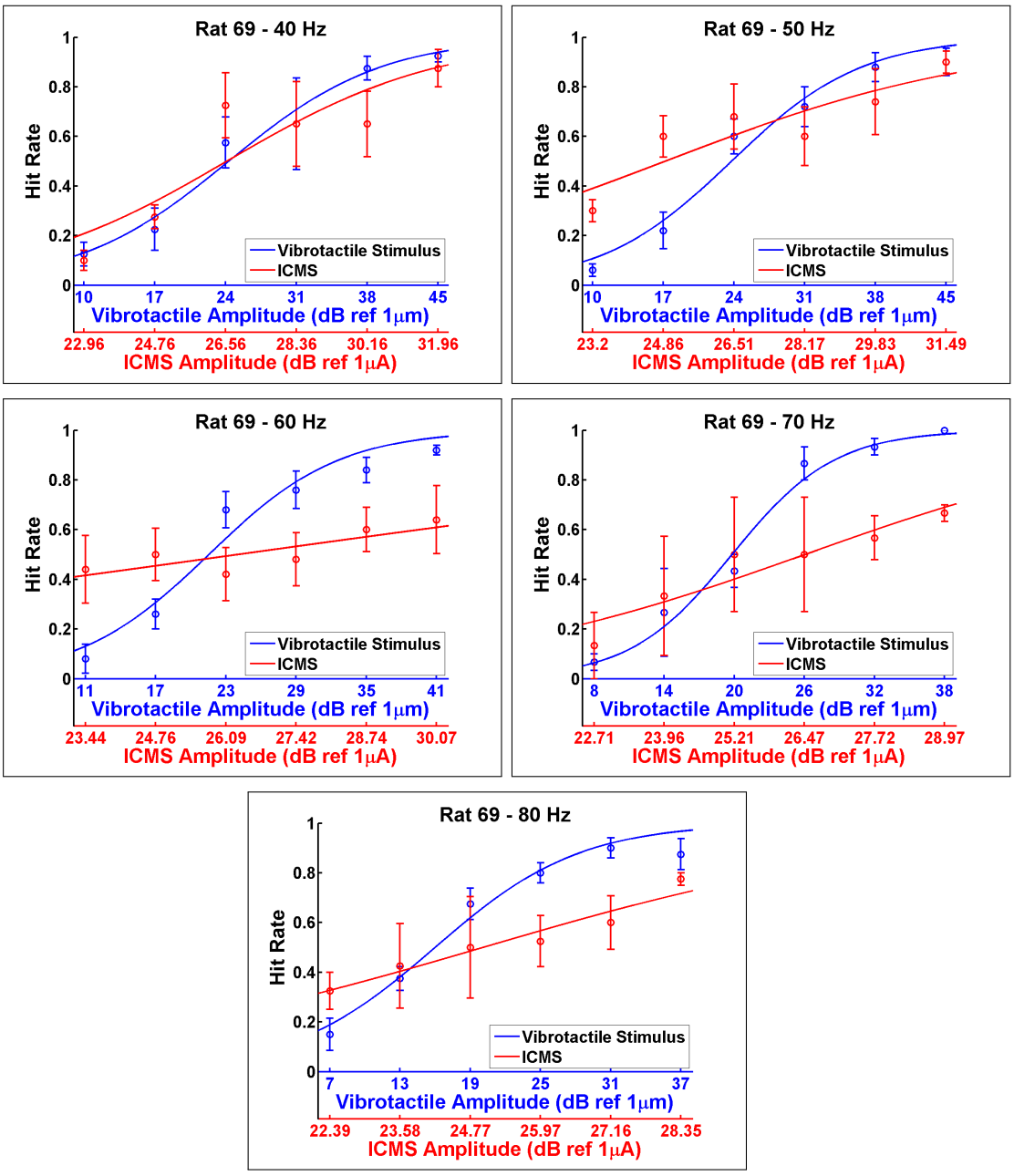

Figure 4.17 Psychometric curves obtained from PCF validation experiments: Rat 69. Data points are the mean of hit rates. Vertical lines represent the standard errors.

changed with frequency for two rats while the slope did not vary too much. Since the sensitivity of the rats increased with increasing frequency in both vibrotactile and ICMS experiments, such a change was expected as the sensations elicited by vibrotactile and ICMS stimuli were similarly effected from the frequency. On the other hand, for other rats, the slope of the curve decreased or increased with frequency. The reason might be the differential effects of frequency on the vibrotactile and the electrical stim-

ulation of these rats. For example, in some cases the range of current level representing the vibrotactile displacements between 0-46 dB ref 1 μm decreased with increasing frequency. I previously mentioned that psychometric curves were the cumulative form of the normal distribution of biological and psychological events (see Section 2.1.4 and Figure 2.14). Therefore, in the case of decreasing slope, the distribution of psychophysical events (i.e., detection) got narrower for ICMS stimuli compared to the vibrotactile stimulation. In the case of increasing slope, the distribution of psychophysical events got wider for ICMS stimuli compared to the vibrotactile stimulation. Nevertheless, the PCFs rescale these distributions to fit them to each other, and this is the ultimate goal of the PCFs.

Furthermore, in this PCF model, I regarded the effects of periodicity of the ICMS on the elicited perception. Romo et al. showed the ability of monkeys to discriminate frequencies of vibrotactile stimuli applied on the monkey's fingers and ICMS trains delivered to the finger representation of the SI [36, 147]. Their results may indicate that a periodic sensation rises when periodic ICMS pulses were delivered to the SI. However ,they have tested frequencies between 6-44 Hz. It is not sure whether the frequencies tested here results in similar sensations or not. On the other hand, it is shown that sensitivity of monkeys to ICMS plateau after 250 Hz [170]. Therefore, frequencies up to this limit may elicit periodic sensations.

On the other hand, Berg et al. and Tabot et al. applied ICMS pulses at 300 Hz [173, 186]. They tested monkeys to discriminate between the amplitude of static skin indentation applied on the monkeys' fingers and ICMS trains delivered to finger representation of SI. They ignored whether the sensations elicited by ICMS were periodic or not. In literature, it is shown that some cortical neurons entrain with vibrotactile stimulation of the glabrous skin [210]. Therefore, the monkeys might generalized to discriminate the magnitudes of the elicited sensations by vibrotactile and ICMS stimuli while ignoring the submodality of the sensations.

In this study, the proposed PCF model considers the effect of ICM frequency on the sensation based on the findings of Romo et al. [36, 147, 210]. Nevertheless, further psychophysical experiments are required to determine whether the artificial sensations elicited by ICMS resembles flutter sensation or not.

In the given context here, the PCFs successfully predicted the current levels for

a given vibrotactile displacement level and frequency in order to generate similar detectability rates for vibrotactile and ICMS stimuli. Although psychometric results were similar according to Kolmogorov-Smirnov test, ICMS intensities were slightly overestimated or underestimated in some cases. This might be related to the fitting errors at some frequencies. Furthermore, the effects of neural damage and the electrode condition should not be totally ignored.

Nevertheless, psychometric correspondence functions seems to be promising for modulating ICMS trains in a cortical somatosensory neuroprosthesis application. At least, ICMS can be used to generate neural activity which results in similar psychophysical performance as in tactile experiments. However, whether the elicited sensations match in perception space or not has yet to be determined.

The PCFs obtained from detection tasks have to be further tested in other behavioral tasks, such as amplitude discrimination [186] and object discrimination with active exploration[155]. Nevertheless, together with improvements in electrode technologies, experiments in human subjects would provide valuable insight into the artificial sensations.

4.6 Conclusions

The correspondence model presented here was constructed based on the corrected hit rates obtained in detection tasks. It successfully represents the psychometric correspondence between vibrotactile and ICMS stimuli in the frequency range of 40-80 Hz. Furthermore, it seems to be feasible for somatosensory neuroprostheses. However, further evaluation is required for how similar the artificial sensations elicited by ICMS and the natural sensations elicited by vibrotactile stimulation of the glabrous skin.

5. GENERAL CONCLUSIONS

The aim of the thesis was to construct a model for converting vibrotactile stimuli into ICMS trains in order to elicit artificial sensations similar to those elicited by natural stimulation in a detection task. The model was constructed based on the psychophysical correspondence between sensations elicited by vibrotactile stimulation of glabrous skin and ICMS trains delivered to the hindpaw representation of SI in rats.

In accordance with this purpose, first of all, I built an operant chamber to train rats in different tasks where bursts of mechanical sinusoidal vibrations were applied on the volar surface of rat's hindpaw. The novel multi-probe design made it possible to deliver mechanical stimuli to the rat's glabrous skin independent of its location in the chamber. Although some rats failed in primitive tasks, approximately 1/3 of the animals completed vibrotactile detection task with accuracies >85%. Behavioral performances of these rats were comparable to those reported in whisker literature. Furthermore, it might be possible to increase the number of rats completed the detection task with environmental enrichment. The rats were further tested in psychophysical experiments and their sensitivity to vibrotactile stimuli at three different frequencies were determined. As reported in literature, detection thresholds decreased with increasing frequency. However, detection thresholds found in rats were higher than those reported for humans and primates. This might be due to the differences between experimental setups and the physiological differences between species. The rats tested here were unrestrained and freely moving whereas fingers of humans and primates were fixed. Furthermore, mechanical properties of the skin and innervation densities are important factors effecting the detection thresholds.

Rats which completed vibrotactile experiments were implanted with microelectrodes in their hindpaw representation of primary somatosensory cortex. All rats but one successfully completed ICMS detection tasks with accuracies >85%. These rats were further tested in ICMS psychophysical experiments at different frequencies. As shown in the literature, the 50% detection thresholds showed a decreasing trend with increasing frequency.

The psychometric data collected from vibrotactile and ICMS experiments were fitted with sigmoidal surface functions based on the stimulus intensity and the frequency. These psychometric functions were used to construct psychometric correspondence functions (PCFs). PCFs mapped the vibrotactile and ICMS intensity levels that are equally detectable for a given frequency. For each rat, a separate PCF was constructed. PCFs were tested in a third experiment. In this experiment, the rats performing vibrotactile detection were presented with probe trials where either a vibrotactile or ICMS stimuli was presented. The current levels were calculated from PCFs based on vibrotactile intensity levels. The rats were expected to perform similar psychophysical performances in vibrotactile and ICMS probe trials. The model was constructed based on three frequencies (40 Hz, 60 Hz and 80 Hz) and tested with five frequencies (40 Hz, 50 Hz, 60 Hz, 70 Hz and 80 Hz). The results showed that the psychometric performances of rats were similar for vibrotactile and corresponding ICMS stimuli. Therefore, PCFs seems to be feasible for determining the current levels for ICMS stimulation in a somatosensory neuroprosthesis.

6. FUTURE WORK

The psychometric correspondence functions proposed here can be used to modulate the intensity of ICMS trains based on vibrotactile stimuli applied on a sensorized robotic finger. These ICMS trains can generate neural activity which results in similar detection rates as the tactile stimuli would do. However, we cannot be sure whether sensations elicited by tactile and ICMS match in perception space. Therefore, PCFs have to be further tested in other behavioral tasks such as amplitude discrimination or feature discrimination by active exploration. For example, Klaes et al. used *match-to-sample task* to test a monkey controlling a virtual arm with ICMS feedback [155]. In the task, the monkey touched a surface appeared on the screen with the virtual arm and it was presented with an ICMS pattern. Then, they were trained to explore the virtual environment and discriminate among two hidden targets based on the ICMS patterns presented when the virtual hand touched the targets. In order to test the PCF model, a modified version of this task can be used. While we explore a surface, mechanical oscillations on the skin surface are encoded by the mechanoreceptors [211]. Therefore, different surfaces can be encoded with different ICMS patterns by using PCF based on the surface texture. Then, the monkey samples a random surface with its own hand and uses the virtual hand to explore hidden surfaces encoded with different ICMS patterns. If the monkey successfully matches the targets to the samples, then the PCF is correctly encoded the texture into ICMS patterns.

In addition, effects of other ICMS parameters on the perception has to be further evaluated. Kim et al. studied the effects of pulse width, frequency and duration of ICMS on the detection thresholds [170]. They showed that increasing any of these parameters caused the detection threshold to decrease. On the other hand, to my knowledge, there is not any study on whether the animals can discriminate between two ICMS stimuli with same charge densities but different, e.g., pulse widths and frequencies. It might be possible to elicit different patterns of sensations by modulating two or more dimensions of the ICMS stimuli.

Higher order sensory cortices might be also targeted for somatosensory neuro-

prosthesis applications. BMI applications usually use recordings from motor cortices [145, 146], but recently other control methods using neural activity in posterior parietal cortex has been proposed [22]. Similarly, alternative approaches has been proposed for sensory feedback. Heming et al. electrically stimulated the thalamic sensory nuclei in human subjects underwent DBS surgery [212, 213]. They reported that persistent or transient tactile perception could be elicited by stimulation of these sensory nuclei. However, the location and the size of the thalamus are the drawbacks of this method. On the other hand, higher order somatosensory cortices might be targeted in order to elicit more abstract sensations, such as clenching hands or touching a rough surface.

However, animal experiments help us to improve cortical neuroprosthesis up to some certain extent. Since they can not tell exactly how similar two sensations are, we can only speculate on the behaviors of the animals. On the other hand, human studies would speed up the progress by reporting verbally how an artificial sensation is similar to the natural one. Furthermore, since each neuroprosthesis is a personalized device, which is designed and/or programmed depending on the individuals, the satisfaction of the end users with the device is important. With human studies, subjects could report how they are satisfied with the prosthesis control and the sensory feedback from the device.

Nevertheless, before human experiments, long-term stability and durability of electrodes have to be assured. Although there are studies reporting minimal damage to the brain tissue with penetrating microelectrode arrays [165], the results may change by prolonged use of these arrays in humans. Recently in literature, drug-loaded electrode coatings have been proposed to reduce the foreign body response of the nervous tissue [158, 214, 215]. Yet, use of these electrodes under both recording and stimulation conditions for prolonged periods has to be extensively studied.

APPENDIX A. Operant Conditioning Graphs

A.1 Vibrotactile operant conditioning

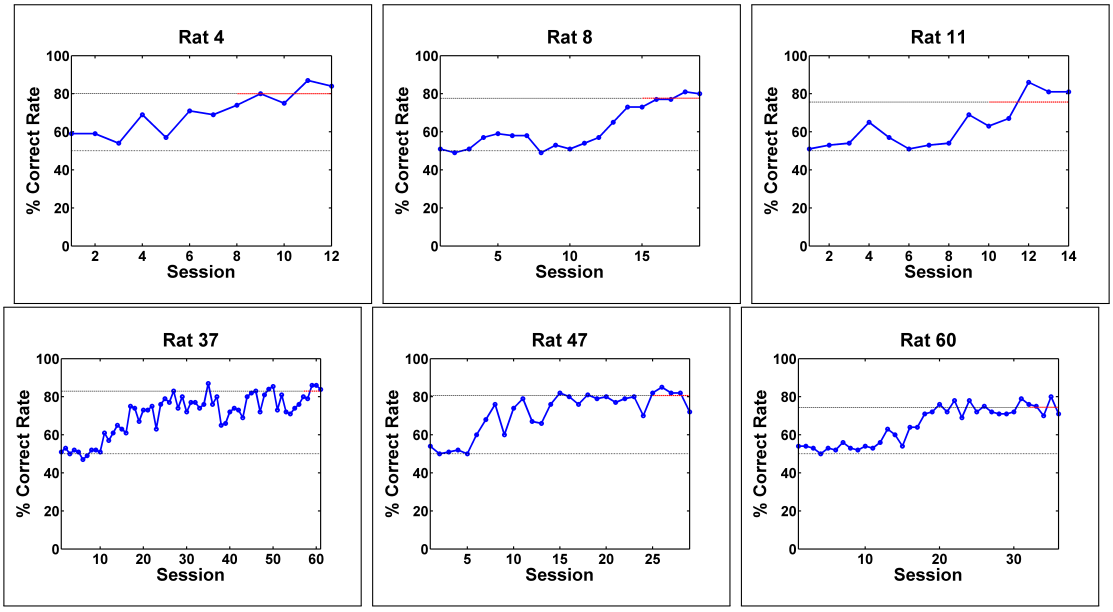

Figure A.1 Behavioral performance of rats in Task-D: Rats performed correct rates between 70%-85%. Red dashed lines show the mean accuracy for last five sessions. 50% is the chance level.

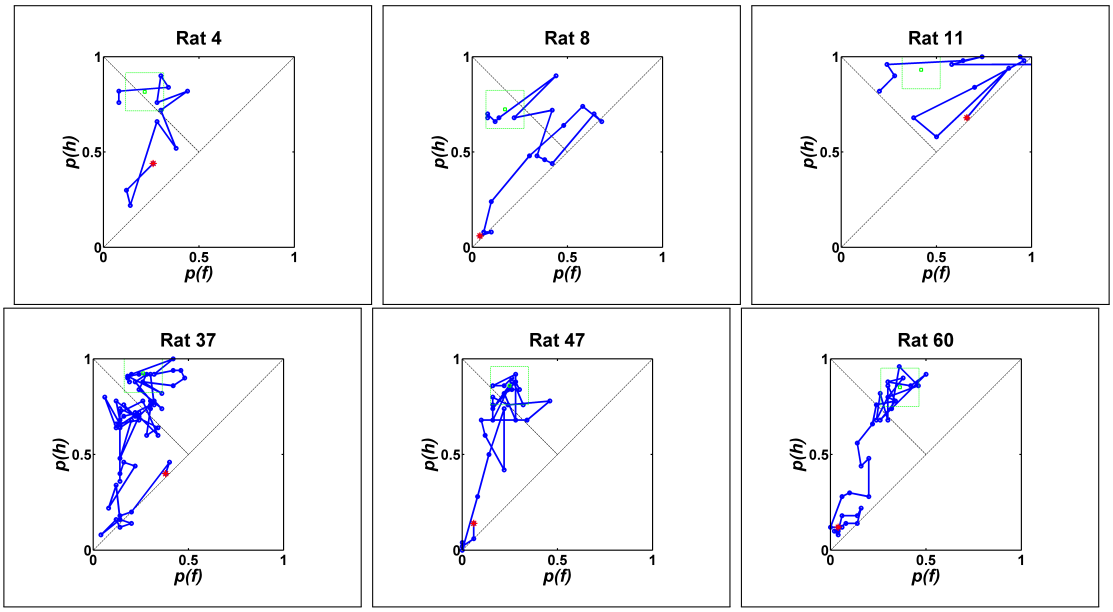

Figure A.2 Receiver operant characteristics of rats in Task-D: Rats performed correct rates between 70%-85%. Red asterisk indicates the first session. Green rectangle shows a region of mean±0.1. [0.0,0.0]-[1.0,1.0] diagonal shows the zero sensitivity. [0.0,1.0]-[0.5,0.5] diagonal is the zero-bias line.

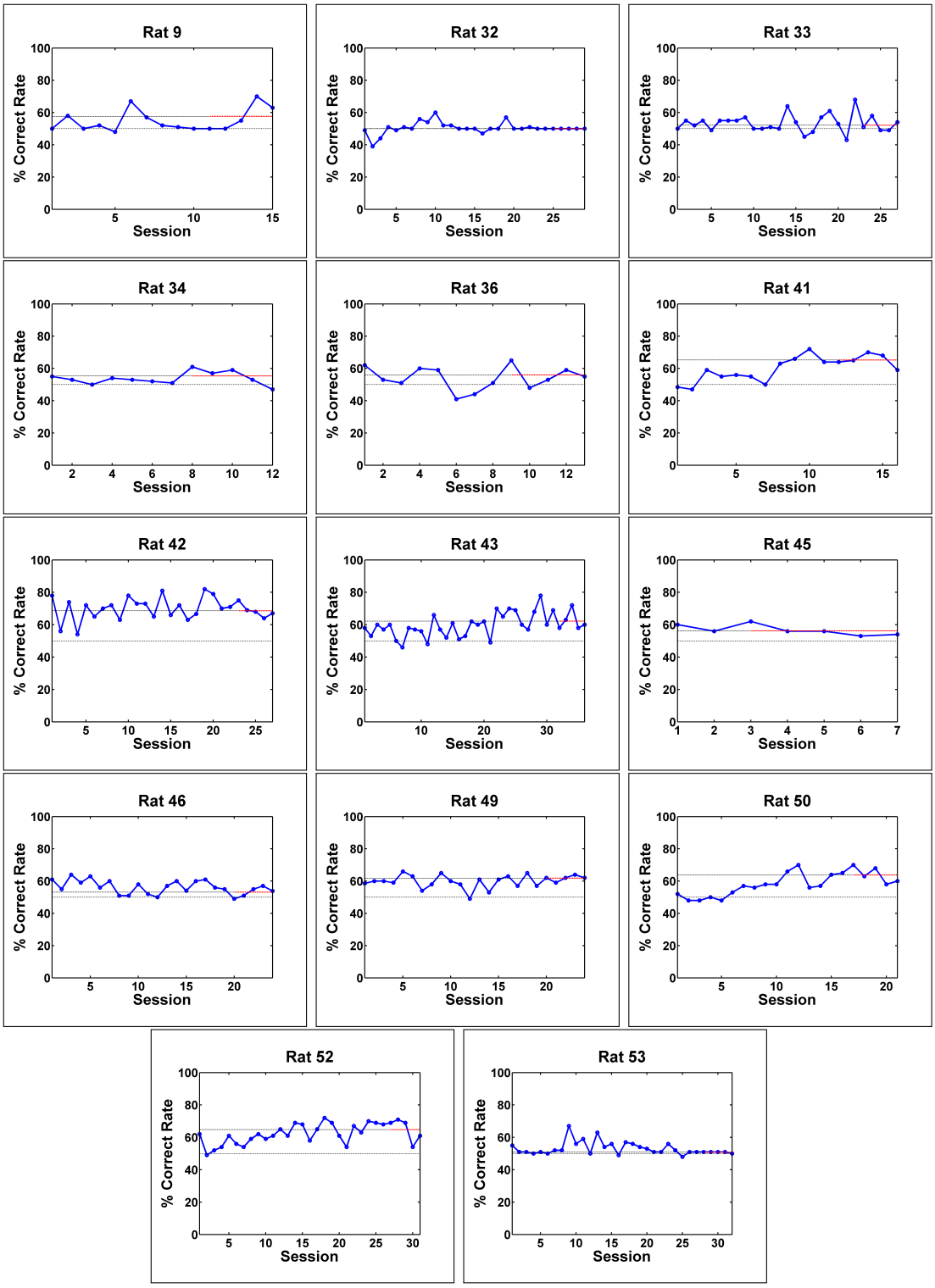

Figure A.3 Behavioral performance of rats in Task-D: Rats performed <70% correct rate. Red dashed lines show the mean accuracy for last five sessions. 50% is the chance level.

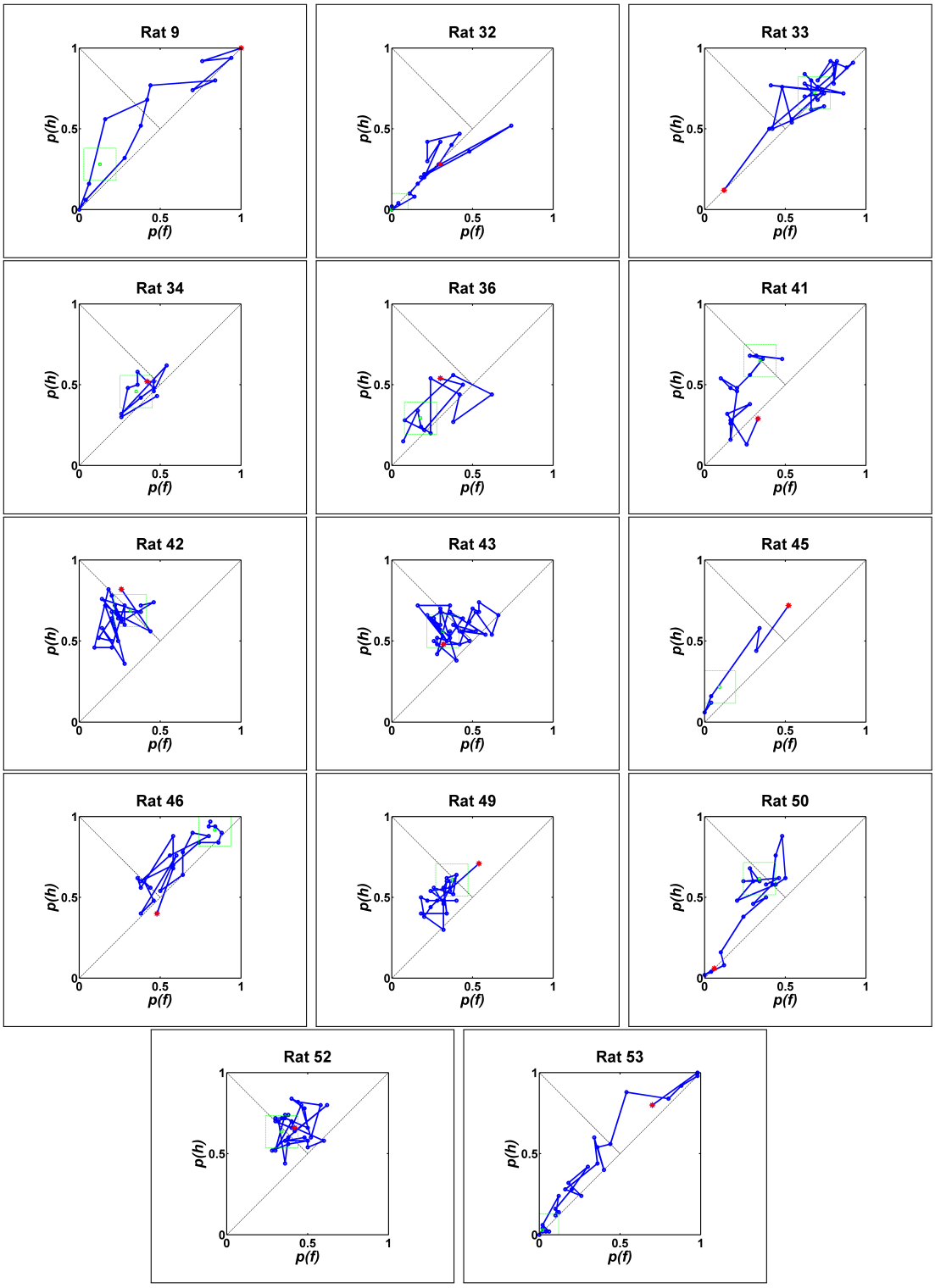

Figure A.4 Receiver operant characteristics of rats in Task-D: Rats performed correct rates between <70%. Red asterisk indicates the first session. Green rectangle shows a region of mean±0.1. [0.0,0.0]-[1.0,1.0] diagonal shows the zero sensitivity. [0.0,1.0]-[0.5,0.5] diagonal is the zero-bias line.

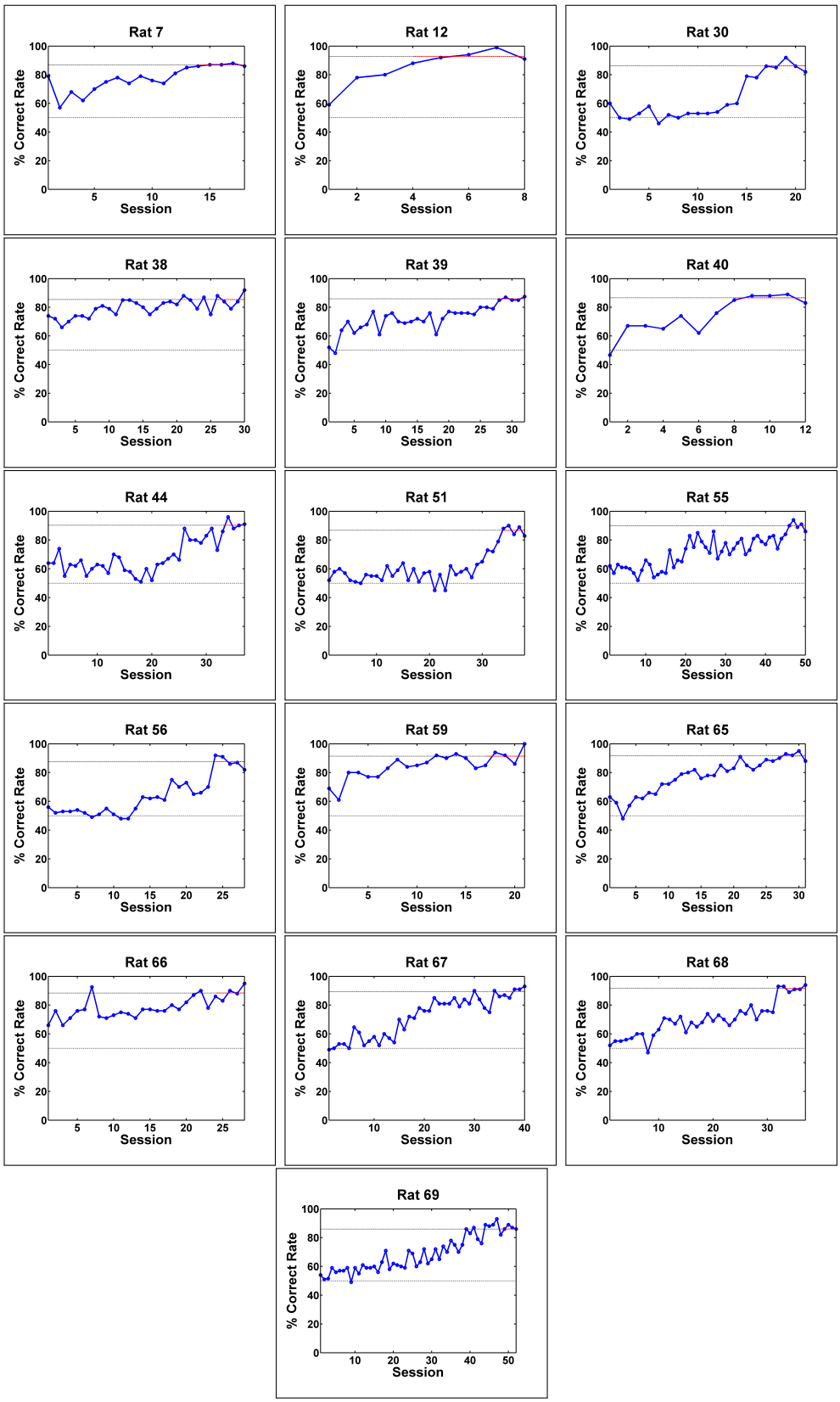

Figure A.5 Behavioral performance of rats in Task-D: Rats performed >85% correct rate. Red dashed lines show the mean accuracy for last five sessions. 50% is the chance level.

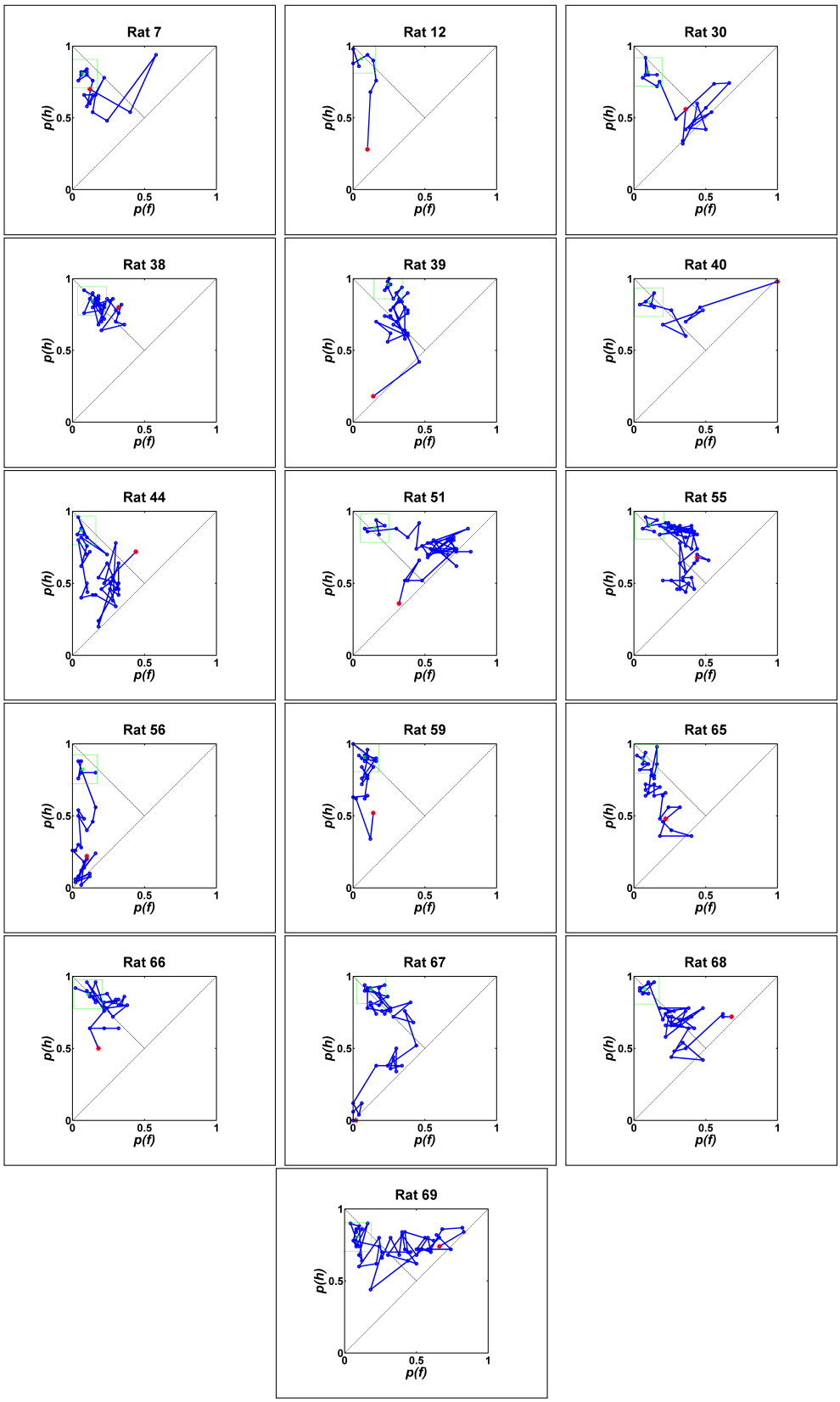

Figure A.6 Receiver operant characteristics of rats in Task-D: Rats performed correct rates between >85%. Red asterisk indicates the first session. Green rectangle shows a region of mean±0.1. [0.0,0.0]-[1.0,1.0] diagonal shows the zero sensitivity. [0.0,1.0]-[0.5,0.5] diagonal is the zero-bias line.

A.2 Auditory operant conditioning

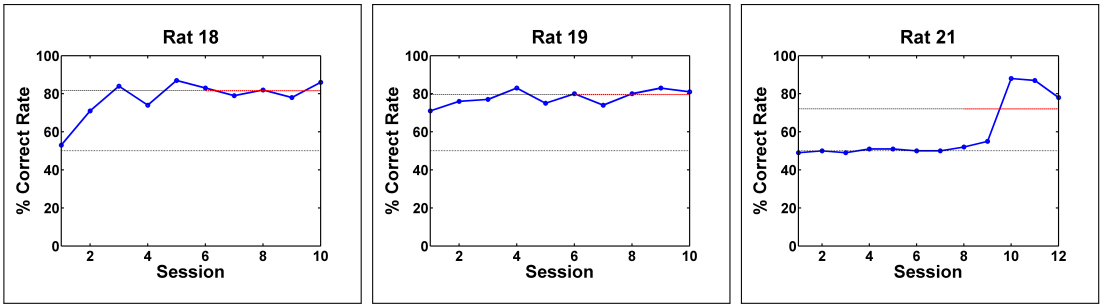

Figure A.7 Behavioral performance of rats in auditory version of Task-D. Red dashed lines show the mean accuracy for last five sessions. 50% is the chance level.

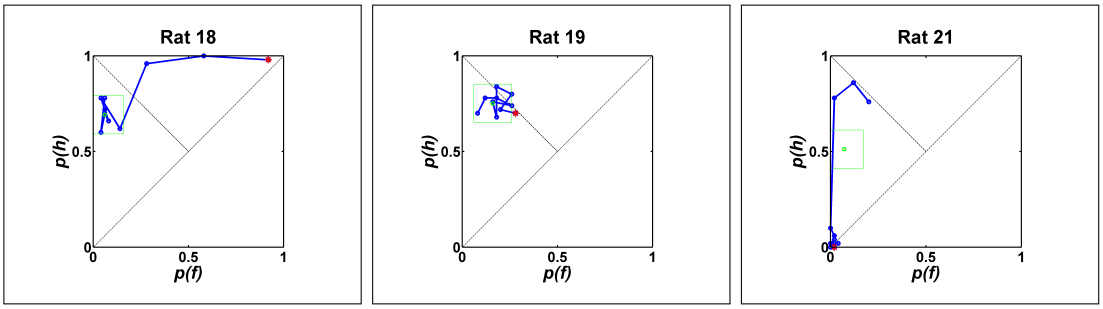

Figure A.8 Receiver operant characteristics of rats in auditory version of Task-D. Red asterisk indicates the first session. Green rectangle shows a region of mean±0.1. [0.0,0.0]-[1.0,1.0] diagonal shows the zero sensitivity. [0.0,1.0]-[0.5,0.5] diagonal is the zero-bias line.

A.3 ICMS operant conditioning

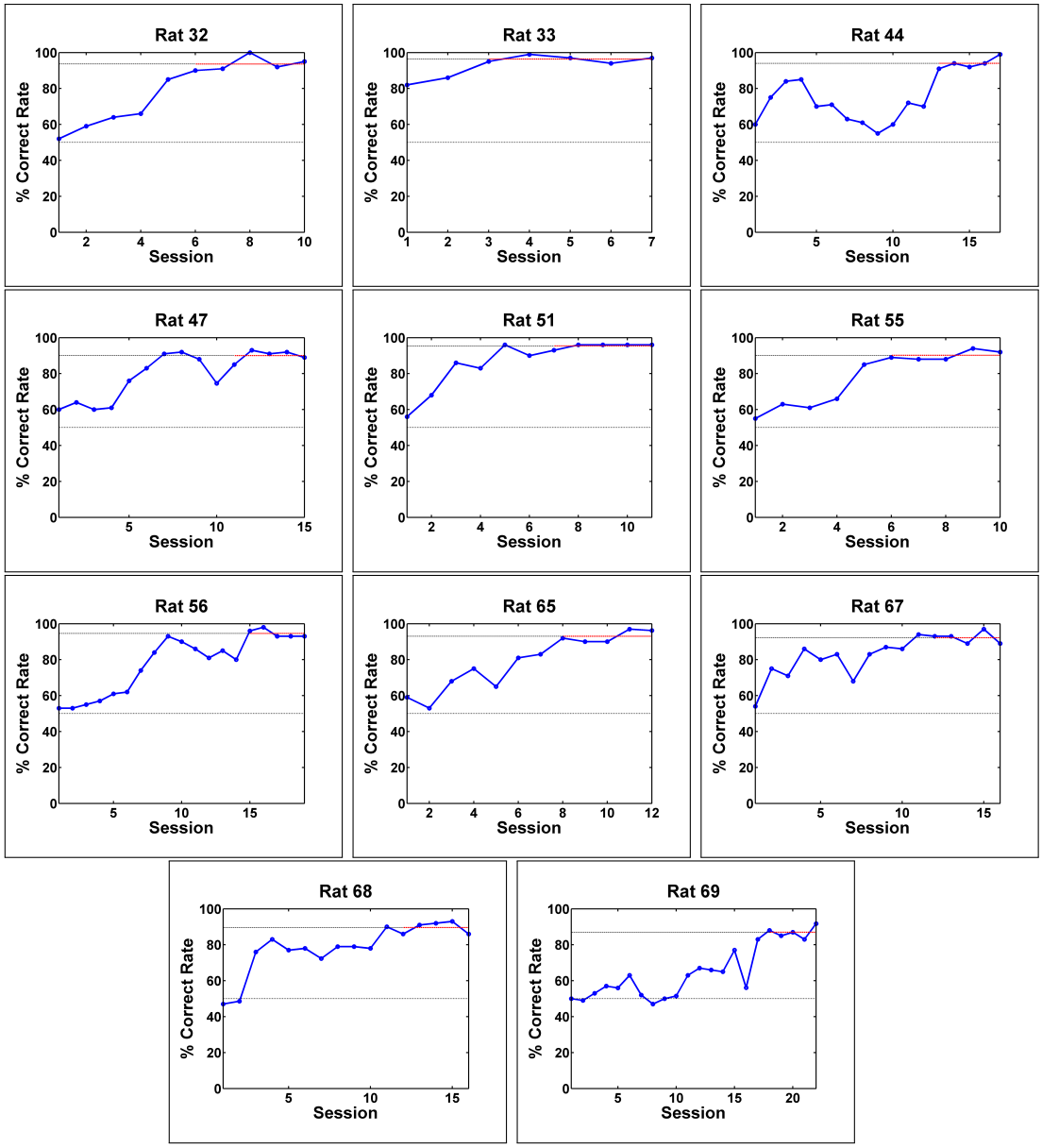

Figure A.9 Behavioral performance of rats in Task-E: ICMS Detection. Red dashed lines show the mean accuracy for last five sessions. 50% is the chance level.

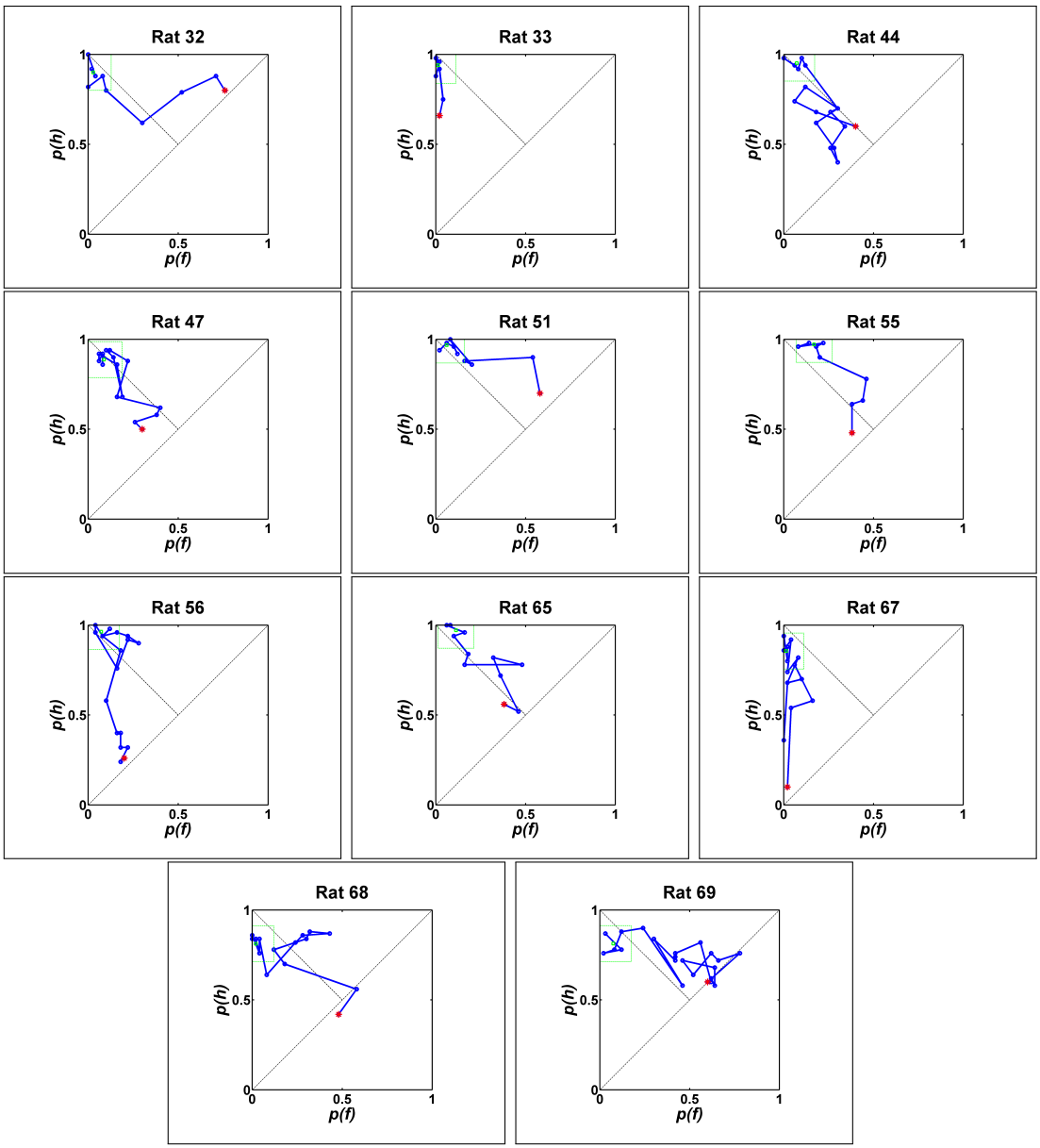

Figure A.10 Receiver operant characteristics of rats in Task-E: ICMS Detection. Red asterisk indicates the first session. Green rectangle shows a region of mean±0.1. [0.0,0.0]-[1.0,1.0] diagonal shows the zero sensitivity. [0.0,1.0]-[0.5,0.5] diagonal is the zero-bias line.

APPENDIX B. Publications

Articles

- Devecioğlu İ. and Güçlü B., A novel vibrotactile system for stimulating the glabrous skin of awake freely behaving rats during operant conditioning. *J Neuroscience Methods* 242: 41-51, 2015.
- Devecioğlu İ. and Güçlü B., Behavioral correspondence between vibrotactile stimulation and intracortical microstimulation: Towards a vibrotactile somatosensory prosthesis. *In progress.*

Conference Proceedings

International Conference Proceedings

- Devecioğlu İ. and Güçlü B., Psychophysical correspondence between vibrotactile stimulation of glabrous skin and intracortical microstimulation of the primary somatosensory cortex in the rat. ***Submitted to*** *Neuroscience 2016.* San Diego, CA: Society for Neuroscience, 2016.
- Devecioğlu İ. and Güçlü B., Vibrotactile sensitivity of freely behaving rats and operant conditioning by intracortical microstimulation. *The Third Joint Satellite Meeting of Turkey Chapter of Society for Neuroscience and Neuroscience Society of Turkey.* Chicago, IL. 2015.
- Devecioğlu İ. and Güçlü B., Electrical microstimulation of hindpaw representation in rat SI cortex yields better detection probability compared to vibrotactile stimulation of the glabrous skin during operant conditioning. Program No. 64.12. *Neuroscience 2014 Abstracts.* Washington, DC: Society for Neuroscience, 2014. Online.

- Devecioğlu İ. and Güçlü B., Development of a training schedule for tactile operant conditioning of rats. Program No. 72.04. *Neuroscience 2013 Abstracts.* San Diego, CA: Society for Neuroscience, 2013. Online.

- Devecioğlu İ. and Güçlü B., Multimodal psychophysical experiments reveal ineffective tactile inputs from the rat glabrous skin. Program No. 269.05. *Neuroscience 2012 Abstracts.* New Orleans, LA: Society for Neuroscience, 2012. Online.

National Conference Proceedings

- Devecioğlu İ. ve Güçlü B., Davranış halindeki sıçanların mekanik titreşimlere duyarlılığının belirlenmesi ve korteks içi mikro-uyarım yöntemi ile edimsel koşullandırılmaları. *Biyomedikal Mühendisliği Ulusal Toplantısı*, 2015.

- Devecioğlu İ. and Güçlü B., Sıçan tüysüz derisinde dokunsal psikofizik deneyleri için enstrümental kabin tasarımı. *Biyomedikal Mühendisliği Ulusal Toplantısı*, 2012.

REFERENCES

1. Karacan, I., H. Koyuncu, O. Pekel, G. Sumbuloglu, M. Kirnap, H. Dursun, A. Kalkan, A. Cengiz, A. Yalinkilic, H. I. Unalan, K. Nas, S. Orkun, and I. Tekeoglu, "Traumatic spinal cord injuries in turkey: a nation-wide epidemiological study," *Spinal Cord*, Vol. 38, pp. 697–701, 2000.

2. Chritopher and Dana Reeve Foundation, "Paralysis facts and figures." `http://www.christopherreeve.org/site/c.mtKZKgMWKwG/b.5184189/k.5587/Paralysis_Facts__Figures.htm`, 2009 (accessed February 11, 2016).

3. Singh, A., L. Tetreault, S. Kalsi-Ryan, A. Nouri, and M. Fehlings, "Global prevalence and incidence of traumatic spinal cord injury," *Clinical Epidemiology*, Vol. 6, pp. 309–331, 2014.

4. Dogan, A., I. Sungur, S. Bilgic, M. Uslu, B. Atik, O. Tan, S. Ozgokce, D. Uluc, H. Coban, M. Turkoglu, and F. Akpinar, "Amputations in eastern turkey (van): a multicenter epidemiological study," *Acta Orthop Traumatol Turc*, Vol. 42, pp. 53–58, 2008.

5. U.S. Dept. Health Human Serv., "Current estimates from the national health interview survey, 1994," *Vital Health Stat.*, Vol. 193(Pt. 1), pp. 1–260, 1995.

6. Owings, M. F., and L. J. Kozak, "Ambulatory and inpatient procedures in the united states, 1996," *Vital and health statistics. Series 13, Data from the National Health Survey*, no. 139, pp. 1–119, 1998.

7. Ziegler-Graham, K., E. J. MacKenzie, P. L. Ephraim, T. G. Travison, and R. Brookmeyer, "Estimating the prevalence of limb loss in the united states: 2005 to 2050," *Arch Phys Med Rehabil*, Vol. 89, no. 3, pp. 422–9, 2008.

8. Davidson, J., "A comparison of upper limb amputees and patients with upper limb injuries using the disability of the arm, shoulder and hand (dash)," *Disability & Rehabilitation*, Vol. 26, no. 14-15, pp. 917–923, 2004.

9. Noble, D., D. B. Price, and R. Gilder, "Psychiatric disturbances following amputation," *Am J Psychiatry*, Vol. 110, no. 8, pp. 609–13, 1954.

10. Opalic, P., and A. Lesic, "Investigation of psychopathological state of patients depending on specific clinical characteristics of physical trauma," *Panminerva Med*, Vol. 44, no. 1, pp. 11–7, 2002.

11. Horgan, O., and M. MacLachlan, "Psychosocial adjustment to lower-limb amputation: A review," *Disability & Rehabilitation*, Vol. 26, no. 14-15, pp. 837–850, 2004.

12. Cavanagh, S. R., L. M. Shin, N. Karamouz, and S. L. Rauch, "Psychiatric and emotional sequelae of surgical amputation," *Psychosomatics*, Vol. 47, no. 6, pp. 459–64, 2006.

13. Bhuvaneswar, C. G., L. A. Epstein, and T. A. Stern, "Reactions to amputation: recognition and treatment," *Prim Care Companion J Clin Psychiatry*, Vol. 9, no. 4, pp. 303–8, 2007.

14. Bosmans, J. C., T. P. Suurmeijer, M. Hulsink, C. P. van der Schans, J. H. Geertzen, and P. U. Dijkstra, "Amputation, phantom pain and subjective well-being: a qualitative study," *Int J Rehabil Res*, Vol. 30, no. 1, pp. 1–8, 2007.

15. Burger, H., and C. Marincek, "Return to work after lower limb amputation," *Disability & Rehabilitation*, Vol. 29, no. 17, pp. 1323–9, 2007.

16. Lewis, E., D. M. Lloyd, and M. J. Farrell, "The role of the environment in eliciting phantom-like sensations in non-amputees," *Front Psychol*, Vol. 3, p. 600, 2012.

17. Czerniecki, J. M., "Rehabilitation in limb deficiency. 1. gait and motion analysis," *Arch Phys Med Rehabil*, Vol. 77, no. 3 Suppl, pp. S3–8, 1996.

18. Esquenazi, A., and r. Meier, R. H., "Rehabilitation in limb deficiency. 4. limb amputation," *Arch Phys Med Rehabil*, Vol. 77, no. 3 Suppl, pp. S18–28, 1996.

19. Sears, H. H., and J. Shaperman, "Proportional myoelectric hand control: an evaluation," *Am J Phys Med Rehabil*, Vol. 70, no. 1, pp. 20–8, 1991.

20. Chapin, J. K., K. A. Moxon, R. S. Markowitz, and M. A. Nicolelis, "Real-time control of a robot arm using simultaneously recorded neurons in the motor cortex," *Nat Neurosci*, Vol. 2, no. 7, pp. 664–70, 1999.

21. Fagg, A. H., N. G. Hatsopoulos, V. de Lafuente, K. A. Moxon, S. Nemati, J. M. Rebesco, R. Romo, S. A. Solla, J. Reimer, D. Tkach, E. A. Pohlmeyer, and L. E. Miller, "Biomimetic brain machine interfaces for the control of movement," *J Neurosci*, Vol. 27, no. 44, pp. 11842–6, 2007.

22. Andersen, R. A., E. J. Hwang, and G. H. Mulliken, "Cognitive neural prosthetics," *Annu Rev Psychol*, Vol. 61, pp. 169–190, 2010.

23. OttoBock, "Upper limb prosthesis." http://www.ottobockus.com/prosthetics/upper-limb-prosthetics/solution-overview/michelangelo-prosthetic-hand/, accessed February 18, 2016.

24. Hochberg, L. R., D. Bacher, B. Jarosiewicz, N. Y. Masse, J. D. Simeral, J. Vogel, S. Haddadin, J. Liu, S. S. Cash, P. van der Smagt, and J. P. Donoghue, "Reach and grasp by people with tetraplegia using a neurally controlled robotic arm," *Nature*, Vol. 485, no. 7398, pp. 372–5, 2012.

25. Wolpert, D. M., K. G. Pearson, and C. P. J. Ghez, "The organization and planning of movement," in *Principles of neural science, 5th ed.* (Kandel, E. R., J. H. Schwartz, T. M. Jessell, S. A. Siegelbaum, and A. J. Hudspeth, eds.), book section Movement, pp. 743–767, New York, NY, USA: McGraw-Hill, 2012.

26. Gardner, E. P., and K. O. Johnson, "The somatosensory system: Receptors and central pathways," in *Principles of neural science, 5th ed.* (Kandel, E. R., J. H. Schwartz, T. M. Jessell, S. A. Siegelbaum, and A. J. Hudspeth, eds.), book section Perception, pp. 475–497, New York, NY, USA: McGraw-Hill, 2012.

27. Gardner, E. P., and K. O. Johnson, "Touch," in *Principles of neural science, 5th ed.* (Kandel, E. R., J. H. Schwartz, T. M. Jessell, S. A. Siegelbaum, and A. J. Hudspeth, eds.), book section Perception, pp. 498–529, New York, NY, USA: McGraw-Hill, 2012.

28. Gaunt, R. A., J. L. Collinger, B. Wodlinger, D. J. Weber, and M. L. Boninger, "Proprioceptive feedback enables brain computer interface (BCI) controlled prosthetic arm movement in the absence of visual input," *Program No. 374.12. Neuroscience 2013 Abstracts.*, San Diego, CA: Society for Neuroscience, 2013. Online.

29. Ehrsson, H. H., N. P. Holmes, and R. E. Passingham, "Touching a rubber hand: feeling of body ownership is associated with activity in multisensory brain areas," *J Neurosci*, Vol. 25, no. 45, pp. 10564–73, 2005.

30. Ehrsson, H. H., B. Rosen, A. Stockselius, C. Ragno, P. Kohler, and G. Lundborg, "Upper limb amputees can be induced to experience a rubber hand as their own," *Brain*, Vol. 131, no. Pt 12, pp. 3443–52, 2008.

31. Petkova, V. I., M. Bjornsdotter, G. Gentile, T. Jonsson, T. Q. Li, and H. H. Ehrsson, "From part- to whole-body ownership in the multisensory brain," *Curr Biol*, Vol. 21, no. 13, pp. 1118–22, 2011.

32. de Vignemont, F., "Embodiment, ownership and disownership," *Conscious Cogn*, Vol. 20, no. 1, pp. 82–93, 2011.

33. Maravita, A., and A. Iriki, "Tools for the body (schema)," *Trends Cogn Sci*, Vol. 8, no. 2, pp. 79–86, 2004.

34. Hatsopoulos, N. G., and J. P. Donoghue, "The science of neural interface systems," *Annu Rev Neurosci*, Vol. 32, pp. 249–266, 2009.

35. Grill, W. M., S. Norman, and R. V. Bellamkonda, "Implanted neural interfaces: biochallenges and engineered solutions," *Annu Rev Biomed Eng*, Vol. 11, pp. 1–24, 2009.

36. Romo, R., A. Hernandez, A. Zainos, C. D. Brody, and L. Lemus, "Sensing without touching: psychophysical performance based on cortical microstimulation," *Neuron*, Vol. 26, no. 1, pp. 273–8, 2000.

37. Rossini, P. M., S. Micera, A. Benvenuto, J. Carpaneto, G. Cavallo, L. Citi, C. Cipriani, L. Denaro, V. Denaro, G. Di Pino, F. Ferreri, E. Guglielmelli, K. P. Hoffmann, S. Raspopovic, J. Rigosa, L. Rossini, M. Tombini, and P. Dario, "Double nerve intraneural interface implant on a human amputee for robotic hand control," *Clin Neurophysiol*, Vol. 121, no. 5, pp. 777–83, 2010.

38. Penfield, W., "The radical treatment of traumatic epilepsy and its rationale," *Can Med Assoc J*, Vol. 23, no. 2, pp. 189–97, 1930.

39. Talwar, S. K., and G. L. Gerstein, "A signal detection analysis of auditory-frequency discrimination in the rat," *J Acoust Soc Am*, Vol. 105, p. 1784, 1999.

40. Rajan, R., J. P. Clement, and U. S. Bhalla, "Rats smell in stereo," *Science*, Vol. 311, no. 5761, pp. 666–70, 2006.

41. Horner, A. E., C. J. Heath, M. Hvoslef-Eide, B. A. Kent, C. H. Kim, S. R. Nilsson, J. Alsio, C. A. Oomen, A. Holmes, L. M. Saksida, and T. J. Bussey, "The touchscreen operant platform for testing learning and memory in rats and mice," *Nat Protoc*, Vol. 8, no. 10, pp. 1961–84, 2013.

42. Adibi, M., and E. Arabzadeh, "A comparison of neuronal and behavioral detection and discrimination performances in rat whisker system," *J Neurophysiol*, Vol. 105, no. 1, pp. 356–65, 2011.

43. Harris, J. A., R. S. Petersen, and M. E. Diamond, "Distribution of tactile learning and its neural basis," *Proc Natl Acad Sci U S A*, Vol. 96, no. 13, pp. 7587–91, 1999.

44. Tahon, K., M. Wijnants, and E. De Schutter, "The rat-rotadrum: a reaction time task depending on a continuous stream of tactile sensory information to the rat," *J Neurosci Methods*, Vol. 200, no. 2, pp. 153–63, 2011.

45. Walker, J. L., F. Monjaraz-Fuentes, C. R. Pedrow, and D. M. Rector, "Precision rodent whisker stimulator with integrated servo-locked control and displacement measurement," *J Neurosci Methods*, Vol. 196, no. 1, pp. 20–30, 2011.

46. Wiest, M. C., E. Thomson, J. Pantoja, and M. A. Nicolelis, "Changes in s1 neural responses during tactile discrimination learning," *J Neurophysiol*, Vol. 104, no. 1, pp. 300–12, 2010.

47. Ikemoto, S., and L. G. Sharpe, "A head-attachable device for injecting nanoliter volumes of drug solutions into brain sites of freely moving rats," *J Neurosci Methods*, Vol. 110, no. 1, pp. 135–140, 2001.

48. Xu, S., S. K. Talwar, E. S. Hawley, L. Li, and J. K. Chapin, "A multi-channel telemetry system for brain microstimulation in freely roaming animals," *J Neurosci Methods*, Vol. 133, no. 1-2, pp. 57–63, 2004.

49. Willis, W. D., and R. E. Coggeshall, *Sensory Mechanisms of the Spinal Cord: Volume 1 Primary Afferent Neurons and the Spinal Dorsal Horn*, New York, NY, USA: Springer Science+Business Media, 2004.

50. Andres, K. H., and M. von Düring, "Morphology of cutaneous receptors," in *Handbook of Sensory Physiology, Volume II: Somatosensory System* (Iggo, A., ed.), pp. 3–28, Springer-Verlag Berlin-Heidelberg-New York, 1973.

51. Halata, Z., "Sensory innervation of the hairless and hairy skin in mammals including humans," in *The primary afferent neuron* (Zenker, W., and W. Neuhuber, eds.), book section 2, pp. 19–34, New York, NY, USA: Plenum Press, 1990.

52. Lechner, S. G., and G. R. Lewin, "Hairy sensation," *Physiology (Bethesda)*, Vol. 28, no. 3, pp. 142–50, 2013.

53. Lumpkin, E. A., K. L. Marshall, and A. M. Nelson, "The cell biology of touch," *J Cell Biol*, Vol. 191, no. 2, pp. 237–48, 2010.

54. Li, L., M. Rutlin, V. E. Abraira, C. Cassidy, L. Kus, S. Gong, M. P. Jankowski, W. Luo, N. Heintz, H. R. Koerber, C. J. Woodbury, and D. D. Ginty, "The functional organization of cutaneous low-threshold mechanosensory neurons," *Cell*, Vol. 147, no. 7, pp. 1615–27, 2011.

55. Vallbo, A. B., H. Olausson, J. Wessberg, and N. Kakuda, "Receptive field characteristics of tactile units with myelinated afferents in hairy skin of human subjects," *J Physiol*, Vol. 483 (Pt 3), pp. 783–95, 1995.

56. Diamond, M. E., M. von Heimendahl, P. M. Knutsen, D. Kleinfeld, and E. Ahissar, "'where' and 'what' in the whisker sensorimotor system," *Nat Rev Neurosci*, Vol. 9, no. 8, pp. 601–12, 2008.

57. Haidarliu, S., E. Simony, D. Golomb, and E. Ahissar, "Muscle architecture in the mystacial pad of the rat.," *Anatomical Record (Hoboken)*, Vol. 293, pp. 1192–1206, 2010.

58. Grant, R. A., S. Haidarliu, N. J. Kennerley, and T. J. Prescott, "The evolution of active vibrissal sensing in mammals: evidence from vibrissal musculature and function in the marsupial opossum monodelphis domestica," *J Exp Biol*, Vol. 216, pp. 3483–3494, 2013.

59. Kleinfeld, D., E. Ahissar, and M. E. Diamond, "Active sensation: insights from the rodent vibrissa sensorimotor system," *Curr Opin Neurobiol*, Vol. 16, no. 4, pp. 435–44, 2006.

60. Ahissar, E., "And motion changes it all," *Nat Neurosci*, Vol. 11, no. 12, pp. 1369–70, 2008. Ahissar, Ehud eng Comment News 2008/11/22 09:00 Nat Neurosci. 2008 Dec;11(12):1369-70. doi: 10.1038/nn1208-1369.

61. Burgess, P. R., D. Petit, and R. M. Warren, "Receptor types in cat hairy skin supplied by myelinated fibers," *J Neurophysiol*, Vol. 31, pp. 833–848, 1968.

62. Wessberg, J., H. Olausson, K. W. Fernstrom, and A. B. Vallbo, "Receptive field properties of unmyelinated tactile afferents in the human skin," *J Neurophysiol*, Vol. 89, no. 3, pp. 1567–75, 2003.

63. Greenspan, J. D., and S. J. Bolanowski, "The psychophysics of tactile perception and its peripheral physiological basis," in *Pain and touch* (Kruger, L., ed.), pp. 25–104, San Diego, CA: Acedemic Press, 1996.

64. Güçlü, B., and S. J. Bolanowski, "Frequency responses of cat rapidly adapting mechanoreceptive fibers," *Somatosens Mot Res*, Vol. 20, no. 3-4, pp. 249–63, 2003.

65. Bolanowski, S., "Somatosensory coding," in *Signals and Perception: Fundamentals of Human sensation* (Roberts, D., ed.), pp. 233–243, Basingstoke, UK: Palgrave Macmillan, 2002.

66. Archer, C. B., "Functions of the skin," in *Rook's Textbook of Dermatology* (Burns, T., S. Breathnach, N. Cox, and C. Griffiths, eds.), West Sussex, UK: Wiley-Blackwell, 2010.

67. Iggo, A., and A. R. Muir, "The structure and function of a slowly adapting touch corpuscle in hairy skin," *J Physiol*, Vol. 200, no. 3, pp. 763–96, 1969.

68. Johansson, R. S., "Tactile sensibility in the human hand: receptive field characteristics of mechanoreceptive units in the glabrous skin area," *J Physiol*, Vol. 281, pp. 101–25, 1978.

69. Lynn, B., and S. E. Carpenter, "Primary afferent units from the hairy skin of the rat hind limb," *Brain Res*, Vol. 238, no. 1, pp. 29–43, 1982.

70. Bolanowski, S. J., and J. J. Zwislocki, "Intensity and frequency characteristics of pacinian corpuscles. i. action potentials," *J Neurophysiol*, Vol. 51, no. 4, pp. 793–811, 1984.

71. Leem, J. W., W. D. Willis, and J. M. Chung, "Cutaneous sensory receptors in the rat foot," *J Neurophysiol*, Vol. 69, no. 5, pp. 1684–99, 1993.

72. Leem, J. W., W. D. Willis, S. C. Weller, and J. M. Chung, "Differential activation and classification of cutaneous afferents in the rat," *J Neurophysiol*, Vol. 70, no. 6, pp. 2411–24, 1993.

73. Koltzenburg, M., C. L. Stucky, and G. R. Lewin, "Receptive properties of mouse sensory neurons innervating hairy skin," *J Neurophysiol*, Vol. 78, no. 4, pp. 1841–50, 1997.

74. Johnson, K. O., "The roles and functions of cutaneous mechanoreceptors," *Curr Opin Neurobiol*, Vol. 11, no. 4, pp. 455–61, 2001.

75. Devecioğlu, I., and B. Güçlü, "Asymmetric response properties of rapidly adapting mechanoreceptive fibers in the rat glabrous skin," *Somatosens Mot Res*, Vol. 30, no. 1, pp. 16–29, 2013.

76. Iggo, A., "Cutaneous receptors," in *The Peripheral Nervous System* (Hubbard, J., ed.), pp. 374–404, New York, NY, USA: Springer, 1974.

77. Ridley, A., "Silver staining of nerve endings in human digital glabrous skin," *J Anat*, Vol. 104, no. Pt 1, pp. 41–8, 1969.

78. Bolanowski, S. J., and L. Pawson, "Organization of meissner corpuscles in the glabrous skin of monkey and cat," *Somatosens Mot Res*, Vol. 20, no. 3-4, pp. 223–31, 2003.

79. Paré, M., R. Elde, J. E. Mazurkiewicz, A. M. Smith, and F. L. Rice, "The meissner corpuscle revised: a multiafferented mechanoreceptor with nociceptor immunochemical properties," *J Neurosci*, Vol. 21, no. 18, pp. 7236–46, 2001.

80. Johansson, R. S., and A. B. Vallbo, "Tactile sensibility in the human hand: relative and absolute densities of four types of mechanoreceptive units in glabrous skin," *J Physiol*, Vol. 286, pp. 283–300, 1979.

81. Darian-Smith, I., and P. Kenins, "Innervation density of mechanoreceptive fibres supplying glabrous skin of the monkey's index finger," *J Physiol*, Vol. 309, pp. 147–55, 1980.

82. Güçlü, B., and S. J. Bolanowski, "Distribution of the intensity-characteristic parameters of cat rapidly adapting mechanoreceptive fibers," *Somatosens Mot Res*, Vol. 20, no. 2, pp. 149–55, 2003.

83. Spencer, P. S., and H. Schaumburg, "An ultrastructural study of the inner core of the pacinian corpuscle," *J Neurocytology*, Vol. 2, pp. 217–235, 1973.

84. Pease, D. C., and T. A. Quilliam, "Electron microscopy of the pacinian corpuscle," *J Biophys Biochem Cytol*, Vol. 3, no. 3, p. 331, 1957.

85. Johnson, K. O., T. Yoshioka, and F. Vega-Bermudez, "Tactile functions of mechanoreceptive afferents innervating the hand," *J Clin Neurophysiol*, Vol. 17, no. 6, pp. 539–58, 2000.

86. Pawson, L., L. T. Prestia, G. K. Mahoney, B. Güçlü, P. J. Cox, and A. K. Pack, "Gabaergic/glutamatergic-glial/neuronal interaction contributes to rapid adaptation in pacinian corpuscles," *J Neurosci*, Vol. 29, no. 9, pp. 2695–705, 2009.

87. Press, D., S. Mutlu, and B. Güçlü, "Evidence of fast serotonin transmission in frog slowly adapting type 1 responses," *Somatosens Mot Res*, Vol. 27, pp. 174–185, 2010.

88. Vega-Bermudez, F., and K. O. Johnson, "Sa1 and ra receptive fields, response variability, and population responses mapped with a probe array," *J Neurophysiol*, Vol. 81, no. 6, pp. 2701–10, 1999.

89. Vega-Bermudez, F., and K. O. Johnson, "Surround suppression in the responses of primate sa1 and ra mechanoreceptive afferents mapped with a probe array," *J Neurophysiol*, Vol. 81, no. 6, pp. 2711–9, 1999.

90. Johansson, R. S., U. Landstrom, and R. Lundstrom, "Responses of mechanoreceptive afferent units in the glabrous skin of the human hand to sinusoidal skin displacements," *Brain Res*, Vol. 244, no. 1, pp. 17–25, 1982.

91. Ruffini, A., "The original slide carrying a gold chloride stained ruffini ending dissected from human." `https://cslide.medsci.ox.ac.uk/items/view/635#markings`, (accessed March 10, 2016).

92. Molnár, Z., and R. E. Brown, "Insights into the life and work of sir charles sherrington," *Nat Rev Neurosci*, Vol. 11, pp. 429–436, 2010.

93. Penfield, W., and T. Rasmussen, *The cerebral cortex of man: A clinical study of localization of function*, New York, NY, USA: The Macmillan Company.

94. Donoghue, J. P., K. L. Kerman, and F. F. Ebner, "Evidence for two organizational plans within the somatic sensory-motor cortex of the rat," *J Comp Neurol*, Vol. 183, pp. 647–663, 1979.

95. Chapin, J. K., and C. S. Lin, "Mapping the body representation in the si cortex of anesthetized and awake rats," *J Comp Neurol*, Vol. 229, no. 2, pp. 199–213, 1984.

96. Neafsey, E. J., E. L. Bold, G. Haas, K. M. Hurley-Gius, G. Quirk, C. F. Sievert, and R. R. Terreberry, "The organization of the rat motor cortex: a microstimulation mapping study," *Brain Research*, Vol. 396, pp. 77–96, 1986.

97. Zwislocki, J. J., *Sensory neuroscience: Four laws of psychophysics*, New York, NY, USA: Springer, 2009.

98. Güçlü, B., and S. J. Bolanowski, "Vibrotactile thresholds of the non-pacinian i channel: I. methodological issues," *Somatosens Mot Res*, Vol. 22, no. 1-2, pp. 49–56, 2005.

99. Güçlü, B., C. Tanidir, N. M. Mukaddes, and F. Unal, "Tactile sensitivity of normal and autistic children," *Somatosens Mot Res*, Vol. 24, pp. 21–33, 2007.

100. Güçlü, B., and C. Öztek, "Tactile sensitivity of children: effects of frequency, masking, and the non-pacinian i psychophysical channel," *J Exp Child Psychol*, Vol. 98, pp. 113–30, 2007.

101. Güçlü, B., "Deviation from weber's law in the non-pacinian i tactile channel: A psychophysical and simulation study of intensity discrimination," *Neural Comput*, Vol. 19, pp. 2638–64, 2007.

102. Güçlü, B., E. Sevinç, and R. Canbeyli, "Duration discrimination by musicians and nonmusicians," *Psychol Rep*, Vol. 108, no. 3, pp. 675–87, 2011.

103. Muniak, M. A., S. Ray, S. S. Hsiao, J. F. Dammann, and S. J. Bensmaia, "The neural coding of stimulus intensity: linking the population response of mechanoreceptive afferents with psychophysical behavior," *J Neurosci*, Vol. 27, no. 43, pp. 11687–99, 2007.

104. Güçlü, B., and S. M. Dinçer, "Neural coding in the non-pacinian i tactile channel: A psychophysical and simulation study of magnitude estimation," *Somatosens Mot Res*, Vol. 30, pp. 1–15, 2013.

105. Bolanowski Jr, S. J., G. A. Gescheider, R. T. Verrillo, and C. M. Checkosky, "Four channels mediate the mechanical aspects of touch," *J Acoust Soc Am*, Vol. 84, p. 1680, 1988.

106. Gescheider, G. A., "The classical psychophysical methods," in *Psychophysics: The fundamentals*, ch. 3, pp. 45–72, Mahwah, NJ, USA: Lawrence Erlbaum Associates, 1997.

107. Prigg, T., D. Goldreich, G. E. Carvell, and D. J. Simons, "Texture discrimination and unit recordings in the rat whisker/barrel system," *Physiol Behav*, Vol. 77, no. 4-5, pp. 671–5, 2002.

108. Butovas, S., and C. Schwarz, "Detection psychophysics of intracortical microstimulation in rat primary somatosensory cortex," *Eur J Neurosci*, Vol. 25, no. 7, pp. 2161–9, 2007.

109. Stebbins, W., *Animal psychophysics: the design and conduct of sensory experiments*, New York, NY, USA: Springer Science+Business Media, 1970.

110. Lawson, R., and L. S. J. Watson, "Learning in the rat (rattus norvegicus) under positive vs. negative reinforcement with incentive conditions controlled," *Ohio J Sci*, Vol. 63, no. 2, pp. 87–91, 1963.

111. Koivuniemi, A. S., and K. J. Otto, "The depth, waveform and pulse rate for electrical microstimulation of the auditory cortex," *Conf Proc IEEE Eng Med Biol Soc*, pp. 2489–2492, 2012.

112. Semprini, M., L. Bennicelli, and A. Vato, "A parametric study of intracortical microstimulation in behaving rats for the development of artificial sensory channels," *Conf Proc IEEE Eng Med Biol Soc*, 2012.

113. May, T., I. Ozden, B. Brush, D. Borton, F. Wagner, N. Agha, D. L. Sheinberg, and A. V. Nurmikko, "Detection of optogenetic stimulation in somatosensory cortex by non-human primates–towards artificial tactile sensation," *PLoS One*, Vol. 9, no. 12, p. e114529, 2014.

114. Walker, J. L., B. M. Walker, F. M. Fuentes, and D. M. Rector, "Rat psychomotor vigilance task with fast response times using a conditioned lick behavior," *Behav Brain Res*, Vol. 216, no. 1, pp. 229–37, 2011.

115. Frederick, D. E., D. Rojas-Libano, M. Scott, and L. M. Kay, "Rat behavior in go/no-go and two-alternative choice odor discrimination: differences and similarities," *Behav Neurosci*, Vol. 125, no. 4, pp. 588–603, 2011.

116. Rousche, P. J., K. J. Otto, M. P. Reilly, and D. R. Kipke, "Single electrode microstimulation of rat auditory cortex: an evaluation of behavioral performance," *Hearing Research*, Vol. 179, no. 1-2, pp. 62–71, 2003.

117. Vazquez, Y., E. Salinas, and R. Romo, "Transformation of the neural code for tactile detection from thalamus to cortex," *Proc Natl Acad Sci U S A*, Vol. 110, no. 28, pp. E2635–44, 2013.

118. Otto, K. J., P. J. Rousche, and D. R. Kipke, "Cortical microstimulation in auditory cortex of rat elicits best-frequency dependent behaviors," *J Neural Eng*, Vol. 2, no. 2, pp. 42–51, 2005.

119. Parthasarathy, K., and U. S. Bhalla, "Laterality and symmetry in rat olfactory behavior and in physiology of olfactory input," *J Neurosci*, Vol. 33, no. 13, pp. 5750–60, 2013.

120. Hernandez, A., A. Zainos, and R. Romo, "Neuronal correlates of sensory discrimination in the somatosensory cortex," *Proc Natl Acad Sci U S A*, Vol. 97, no. 11, pp. 6191–6, 2000.

121. Sanders, K. H., and M. Zimmermann, "Mechanoreceptors in rat glabrous skin: redevelopment of function after nerve crush," *J Neurophysiol*, Vol. 55, no. 4, pp. 644–59, 1986.

122. Gerdjikov, T. V., C. G. Bergner, M. C. Stuttgen, C. Waiblinger, and C. Schwarz, "Discrimination of vibrotactile stimuli in the rat whisker system: behavior and neurometrics," *Neuron*, Vol. 65, no. 4, pp. 530–40, 2010.

123. Martin, C., J. Berwick, D. Johnston, Y. Zheng, J. Martindale, M. Port, P. Redgrave, and J. Mayhew, "Optical imaging spectroscopy in the unanaesthetised rat," *J Neurosci Methods*, Vol. 120, no. 1, pp. 25–34, 2002.

124. Sachdev, R. N., H. Sellien, and F. F. Ebner, "Direct inhibition evoked by whisker stimulation in somatic sensory (si) barrel field cortex of the awake rat," *J Neurophysiol*, Vol. 84, no. 3, pp. 1497–504, 2000.

125. Devecioğlu, I., and B. Güçlü, "A novel vibrotactile system for stimulating the glabrous skin of awake freely behaving rats during operant conditioning," *J Neurosci Methods*, Vol. 242, pp. 41–51, 2015.

126. Yıldız, M. Z., and B. Güçlü, "Relationship between vibrotactile detection threshold in the pacinian channel and complex mechanical modulus of the human glabrous skin," *Somatosens Mot Res*, Vol. 30, no. 1, pp. 37–47, 2013.

127. Verrillo, R. T., "Effect of contactor area on the vibrotactile threshold," *J Acoust Soc Am*, Vol. 35, no. 12, pp. 1962–1966, 1963.

128. Fisch, G. S., "Evaluating data from behavioral analysis: visual inspection or statistical models?," *Behavioural Processes*, Vol. 54, no. 1, pp. 137–154, 2001.

129. Makous, J. C., G. A. Gescheider, and S. J. Bolanowski, "The effects of static indentation on vibrotactile threshold," *The Journal of Acoustical Society of America*, Vol. 99, no. 5, pp. 3149–53, 1996.

130. Gescheider, G. A., B. Güçlü, J. L. Sexton, S. Karalunas, and A. Fontana, "Spatial summation in the tactile sensory system: probability summation and neural integration," *Somatosens Mot Res*, Vol. 22, no. 4, pp. 255–68, 2005.

131. Woolsey, T. A., and H. Van der Loos, "The structural organization of layer iv in the somatosensory region (si) of mouse cerebral cortex. the description of a cortical field composed of discrete cytoarchitectonic units.," *Brain Res.*, Vol. 17, pp. 205–42, 1970.

132. Tütüncüler, B., G. Foffani, B. T. Himes, and K. A. Moxon, "Structure of the excitatory receptive fields of infragranular forelimb neurons in the rat primary somatosensory cortex responding to touch," *Cereb Cortex*, Vol. 16, no. 6, pp. 791–810, 2006.

133. Coq, J. O., and C. Xerri, "Tactile impoverishment and sensorimotor restriction deteriorate the forepaw cutaneous map in the primary somatosensory cortex of adult rats," *Exp Brain Res*, Vol. 129, no. 4, pp. 518–31, 1999.

134. Harker, K. T., and I. Q. Whishaw, "Place and matching-to-place spatial learning affected by rat inbreeding (dark-agouti, fischer 344) and albinism (wistar, sprague-dawley) but not domestication (wild rat vs. long-evans, fischer-norway).," *Behav Brain Res*, Vol. 134, no. 1-2, pp. 467–77, 2002.

135. Talbot, W. H., I. Darian-Smith, H. H. Kornhuber, and V. B. Mountcastle, "The sense of flutter-vibration: comparison of the human capacity with response patterns of mechanoreceptive afferents from the monkey hand," *J Neurophysiol*, Vol. 31, no. 2, pp. 301–34, 1968.

136. Johansson, R. S., and A. Vallbo, "Detection of tactile stimuli. thresholds of afferent units related to psychophysical thresholds in the human hand.," *J Physiology*, Vol. 297, pp. 405–22, 1979.

137. Güçlü, B., and S. J. Bolanowski, "Probability of stimulus detection in a model population of rapidly adapting fibers," *Neural Comput*, Vol. 16, no. 1, pp. 39–58, 2004.

138. Saal, H. P., and S. J. Bensmaia, "Touch is a team effort: interplay of submodalities in cutaneous sensibility," *Trends Neurosci*, Vol. 37, pp. 689–97, 2014.

139. Mountcastle, V. B., R. H. Lamotte, and G. Carli, "Detection thresholds for stimuli in humans and monkeys: Comparison with threshold events in mechanoreceptive afferent nerve fibers innervating the monkey hand," *J Neurophysiol*, Vol. 35, pp. 122–36, 1972.

140. Yıldız, M. Z., I. Toker, F. B. Özkan, and B. Güçlü, "Effects of passive and active movement on vibrotactile detection thresholds of the pacinian channel and forward masking.," *Somatosens Mot Res*, Vol. 32, pp. 262–72, 2015.

141. Kandel, E. R., and A. J. Hudspeth, "The brain and behavior," in *Principles of neural science, 5th ed.* (Kandel, E. R., J. H. Schwartz, T. M. Jessell, S. A. Siegelbaum, and A. J. Hudspeth, eds.), book section Overall Percpective, pp. 5–20, New York, NY, USA: McGraw-Hill, 2012.

142. Costandi, M., *50 ideas you really need to know: The human brain*, London: Quercus Editions Ltd., 2013.

143. Priori, A., G. Foffani, L. Rossi, and S. Marceglia, "Adaptive deep brain stimulation (adbs) controlled by local field potential oscillations," *Exp Neurol*, Vol. 245, pp. 77–86, 2013.

144. Wrobel, S., "Flipping the switch: Targeting depression's neural circuitry." http://emorymedicinemagazine.emory.edu/issues/2015/spring/features/brain-hacking/flipping-the-switch/index.html, accessed April 28, 2016.

145. Fagg, A. H., N. G. Hatsopoulos, B. M. London, J. Reimer, S. A. Solla, D. Wang, and L. E. Miller, "Toward a biomimetic, bidirectional, brain machine interface," *Conf Proc IEEE Eng Med Biol Soc*, pp. 3376–80, 2009.

146. Moxon, K. A., and G. Foffani, "Brain-machine interfaces beyond neuroprosthetics," *Neuron*, Vol. 86, no. 1, pp. 55–67, 2015.

147. Romo, R., A. Hernandez, A. Zainos, and E. Salinas, "Somatosensory discrimination based on cortical microstimulation," *Nature*, Vol. 392, no. 6674, pp. 387–90, 1998.

148. Kandel, E. R., B. A. Barres, and A. J. Hudspeth, "Nerve cells, neural circuitry, and behavior," in *Principles of neural science, 5th ed.* (Kandel, E. R., J. H. Schwartz, T. M. Jessell, S. A. Siegelbaum, and A. J. Hudspeth, eds.), book section Overall Percpective, pp. 21–38, New York, NY, USA: McGraw-Hill, 2012.

149. Siegelbaum, S. A., and J. Koester, "Ion channels," in *Principles of neural science, 5th ed.* (Kandel, E. R., J. H. Schwartz, T. M. Jessell, S. A. Siegelbaum, and A. J. Hudspeth, eds.), book section Cell and molecular biology of the neuron, pp. 100–125, New York, NY, USA: McGraw-Hill, 2012.

150. Koester, J., and S. A. Siegelbaum, "Membrane potential and the passive electrical properties of the neuron," in *Principles of neural science, 5th ed.* (Kandel, E. R., J. H. Schwartz, T. M. Jessell, S. A. Siegelbaum, and A. J. Hudspeth, eds.), book section Cell and molecular biology of the neuron, pp. 126–147, New York, NY, USA: McGraw-Hill, 2012.

151. Koester, J., and S. A. Siegelbaum, "Propagated signaling: The action potential," in *Principles of neural science, 5th ed.* (Kandel, E. R., J. H. Schwartz, T. M. Jessell, S. A. Siegelbaum, and A. J. Hudspeth, eds.), book section Cell and molecular biology of the neuron, pp. 148–176, New York, NY, USA: McGraw-Hill, 2012.

152. Siegelbaum, S. A., E. R. Kandel, and R. Yuste, "Synaptic integration in the central nervous system," in *Principles of neural science, 5th ed.* (Kandel, E. R., J. H. Schwartz, T. M. Jessell, S. A. Siegelbaum, and A. J. Hudspeth, eds.), book section Synaptic transmission, pp. 210–235, New York, NY, USA: McGraw-Hill, 2012.

153. Merrill, D. R., M. Bikson, and J. G. Jefferys, "Electrical stimulation of excitable tissue: design of efficacious and safe protocols," *J Neurosci Methods*, Vol. 141, no. 2, pp. 171–98, 2005.

154. Oddo, C. M., S. Raspopovic, F. Artoni, A. Mazzoni, G. Spigler, F. Petrini, F. Giambattistelli, F. Vecchio, F. Miraglia, L. Zollo, G. Di Pino, D. Camboni, M. C. Carrozza, E. Guglielmelli, P. Rossini, U. Faraguna, and S. Micera, "Intraneural stimulation elicits discrimination of textural features by artificial fingertip in intact and amputee humans," *eLife*, Vol. 5, p. e09148, 2016.

155. Klaes, C., Y. Shi, S. Kellis, J. Minxha, B. Revechkis, and R. A. Andersen, "A cognitive neuroprosthetic that uses cortical stimulation for somatosensory feedback," *J Neural Eng*, Vol. 11, no. 5, p. 056024, 2014.

156. Towe, B. C., "Bioelectricity and its measurement," in *Biomedical engineering and design hadnbook: Volume 1 Fundamentals* (Kutz, M., ed.), pp. 481–637, New York, NY, USA: McGraw-Hill, 2009.

157. Navarro, X., T. B. Krueger, N. Lago, S. Micera, T. Stieglitz, and P. Dario, "A critical review of interfaces with the peripheral nervous system for the control of neuroprostheses and hybrid bionic systems," *J Peripher Nerv Syst*, Vol. 10, no. 3, pp. 229–258, 2005.

158. McDermott, M. D., J. Zhang, and K. J. Otto, "Improving the brain machine interface via multiple tetramethyl orthosilicate sol-gel coatings on microelectrode arrays," in *The 7th International IEEE/EMBS Conference on Neural Engineering*, 2015.

159. Sommakia, S., J. L. Rickus, and K. J. Otto, "Glial cells, but not neurons, exhibit a controllable response to a localized inflammatory microenvironment in vitro," *Front Neuroeng*, Vol. 7, p. 41, 2014.

160. Fernández, E., B. Greger, P. A. House, I. Aranda, C. Botella, J. Albisua, C. Soto-Sánchez, A. Alfaro, and R. A. Normann, "Acute human brain responses to intracortical microelectrode arrays: challenges and future prospects," *Front Neuroeng*, Vol. 7, p. 24, 2014.

161. Liu, J., T.-M. Fu, Z. Cheng, G. Hong, T. Zhou, L. Jin, M. Duvvuri, Z. Jiang, P. Kruskal, C. Xie, Z. Suo, Y. Fang, and C. M. Lieber, "Syringe-injectable electronics," *Nat Nanotechnol*, Vol. 10, pp. 629–36, 2015.

162. Boinagrov, D., J. Loudin, and D. Palanker, "Strength-duration relationship for extracellular neural stimulation: Numerical and analytical models," *J Neurophysiol*, Vol. 104, pp. 2236–48, 2010.

163. Paxinos, G., and W. Charles, *The rat brain in stereotaxic coordinates*, London, UK: Academic Press, 2006.

164. Polikov, V. S., P. A. Tresco, and W. M. Reichert, "Response of brain tissue to chronically implanted neural electrodes," *J Neurosci Methods*, Vol. 148, no. 1, pp. 1–18, 2005.

165. Rajan, A. T., J. L. Boback, J. F. Dammann, F. Tenore, B. A. Wester, K. J. Otto, R. A. Gaunt, and S. Bensmaia, "The effects of chronic intracortical microstimulation on neural tissue and fine motor behavior," *J Neural Engin*, Vol. 12, p. 066018, 2015.

166. Recanzone, G. H., M. M. Merzenich, and H. R. Dinse, "Expansion of the cortical representation of a specific skin field in primary somatosensory cortex by intracortical microstimulation," *Cereb. Cortex*, Vol. 2, pp. 181–96, 1992.

167. Callier, T., E. W. Schluter, G. A. Tabot, L. E. Miller, F. V. Tenore, and S. J. Bensmaia, "Long-term stability of sensitivity to intracortical microstimulation of somatosensory cortex," *J Neural Eng*, Vol. 12, no. 5, p. 056010, 2015.

168. Chen, K. H., J. F. Dammann, J. L. Boback, F. V. Tenore, K. J. Otto, R. A. Gaunt, and S. J. Bensmaia, "The effect of chronic intracortical microstimulation on the electrode-tissue interface," *J Neural Eng*, Vol. 11, no. 2, p. 026004, 2014.

169. Lycke, R. J., A. Schendel, J. C. Williams, and K. J. Otto, "In vivo evaluation of a muecog array for chronic stimulation," *Conf Proc IEEE Eng Med Biol Soc*, pp. 1294–7, 2014.

170. Kim, S., T. Callier, G. A. Tabot, R. A. Gaunt, F. V. Tenore, and S. J. Bensmaia, "Behavioral assessment of sensitivity to intracortical microstimulation of primate somatosensory cortex," *Proc Natl Acad Sci USA*, p. 201509265, 2015.

171. Foffani, G., B. Tutunculer, and K. A. Moxon, "Role of spike timing in the forelimb somatosensory cortex of the rat," *J Neurosci*, Vol. 24, no. 33, pp. 7266–71, 2004.

172. Cohen, J. D., and M. A. Castro-Alamancos, "Detection of low salience whisker stimuli requires synergy of tectal and thalamic sensory relays," *J Neurosci*, Vol. 30, no. 6, pp. 2245–56, 2010.

173. Berg, J. A., r. Dammann, J. F., F. V. Tenore, G. A. Tabot, J. L. Boback, L. R. Manfredi, M. L. Peterson, K. D. Katyal, M. S. Johannes, A. Makhlin, R. Wilcox, R. K. Franklin, R. J. Vogelstein, N. G. Hatsopoulos, and S. J. Bensmaia, "Behavioral demonstration of a somatosensory neuroprosthesis," *IEEE Trans Neural Syst Rehabil Eng*, Vol. 21, no. 3, pp. 500–7, 2013.

174. Sadovsky, A. J., and J. N. MacLean, "Scaling of topologically similar functional modules defines mouse primary auditory and somatosensory microcircuitry," *J Neurosci*, Vol. 33, pp. 14048–60, 2013.

175. Fridman, G. Y., H. T. Blair, A. P. Blaisdell, and J. W. Judy, "Perceived intensity of somatosensory cortical electrical stimulation," *Exp Brain Res*, Vol. 203, no. 3, pp. 499–515, 2010.

176. Ahn, M., M. Lee, J. Choi, and S. C. Jun, "A review of brain-computer interface games and an opinion survey from researchers, developers and users.," *Sensors*, Vol. 14, pp. 14601–33, 2014.

177. Murphy, M. D., D. J. Guggenmos, D. T. Bundy, and R. J. Nudo, "Current challenges facing the translation of brain computer interfaces from preclinical trials to use in human patients," *Front Cell Neurosci*, Vol. 9, p. 497, 2015.

178. Rao, R. P., A. Stocco, M. Bryan, D. Sarma, T. M. Youngquist, J. Wu, and C. S. Prat, "A direct brain-to-brain interface in humans," *PLoS One*, Vol. 9, no. 11, p. e111332, 2014.

179. Hotson, G., D. P. McMullen, M. S. Fifer, M. S. Johannes, K. D. Katyal, M. P. Para, R. Armiger, W. S. Anderson, N. Thakor, B. A. Wester, and N. E. Crone, "Individual finger control of a modular prosthetic limb using high-density electrocorticography in a human subject," *J Neural Engin*, Vol. 13, p. 026017, 2016.

180. Micera, S., J. Carpaneto, and S. Raspopovic, "Control of hand prostheses using peripheral information.," *Biomedical Engin., IEEE Reviews*, Vol. 3, pp. 48–68, 2010.

181. Ruff, R., W. Poppendieck, A. Gail, S. Westendorff, M. Russold, S. Lewis, T. Meiners, and K. P. Hoffmann, "Acquisition of myoelectric signals to control a hand prosthesis with implantable epimysial electrodes," *Conf Proc IEEE Eng Med Biol Soc*, pp. 5070–3, 2010.

182. Raspopovic, S., M. Capogrosso, F. M. Petrini, M. Bonizzato, J. Rigosa, G. Di Pino, J. Carpaneto, M. Controzzi, T. Boretius, E. Fernandez, G. Granata, C. M. Oddo, L. Citi, A. L. Ciancio, C. Cipriani, M. C. Carrozza, W. Jensen, E. Guglielmelli, T. Stieglitz, P. M. Rossini, and S. Micera, "Restoring natural sensory feedback in real-time bidirectional hand prostheses," *Sci Transl Med*, Vol. 6, no. 222, p. 222ra19, 2014.

183. Kuiken, T. A., L. A. Miller, R. D. Lipschutz, B. A. Lock, K. Stubblefield, P. D. Marasco, P. Zhou, and G. A. Dumanian, "Targeted reinnervation for enhanced prosthetic arm function in a woman with a proximal amputation: a case study," *The Lancet*, Vol. 369, no. 9559, pp. 371–380, 2007.

184. Abbott, A., "Neuroprosthetics: in search of the sixth sense," *Nature*, Vol. 442, no. 7099, pp. 125–7, 2006.

185. Tabot, G. A., S. S. Kim, J. E. Winberry, and S. J. Bensmaia, "Restoring tactile and proprioceptive sensation through a brain interface," *Neurobiol Dis*, 2014.

186. Tabot, G. A., J. F. Dammann, J. A. Berg, F. V. Tenore, J. L. Boback, R. J. Vogelstein, and S. J. Bensmaia, "Restoring the sense of touch with a prosthetic hand through a brain interface," *Proc Natl Acad Sci USA*, Vol. 110, no. 45, pp. 18279–84, 2013.

187. Tan, D. W., M. A. Schiefer, M. W. Keith, J. R. Anderson, J. Tyler, and D. J. Tyler, "A neural interface provides long-term stable natural touch perception," *Sci Transl Med*, Vol. 6, no. 257, p. 257ra138, 2014.

188. Millstein, S. G., and G. A. Hunter, "Prosthetic use in adult upper limb amputees: A comparison of the body powered and electrically powered prostheses," *Prosthet Orthot Int*, Vol. 10, pp. 27–34, 1986.

189. Norton, K. M., "A brief history of prosthetics," *inMotion*, Vol. 17, pp. 11–13, 2007.

190. Dudkiewicz, I., R. Gabrielov, I. Seiv-Ner, G. Zelig, and M. Heim, "Evaluation of prosthetic usage in upper limb amputees," *Disability & Rehabilitation*, Vol. 26, pp. 60–63, 2004.

191. Chorost, M., "A true bionic limb remains far out of reach." http://www.wired.com/2012/03/ff_prosthetics/, published March 20, 2012; accessed May 5, 2016.

192. Farina, D., N. Jiang, H. Rehbaum, A. Holobar, B. Graimann, H. Dietl, and O. Aszmann, "The extraction of neural information from the surface emg for the control of upper-limb prostheses: emerging avenues and challenges," *IEEE Trans Neural Syst Rehabil Eng*, Vol. 22, pp. 797–809, 2014.

193. Fougner, A., O. Stavdahl, P. J. Kyberd, Y. G. Losier, and P. A. Parker, "Control of upper limb prostheses: terminology and proportional myoelectric control-a review," *IEEE Trans Neural Syst Rehabil Eng*, Vol. 20, pp. 663–77, 2012.

194. Kuiken, T. A., P. D. Marasco, B. A. Lock, R. N. Harden, and J. P. Dewald, "Redirection of cutaneous sensation from the hand to the chest skin of human amputees with targeted reinnervation," *Proc Natl Acad Sci U S A*, Vol. 104, no. 50, pp. 20061–6, 2007.

195. Ju, J. S., Y. Shin, and E. Y. Kim, "Vision based interface system for hands free control of an intelligent wheelchair," *J Neuroeng Rehabil*, Vol. 6, p. 33, 2009.

196. van de Laar, B., B. D. Plass-Oude, B. Reuderink, M. Poel, and A. Nijholt, "How much control is enough? influence of unreliable input on user experience.," *IEEE Trans Cybern*, Vol. 43, pp. 1584–92, 2013.

197. Ethier, C., E. R. Oby, M. J. Bauman, and L. E. Miller, "Restoration of grasp following paralysis through brain-controlled stimulation of muscles," *Nature*, Vol. 485, no. 7398, pp. 368–71, 2012.

198. Shanechi, M. M., R. C. Hu, and Z. M. Williams, "A cortical-spinal prosthesis for targeted limb movement in paralysed primate avatars," *Nat Commun*, Vol. 5, 2014.

199. Lewis, S., M. F. Russold, H. Dietl, and E. Kaniusas, "User demands for sensory feedback in upper extremity prostheses," in *IEEE International Symposium on Medical Measurements and Applications Proceedings (MeMeA)*, pp. 1–4, IEEE, 2012.

200. de Vignemont, F., "Body schema and body image–pros and cons," *Neuropsychologia*, Vol. 48, no. 3, pp. 669–80, 2010.

201. Blanke, O., "Multisensory brain mechanisms of bodily self-consciousness," *Nat Rev Neurosci*, Vol. 13, no. 8, pp. 556–71, 2012.

202. Evans, N., and O. Blanke, "Shared electrophysiology mechanisms of body ownership and motor imagery," *Neuroimage*, Vol. 64, pp. 216–28, 2013.

203. Marasco, P. D., K. Kim, J. E. Colgate, M. A. Peshkin, and T. A. Kuiken, "Robotic touch shifts perception of embodiment to a prosthesis in targeted reinnervation amputees," *Brain*, Vol. 134, no. Pt 3, pp. 747–58, 2011.

204. Macherey, O., and R. P. Carlyon, "Cochlear implants," *Current Biology*, Vol. 24, pp. R878–R84, 2014.

205. Witteveen, H. J., E. A. Droog, J. S. Rietman, and P. H. Veltink, "Vibro-and electrotactile user feedback on hand opening for myoelectric forearm prostheses," *IEEE Trans Biomed Eng*, Vol. 59, no. 8, pp. 2219–2226, 2012.

206. Cipriani, C., M. D'Alonzo, and M. C. Carrozza, "A miniature vibrotactile sensory substitution device for multifingered hand prosthetics," *IEEE Trans Biomed Eng*, Vol. 59, no. 2, pp. 400–408, 2012.

207. Dhillon, G. S., and K. W. Horch, "Direct neural sensory feedback and control of a prosthetic arm," *IEEE Trans Neural Syst Rehabil Eng*, Vol. 13, no. 4, pp. 468–72, 2005.

208. Horch, K., S. Meek, T. G. Taylor, and D. T. Hutchinson, "Object discrimination with an artificial hand using electrical stimulation of peripheral tactile and proprioceptive pathways with intrafascicular electrodes," *IEEE Trans Neural Syst Rehabil Eng*, Vol. 19, no. 5, pp. 483–9, 2011.

209. Romo, R., and E. Salinas, "Flutter discrimination: neural codes, perception, memory and decision making," *Nat Rev Neurosci*, Vol. 4, no. 3, pp. 203–18, 2003.

210. Romo, R., A. Hernandez, A. Zainos, and E. Salinas, "Correlated neuronal discharges that increase coding efficiency during perceptual discrimination," *Neuron*, Vol. 38, no. 4, pp. 649–57, 2003.

211. Yau, J. M., M. Hollins, and S. J. Bensmaia, "Textural timbre: The perception of surface microtexture depends in part on multimodal spectral cues," *Commun Integr Biol*, Vol. 2, no. 4, pp. 1–3, 2009.

212. Heming, E., A. Sanden, and Z. H. Kiss, "Designing a somatosensory neural prosthesis: percepts evoked by different patterns of thalamic stimulation," *J Neural Eng*, Vol. 7, no. 6, p. 064001, 2010.

213. Heming, E. A., R. Choo, J. N. Davies, and Z. H. T. Kiss, "Designing a thalamic somatosensory neural prosthesis: Consistency and persistence of percepts evoked by electrical stimulation," *IEEE Trans Neural Syst Rehabil Engin*, Vol. 19, no. 5, pp. 477–482, 2011.

214. Seifert, J. L., V. Desai, R. C. Watson, T. Musa, Y.-t. Kim, E. W. Keefer, and M. Romero, "Normal molecular repair mechanisms in regenerative peripheral nerve interfaces allow recording of early spike activity despite immature myelination," *IEEE Trans Neural Syst Rehabil Eng*, Vol. 20, no. 2, pp. 220–227, 2012.

215. Peppas, N. A., and A. S. Hoffman, "Hydrogels," in *Biomaterials Science: An Introduction to Materials in Medicine* (Ratner, B. D., A. S. Hoffman, F. J. Schoen, and J. E. Lemons, eds.), book section I.2.5, pp. 166–178, Oxford, UK: Academic Press, 2013.